Fatigue Damage Assessment of Materials Under Uniaxial Variable Amplitude Loading Conditions

By

Mitesh Sharma

A thesis presented to the Ryerson University
in fulfillment of the
thesis requirement for the degree of
Master of Applied Science
in
Mechanical Engineering

Toronto, Ontatio, Canada, 2003

AUTHOR'S DECLARATION

I hereby declare that I am the sole author of this thesis.

I authorize the Ryerson University to lend this thesis to other institutions or individuals for the purpose of scholarly research.

I further authorize the Ryerson University to reproduce this thesis by photocopying or by other means, in total or in part, at the request of other institutions or individuals for the purpose of scholarly research.

The Ryerson University requires the signatures of all persons using or photocopying this thesis. Please sign below, and give address and date.

ABSTRACT

This thesis intends to further apply an earlier developed energy based-critical fatigue damage parameter to assess the fatigue damage of different materials subjected to repeated random block histories. In fatigue damage assessment under variable loading conditions, further phenomenological factors of:

(i) sequence loading effect,

(ii) memory effect, and

(iii) the effect of small amplitude cycles below the material endurance limit have been introduced.

The effect due to sequence loading is studied for variable amplitude loading conditions. It is found that the loading sequence has a great influence on the cyclic stress-strain hysteresis loops and therefore on fatigue damage of materials. Memory effect concept has been carefully monitored and programmed to correspond to the closed hysteresis loops in each block loading history. The small cycles exceeding 50% of the fatigue endurance limit contributed to the accumulated damage.

A comparison of the predicted fatigue life results based on energy based-critical parameter including the phenomenological factors with the experimental live data reported in the literature has shown a good agreement.

ACKNOWLEDGEMENTS

I wish to acknowledge and thank my supervisor Professor A. Varvani-Farahani for his strong support and insightful guidance in the course of this study.

I would like to thank my co-supervisor Professor M.R. Kianoush for his encouragement and advice that greatly helped me through this work.

The financial support of NSERC through Professor A. Varvani-Farahani of Department of Mechanical Engineering- Ryerson University as well as a partial support of Civil Engineering Department through Professor M.R. Kianoush are greatly appreciated.

Finally, I would like to thank all my fellow graduate students and family members for their support, encouragement and constructive criticisms.

To my dear late grandmother

Parvati

TABLE OF CONTENTS

LIST OF FIGURES

NOMENCLATURE

ASME	-	American Society of Mechanical Engineering
CPE	-	Critical Plane Energy
DCA	-	Damage Curve Approach
DLDR	-	Double Linear Damage Rule
DDCA	-	Double-Damage Curve Approach
E	-	Modulus of elasticity
HCF	-	High cycle fatigue
LCF	-	Low cycle fatigue
S-N	-	Stress –Life
ϵ-N	-	Strain-Life
LDR	-	Linear Damage Rule
MSC	-	Microstructurally short crack
PSC	-	Physically small crack
CAL	-	Constant amplitude loading
VAL	-	Variable amplitude loading
S	-	Alternating stress
K	-	Cyclic strength coefficient
n_1	-	Cyclic hardening exponent
n*	-	Constant unifies shear and tensile fatigue data.
k	-	mathematical exponent to give close fit to the double linear damage rule.
N_f	-	Cycles to failure
N_r	-	Number of cycle at reference level.
D_i	-	Damage fraction
c_i	-	Retardation factor.
d	-	Material sensitivity constant.
p	-	Constant measured from the slope of the first damage accumulation line.
p_1	-	Empirical shaping parameter depending on the material properties.
A	-	Material constant for refined double linear damage rule.
β		Material constant (slope of regression line).

$\beta_1, \beta_2, \beta_3$ Material constant determined experimentally.

$\Delta\lambda, \Delta\lambda^*$ Sequenced related parameters.

a_0, a, a_f Initial, Instantaneous and Final crack length.

N_1, N_{11} Two stages of damage linear rule.

$\Delta\varepsilon_{ap}$, $\Delta(\frac{\gamma_{ap}}{2})$ The shear and axial strain ranges respectively.

$\Delta\varepsilon_n, \Delta(\frac{\gamma_{\max}}{2})$ Maximum shear strain range and normal strain range acting on the critical plane, respectively.

$\Delta\sigma_a, \Delta\tau_a, \Delta\varepsilon_a$ Applied tensorial strain range, stress range, and shear stress range, respectively

$\Delta\tau_{\max}, \Delta\sigma_n$ Maximum shear stress range and normal stress range, respectively

$\varepsilon_1, \varepsilon_2, \varepsilon_3$ Principal strains ($\varepsilon_1 > \varepsilon_2 > \varepsilon_3$)

$\varepsilon_e, \varepsilon_p$ Elastic strain and plastic strain respectively

ν_e, ν_p, ν_{eff} Elastic, plastic, and effective Poisson's ratios respectively

$\sigma_1, \sigma_2, \sigma_3$ Principal stresses ($\sigma_1 > \sigma_2 > \sigma_3$)

σ_n^m Mean normal stress

α Life fraction factor for the initiation stage.

α_1 Material constant determined from regression analysis experimentally

λ_1, λ_2 First and second fictitious load levels.

$\sigma_n^{\max}$ Maximum normal stress

$\sigma_n^{\min}$ Minimum normal stress

$\sigma_{\max}$ Maximum stress amplitude

$\sigma_f', \varepsilon_f'$ The axial fatigue strength coefficient and axial fatigue ductility coefficient, respectively.

τ_f', γ_f' The shear fatigue strength coefficient and shear fatigue ductility coefficient, respectively.

$\varepsilon_{a1}, \varepsilon_{a2}, \varepsilon_{a3}$ Applied strain amplitudes in a step loading conditions ($\varepsilon_{a1} > \varepsilon_{a2} > \varepsilon_{a3}$).

$\Delta\gamma_p$ Plastic strain range.

OBJECTIVE AND SCOPE OF PRESENT STUDY

The present study intends to further apply a recently developed Varvani's fatigue damage parameter to assess the fatigue damage of smooth 1045 steel components subjected to repeated variable block histories. The parameter is the sum of the normal energy range and shear energy calculated for critical plane on which the stress and strain Mohr's circles are largest during each peak-valley cyclic loads. Fatigue damage has been accumulated on the basis of peaks and valleys throughout the variable block loading histories using a computer algorithm developed in this study. In fatigue damage assessment under variable loading conditions, further phenomenological factors of (i) loading sequence effect, (ii) the effect of small amplitude cycles below the materials endurance limit, and (iii) hysteresis memory effect have been taken into account.

The effect due to sequence loading is studied for variable loading. It is found that the loading sequence has a great influence in the stress-strain response of hysteresis loops. Memory effect concept has been carefully monitored and programmed to correspond to the closed hysteresis loop in each block loading history. The small amplitude cycles corresponds to 50% to 100% of the materials endurance limit are also studied. Results indicate that small cycles exceeding 50% of the fatigue endurance limit contribute to the accumulated damage. The variation of mean stress as peaks and valleys of a block loading history fluctuate has been included in fatigue damage calculation.

A comparison of the predicted fatigue life results based on energy based-critical parameter including the phenomenological factors with the experimental fatigue life data has been found in a good agreement.

PREFACE OF THESIS

The following provides a brief description of material covered in this thesis. This discussion emphasizes practical application, evaluation of fatigue damage assessment subjected to variable amplitude loading conditions.

Chapter 1 covers the introduction and background of three basic approach stress, strain and fracture mechanics. The chapter discusses about early fatigue damage model such as well-known Miner's rule, non-linear damage rule. It also covers the early approaches developed in1970's to some of the latest models developed such as critical plane damage theories, continuum damage mechanics approaches, energy based-critical plane damage approaches.

Chapter 2 reviews the practical application in the field of aeronautics, automobile and civil industries (such as bridge, chimney and offshore structures). These applications will give the brief idea on how fatigue damage analysis is used in the diverse engineering fields.

Chapter 3 discusses Varvani's fatigue damage approach and includes all terms required for damage assessment using this approach. This chapter further discusses the states of stress and strain and phenomenological factors such as sequence effect, memory effect and small cycle effect, for fatigue damage assessment under variable amplitude loading conditions.

Chapter 4 addresses the detailed description of computer method developed for the analysis of fatigue damage model. It also describes detailed steps involved in computer program, for Varvani's parameter as well as phenomenological factors.
Chapter 5 evaluates the damage analysis results for various fatigue data available in the literature. The model is tested with diverse engineering applications in order to prove the

applicability of the approach. The experimental data referenced from literature are explained in detail because each data set corresponded to specific loading conditions. Chapter 6 discusses the advantages of a new proposed model and comparison of a new proposed approach with other critical plane approaches.

Chapter 7 summarizes the conclusions obtained by evaluating the fatigue damage model. It gives details about how accurately this approach can be used for variable loading conditions. It also includes recommendations for researchers who are interested to carry out further studies on the topic.

CHAPTER ONE

Introduction and Background

1.1 Introduction:

Fatigue failures are common modes of failure observed in various mechanical components and structures. In real engineering applications where fatigue is an important failure mode, the alternating stress amplitude usually changes in irregular manner. Proper prediction of life of those objects is a very important problem and any underestimation can cause catastrophic failure.

Fatigue is a process which causes premature failure or damage of component subjected to repeated loading. It is a complicated metallurgical process to accurately describe and model on the microscopic level. Despite this complexity, fatigue analysis methods have been developed. The three primary fatigue analysis methods are stress-life approach, the strain-life approach, and the fracture mechanics approach.

(i) The Stress –Life (S-N) approach: This method was the first approach used in an attempt to understand and quantify metal fatigue. It was the standard fatigue design method for almost 100 years. The S-N approach is still widely used in design applications where the applied stress is primarily within the elastic range of the material and resultant lives are long. The basis of the stress-life method is the S-N diagram, which is a plot of alternating stress, S, versus cycles to failure, N_f. This method does not work well in low-cycle applications. The dividing line between the low and high cycle fatigue depends on the material being considered, but usually falls between 10 and 10^5 cycles. One of the major drawbacks of the stress-life approach is that it ignores true stress-strain behavior and treats all

strains in the elastic range. This method is completely empirical in nature and lacks the physical insights. The plastic strains, which are critical at the short lives, are ignored and at long lives most of steels have only a small plastic component of cyclic strain. The S-N approach does not distinguish between crack initiation and propagation stages.

(ii) Strain-Life (ϵ-N) Approach: This method takes into account actual stress-strain response of the material, plastic strain, and the mechanism that is modeled and is used in high strain/low cycle regime. In most engineering components [1], the response in critical locations is either dependent on strain or deformation. When the load levels are low, stresses and strains are linearly related. At high load levels [1], in the low cycle fatigue (LCF) regime, the cyclic stress-strain response and material behavior are best modeled under strain-controlled condition. Fatigue research showed [1] that damage is dependent on plastic deformation or strain. In the strain-life approach the plastic strain or deformation is directly measured and quantified. The strain-life method assumes that smooth specimen tested under strain-controlled can stimulate fatigue damage at the notch root of an engineering component. Crack growth is not explicitly accounted for in the strain-life method. This method can model the residual mean stresses resulting from the sequence effect in load histories. This allows for more accurate accounting of cumulative damage under variable amplitude loading. It is used in high temperature application where fatigue creep interaction is critical. This method involves a more complicated level of analysis like Neuber analysis, finite element analysis or strain gauge measurement.

(iii) Fracture Mechanics Approach: The fatigue life of a component comprises of two stages: initiation and propagation stages. The size of the crack at the transition from initiation to propagation is usually unknown and often depends on the point of view of the analyst. At low strain amplitude [1], about 90% of the life is spent at initiation stage, while at high amplitude the majority of the fatigue life may be spent propagating a crack. Fracture mechanics approaches are used to estimate the propagation life. It requires an initial crack size be known for component with imperfections or defects, such as welding porosities, inclusions and casting defects, etc. Linear elastic fracture mechanism

principles are used to relate the stress magnitude and distribution near the crack tip to remote stress applied to the cracked component, the crack size and shape, the material properties of the crack component. Griffith [2] formulated the concept that a crack in a component will propagate if the energy is lowered with crack propagation the total energy of the system is lowered. Irwin [3] extended the theory for ductile materials. He postulated that the energy due to plastic deformation must be added to the surface energy associated with the creation of new crack surfaces. He recognized that for ductile materials, the surface energy term is often negligible compared to the energy associated with plastic deformation. Irwin [4] made another significant contribution, which states that the local stresses near the crack tip are of the general form as shown in the Figure 1.1.

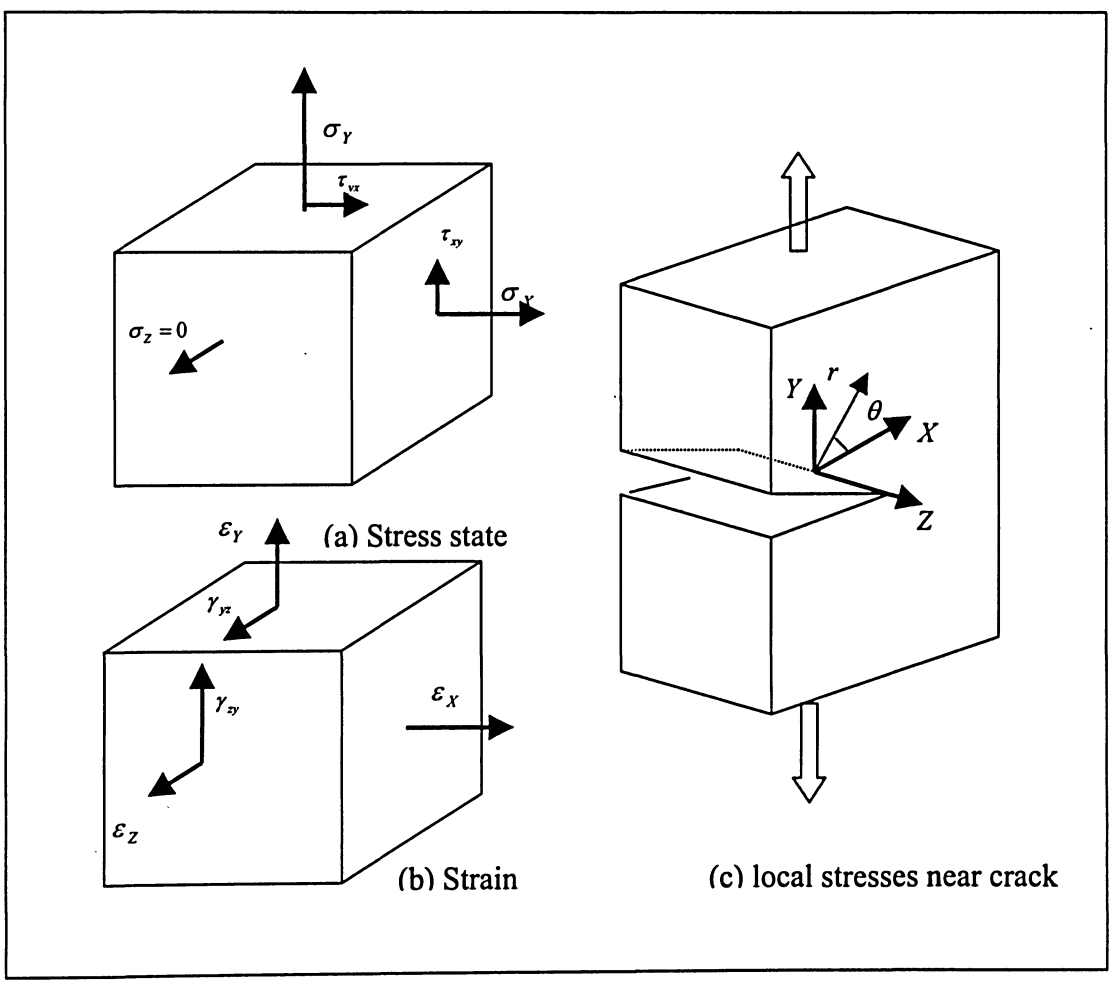

Figure 1.1 Schematic presentation of local stresses near crack tips for plane stress condition.

Historically, two considerations have promoted the development of fatigue analysis methods. The first has been the need to provide designers and engineers with methods that are practical and easily implemented, and cost effective. The second consideration has been the need to reconcile these analytical considerations with physical considerations. Economics of time and money is an important consideration when selecting an analysis technique. The S-N approach is the quickest and cheapest of the approaches, but the advantages of the other methods may far outweigh cost consideration. Any of the fatigue life estimation techniques can be used for either initial sizing or design of new component or for the analysis of an existing component.

1.2 Theories on cumulative fatigue damage:

Several researchers have reviewed theories on cumulative fatigue damage and divided these theories into the following categories:

1. Linear damage rules.
2. Non-linear damage curve.
3. Two stage linearization approaches.
4. Life curve modification methods.
5. Approaches based on crack growth concepts.
6. Energy based theories.
7. Continuum damage mechanics model.
8. Critical plane Damage theories, and
9. Energy-based critical plane damage theories.

1.2.1 Linear damage rules (LDR):

The first cumulative damage rule was proposed by Palmgren [5] in 1924 and later developed by Miner [6] in 1945. This linear theory, which is still widely used now, is referred to as the Palmgren-Miner rule or Miner's rule.

It simply states that fatigue failure is expected when the summation of all the fatigue damage caused by different stress level reaches unity.

$$\sum_{i=1}^{n} \frac{n}{N_f} = \text{Cycle ratio}, \tag{1.1}$$

where n and N_f are the number of cycles and the fatigue life in cycles at stress level S respectively.

The damage fraction, D, is defined as the fraction of life used up by an event or a series of events. Failure in any of the cumulative damage theories is assumed to occur when the summation of damage fraction equals 1:

$$\sum D_i = 1 \tag{1.2}$$

The linear damage rule states that the damage fraction, D_i, at stress level S_i is equal to the cycle ratio n_i/N_i.

$$D_i = \sum \frac{n_i}{N_i} = 1 \tag{1.3}$$

Linear damage rules cannot account for load sequence and load interaction effect due to their linear nature. The Linear damage rule has two main shortcomings when it describes observed material behavior. First, it does not consider sequence effect. The linear damage rule does not hold a term to show the effect of stress amplitude. Miner's rule can also be interpreted graphically by showing its effect on the S-N curve as shown in Figure 1.2.

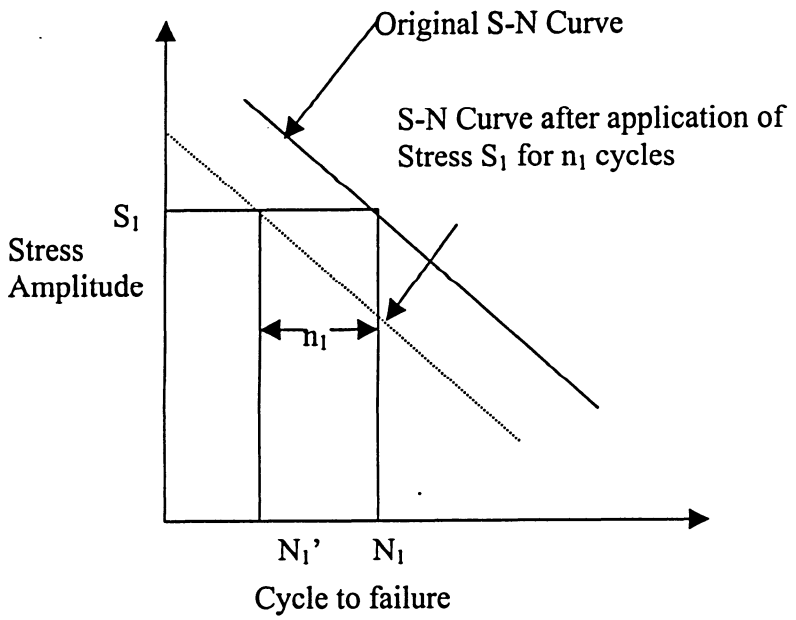

Figure 1.2 Effect of Miner's rule on S-N Curve [1].

1.2.2 Non-Linear Theories:

Many nonlinear damage theories have been proposed which attempt to overcome the shortcomings of Miner's rule. There are some practical problems involved when trying to use these methods. Firstly, they require material constants, which must be determined from a series of step tests. This requires a considerable number of tests to conduct. Secondly, since some of the methods take into account sequence effects, the number of calculations and lengthy procedure can become a problem in complicated histories. Another point is that although the nonlinear methods may give better predictions than Miner's rule for two-step histories, it cannot be guaranteed that they will work better for actual service load histories.

Macro and Starkey [7] proposed the first non-linear load dependent damage theory in 1954, represented by a power relationship as:

$$D = \sum r_i^{x_i} \tag{1.4}$$

where x_i is a variable quantity related to the i^{th} loading level. The concept of change in endurance limit due to pre-stress exerted an important influence on subsequent cumulative fatigue damage research. Kommers [8] and Bennelt [9] further investigated the effect of fatigue pre-stressing on endurance properties using a two-level step loading method. Their experimental results suggested that the reduction in the endurance strength could be used as a damage measure, but they did not correlate this damage parameter to the life fraction. All of these damage models based on endurance limit reduction are non-linear and able to account for the load sequence effect. None of these models, however, take into account the interaction effect. The use of above method is shown in Figure 1.3, which is plot of damage fraction versus cycle ratio for two stress levels, where $S_1 > S_2$ and damage calculation is done along OA'AB (dotted line shown in the Figure).

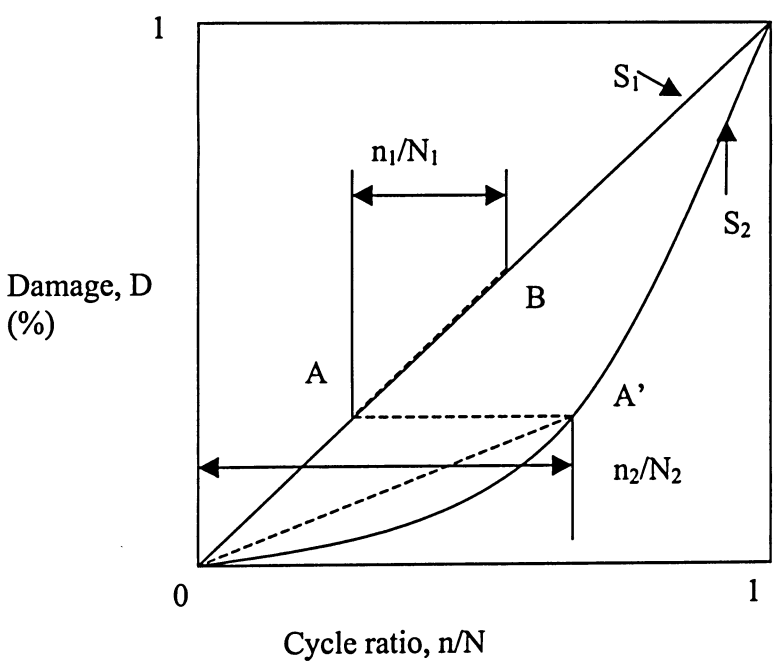

Figure 1.3 Demonstration of Non-linear theory [1].

1.2.3 Early theories accounting for load interaction effect:

Splitzer-Corten [10] and Freudenthal-Heller [11] approaches are based on the modification of the S-N diagram, which is simply a clockwise rotation of S-N line around a reference point on the line. In Splitzer-Corten model the reference point corresponds to the highest level, while in Freudenthal-Heller approach, this reference is chosen at the stress level corresponding to the fatigue life of 10^3- 10^4 cycles. Manson et al. [12] also examined the approach based on the S-N line rotation and convergence concept. They suggested that a point corresponding to failure life between 10^2 and 10^3 cycles on the original S-N line can be selected as the convergence point. Their approach also provides a method for predicting the reduction in endurance limit due to pre-cycling damage, and is therefore able to account not only for the load interaction effect, but also for small cycle damage. Marrow [13] has proposed a plastic work interaction damage rule which modifies Miner's rule by multiplying a given stress cycle ratio (the given stress to the maximum stress) to power factor to incorporate the interaction effect. The factor is called the plastic work exponent and can be interpreted as the material sensitivity to the variable-amplitude stress history. According to Marrow, when a component is subjected to variable-amplitude loading, the damage accumulation is given by the following:

$$D = \sum_{i=1}^{n} \frac{n_i}{N_{fi}} \left(\frac{\sigma_i}{\sigma_{\max}} \right)^d \tag{1.5}$$

in which N_{fi} indicates the number of cycles to failure when the specimen or component is subjected to strain of amplitude ε_i (or stress amplitude σ_i), n_i is the applied strain cycle of ε_i(or stress cycles of σ_i), σ_{max} is the maximum stress amplitude among all stress amplitude applied to the component, d is the material's sensitivity to the variable amplitude loading. It is noted that equation (1.5) reduces to equation (1.3) when d=0, which indicated that Palmgren-Miner's linear damage rule is a special case of the proposed non-linear damage rule. Figure 1.4 shows the schematic representation for two-level L-H and H-L stressing. In these Figures, solid lines represent the Miner rule, dash line represents rotation from S-N curve to LDR, which is parallel to the original S-N

curves. It can be seen that the LDR and the S-N line rotation approaches differ in their abilities to account for the load interaction effects.

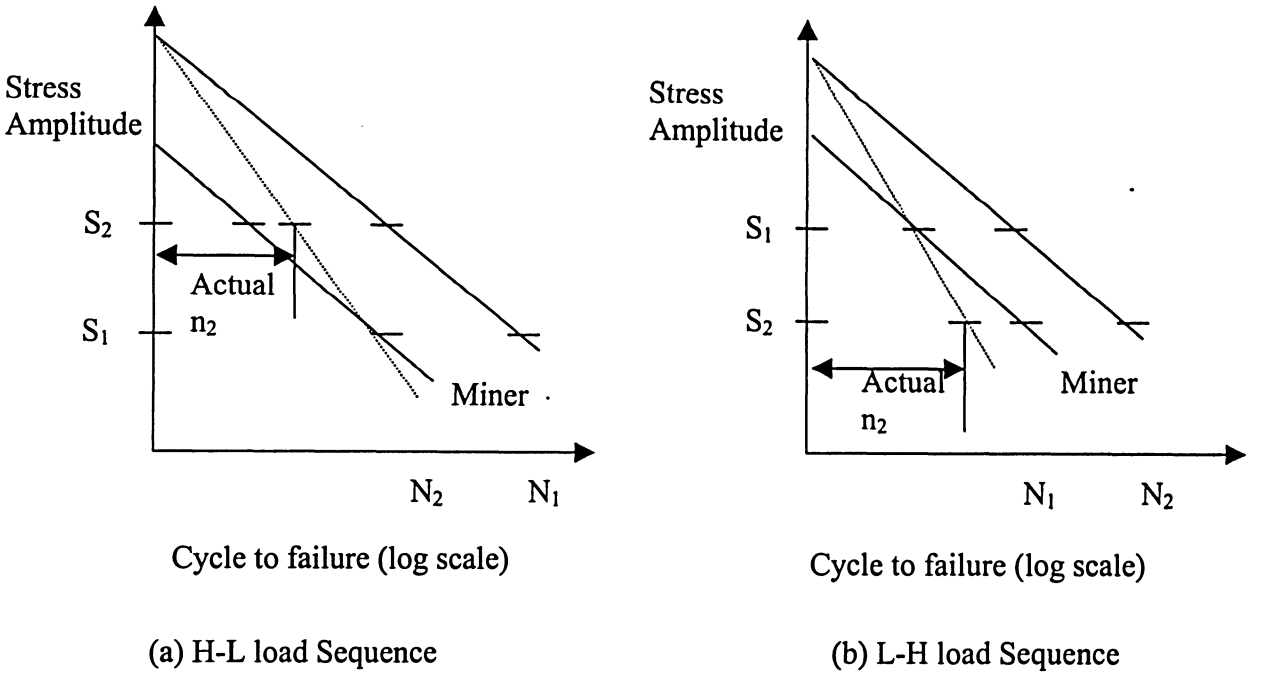

Figure 1.4 Load Interaction Effect [12].

1.2.3.1 Two stage linear damage theories:

The two-stage damage approach improves on the LDR shortcomings, while still retains its simplicity in form. Grover [14] considered cycle ratio for two separate stages in the fatigue damage process of constant amplitude stressing:(i) Damage due to crack initiation $N_1 = \alpha N_f$; and (ii) Damage due to crack propagation $N_{11} = (1+\alpha)N_f$. The term α is the life fraction factor for the initiation stage and N_f is fatigue life in cycles. In two stage linearization approaches, the damage process is divided into two stages of crack initiation and crack propagation and the LDR is applied in each stage. Later, Mason [15] reverted to Grover's work and proposed the double linear damage rule (DLDR). In DLDR, the two stages were separated by equations of $N_1 = N_f - PN_f^{0.6}$ and $N_{11} = PN_f^{0.6}$ where P is a coefficient of the second stage fatigue life.

1.2.4 Life Curve Modification Methods:

1.2.4.1 Damage curve approach (DCA):

This approach was developed to refine DDLR through a reliable physical basis. It is recognized that the major manifestation of damage is crack growth, which involves many complicated processes such as dislocation, agglomeration, sub cell formation, multiple crack formation and independent growth of these cracks until they link and form a dominant crack. Mason and Halford [16] empirically formulated the 'effective crack growth' model that accounts for the effects of these processes. This model is represented as:

$$a = a_0 + (a_f + a_0)\sigma^q \tag{1.6}$$

where a_0, a, a_f are initial (at which r = 0), instantaneous and final (at which r = 1) crack lengths, respectively. The exponent q is defined as $q = BN^{\beta}$ where B and β are two material constants. Damage is then defined as the ratio of instantaneous to final crack length, $D = \frac{a}{a_f}$. In most cases $a_0 = 0$, and the damage function of DCA becomes:

$$D = r^q \tag{1.7}$$

This form is similar to Marco-Starkey theory [7] equation (1.4). Through a series of two level tests, the constant β can be determined from the slope of the regression line of the experimental data. If a reference level, Nr, is selected, the other constant, B, can then be expressed as $N_r^{-\beta}$. Therefore exponent q in equation (1.7) can be written as:

$$q = \left(\frac{N_f}{N_r}\right)^{\beta} \tag{1.8}$$

which is a load level dependent term.

1.2.4.2 Refined double linear damage rule (Refined DLDR):

The original DLDR can be refined by linearization of damage rule curves defined by DCA model. In the refined DLDR, the knee points in a damage vs. cycle ratio (D-r) plot divide the damage process into two phases, and these two phases are determined by using below mentioned equations:

$$D_{knee} = A\left(\frac{N_r}{N_f}\right)^{\alpha_1} \quad And \quad v_{knee} = 1-(1-A)\left(\frac{N_r}{N_f}\right)^{\alpha_1} \tag{1.9}$$

where A and α_1 are two constants determined from regression analysis of the experimental data [16]. The empirical values of these two constants were found to be A = 0.35 and $\alpha_1 = 0.25$ for high strength steel.

1.2.4.3 Double-damage curve approach (DDCA):

This approach is developed by adding a linear term to the DCA equation with some mathematical manipulation and can be presented as:

$$D = \left[(pr)^k + (1-p)^k r^{kq}\right]^{1/k} \tag{1.10}$$

where k is a mathematical exponent to give a close fit to the double linear damage line, and p is a constant measured from the slope of the first damage accumulation line DLDR:

$$P = \frac{D_{knee}}{v_{knee}} = \frac{A\left(\frac{N_r}{N_f}\right)^{\alpha_1}}{1-(1-A)\left(\frac{N_r}{N_f}\right)^{\alpha_1}} \tag{1.11}$$

The DDCA represents a continuous damage curve, which conforms to the DLDR line in the early portion of phase I regime, but blends into DCA curve, which is also close to the DLDR in phase II. To evaluate the effectiveness of the developed DDCA, Mason et al. [17] conducted cumulative damage experiments on the both 316 stainless steel and

Haynes Alloy 188. A comparison of their experimental results with DDCA predictions indicated good agreement. The above models possess similar characteristics. They are all load-level dependent; but do not account for the load interaction effect and small-amplitude cycle damage. Figure 1.5 shows the comparison between three methods.

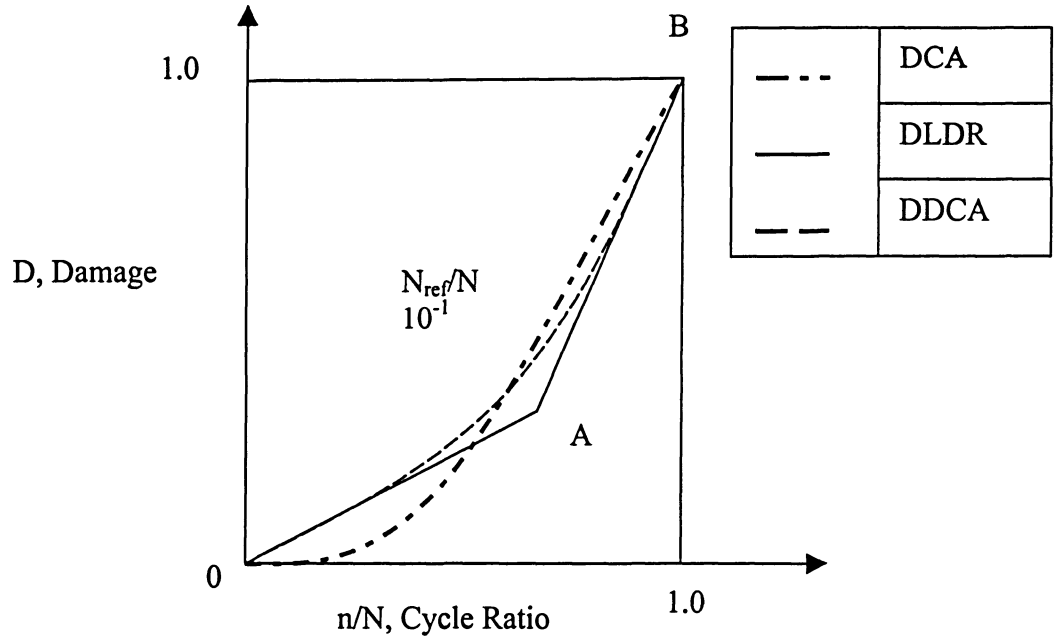

Figure 1.5 Comparison of DDCA with DLCR and DCA [17].

1.2.4.4 Modified version to account for load interaction effect:

To account for load interaction effect, Bui-Quoc[18] developed two approaches to improve the model. One is the fictitious load approach and another is the cycle ratio modification approach. The fictitious load approach was developed only for two-step load cycling. In this approach, there is no modification of the load parameter for first level λ_1. For the second load level; the load parameter λ_2 is replaced by an imaginary strain, therefore λ_2 are called 'fictitious load'. To determine the fictitious value λ_2, parameter Y used in regression analysis as:

$$Y = 1 + \beta_1 \left(\frac{|\Delta\lambda|}{\Delta\lambda^*} \right)^{\beta 2} r_1^{\beta 3} \tag{1.12}$$

where $\beta_1\ \beta_2\ \beta_3$ are determined experimentally; $\Delta\lambda$ is the difference between strain levels $\Delta\lambda = \lambda_2 - \lambda_1$; Y and $\Delta\lambda^*$ are sequence related parameters defined as follows:

for the Low-High increasing steps.

$$Y = \lambda_f^* - \frac{\lambda_2}{\lambda_f^*} - \lambda_2 \text{ and } \Delta\lambda^* = \lambda_f^* - \lambda_1 \tag{1.13}$$

where $\lambda_f^* = \frac{8}{7}\lambda_f$;

and for the High-Low decreasing steps.

$$Y = \lambda_2 - \frac{1}{\lambda_2} - 1, \text{ and } \Delta\lambda^* = \lambda_1 - 1 \tag{1.14}$$

In the cycle ratio modification approach, introducing an exponent in stress/strain version [18] modifies the damage function equation, ν, to the cycle ratio r^{ν} therefore, ν is called a load – interaction parameter. For two-step cycling, ν is related to another parameter, α_1, by empirical equation of:

$$\nu = \left[1 - \left(\frac{|\Delta\lambda|}{\lambda_f - 1}\right)^{\alpha_1}\right]^{\frac{\Delta\lambda}{|\Delta\lambda|}} \tag{1.15}$$

where $\Delta\lambda = \lambda_2 - \lambda_1$. The value of the material constant α_1 is in the range of 0-1. It can be experimentally determined from two-step fatigue test, or empirically estimated by taking $\alpha_1 = 0.5$ as a reasonable approximation.

1.2.5 Theories using the crack growth concept:

The crack growth concepts developed in 1950s and 1960s have been widely accepted. This is due to the fact that damage concept was defined based on cracking response of materials, and the development of technology provided sophisticated tools and techniques in measuring of very small cracks of the order of 1μm.

1.2.5.1 Macro fatigue crack growth model:

A popular macro fatigue crack growth retardation model is the wheeler model [19]. This model assumes the crack growth rate to be related to the interaction of crack-tip plastic zone under residual compressive stresses created by overloads. This model modifies the constant amplitude growth rate equation, $\frac{da}{dN} = [A(\Delta k)^m]$ by empirical retardation factor c_i.

$$\frac{da}{dN} = c_i[A(\Delta k)^m] \text{ Where } c_i = \left(\frac{r_{pi}}{r_{max}}\right)^{p_1} \quad (1.15a)$$

where r_{pi} is the plastic zone size associated with the i^{th} loading cycle, r_{max} is the distance from the current crack tip to the largest prior elastic-plastic zone created by the overload, and p_1 is an empirical shaping parameter depending on material properties and load spectrum. Constants A and m are material constants. A similar retardation model based on the crack tip plasticity is the Willenburg model [16]. This model uses an effective stress intensity factor at the crack tip, (Δk_{eff}), which is caused due to the increased crack tip residual compressive stress induced by the overloads. The reduction in the applied (Δk) is a function of the instantaneous plastic zone size at the i^{th} load cycle and if the maximum plastic zone at the i^{th} load cycle

1.2.5.2 Double exponential law:

For the accumulation of fatigue damage in crack initiation and stage I growth, Miller and Zachariah [21] introduced an exponential relation between the crack length and elapsed life for each phase. The approach is thus termed double exponential law. In this model damage is normalized as $D = \frac{a}{a_f}$, where a and a_f are instantaneous and final crack lengths respectively. Later, Ibrahim and Miller [22] significantly modified this model. Based on the growth mechanism of very small cracks, propagation behavior in stage I was then mathematically described in a manner similar to that expressed by LEFM for stage II growth as:

$$\frac{da}{dN} = \phi(\Delta\gamma_p)^{\alpha_1}\alpha_1 \quad (1.15b)$$

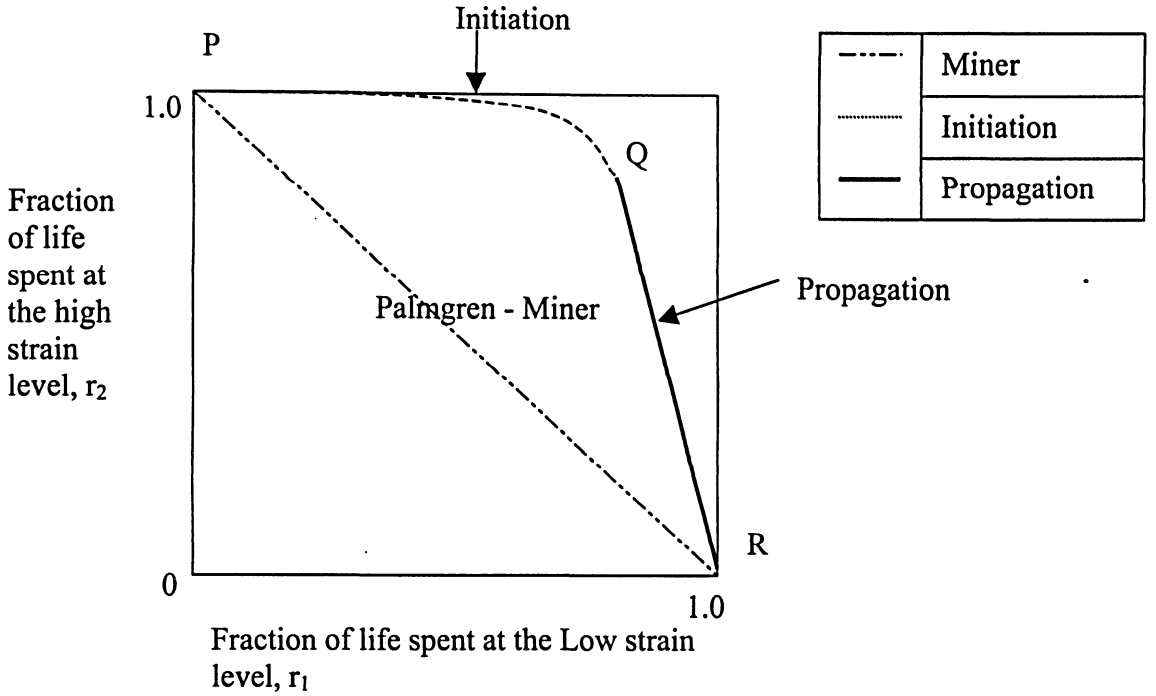

Figure 1.6 Schematic representation of the cumulative damage curve based on the modified Ibrahim-Miller model [22].

where ϕ and α_1 in equation (1.15b) are material constants, and $(\Delta\gamma_p)$ is the plastic shear strain range. From this equation, a linear relationship between the initial cycle ratio, r_1, and the final ratio, r_2, in two level cycling can be found for r_1 in excess of the initiation boundary $r_{I,1} = N_{I,1}/N_{f,1}$. To determine the phase boundary between initiations and stage I propagation, data from a series of two level strain-controlled tests are then collected and plotted in the $r_1 - r_2$ frame. An example of this type of plot and its comparison with linear rule is shown in Figure 1.6. In further study by Miller and Ibrahim, the damage equation for stage I propagation has been described as:

$$D = \frac{a}{a_f} = \left(\frac{a_i}{a_f}\right)^{(1-r)(1-r_1)} \tag{1.16}$$

Where a_i and a_f are initial and final crack length; r and r_1 are initial and final cycle ratio.

1.2.6 Energy Based Damage Theories:

Garud [24] has proposed a new approach to the evaluation of fatigue under complex loading; it relates fatigue life to the plastic work per cycle. The plastic work essentially represents an integrated effect of the two most important quantities generally believed to govern the fatigue process, namely the shear stresses and the plastic strains. The constitutive relations used in his analysis are time-independent and thus the phenomena such as strain-rate sensitivity and creep are excluded. Fatigue life prediction using this approach requires only the uniaxial cyclic stress-strain curve and uniaxial fatigue test results on the smooth specimens. The effect of hydrostatic stress and of mean stress yielding on fatigue life can be included in the analysis when test data are available.

Golos and Ellyin [25] developed a preliminary damage model by using plastic strain energy density as a parameter. Numerous investigations have been carried out to correlate the fatigue life of material with either the strain or stress range. More recently, attempts have been made to relate the fatigue life with plastic strain energy absorbed during a cycle. Ellyin [26] have proposed a special form of the cyclic strain energy density as a damage parameter. This form of the strain energy density combines the plastic strain energy associated with tensile mode, which facilitates crack growth. It is termed the total strain energy density, Δw_t and is shown in Figure 1.7. This theory has a number of desirable features such as being consistent with the notion both low and high-cycle fatigue regimes, and it is related to the mechanical input energy. Theoretically, plastic strain energy absorbed in a complete cycle can be obtained by integrating the area included in a hysteresis. It is, therefore, also referred to as the hysteresis energy and denoted by Δw_p.

It was later found that some inefficiency was associated with plastic strain approach. For example, the effect of mean stress cannot be directly incorporated in the determination of the hysteresis energy. Also, for the low strain-high cycle fatigue, the plastic strain energy density is very small. In some case though the macroscopic (bulk) response of the material is elastic or quasi-elastic, microscopic (local) plastic deformation may still exist in the material due to the non-uniformity of the local strain distribution or due to the

strain concentration by high pre-straining. To overcome these shortcomings, Golos and Ellyin [27] modified the plastic strain energy-based model by using total strain energy density Δw^t. The total strain energy density combines both plastic Δw_p and elastic Δw_e portion. The calculation of total energy range Δw_t is obtained from:

$$\Delta w_t = \Delta w_e + \Delta w_p \tag{1.17}$$

All stress or strain based criteria lack the consideration of the multiaxial stress-strain response of the material as a crucial part of the fatigue process. The fatigue process is generally believed to involve cyclic plastic deformations, which are dependent on the path dependence of the fatigue process sufficiently. The energy concept includes the explicit consideration of the multiaxial stress-strain response. One of the major shortcoming of this approach is, energy is a scalar quantity whereas damage is a vector quantity hence you cannot relate these quantities which is violation of physics.

Lachowicz [28] proposed a method of identification and calculation of components of strain energy density under cyclic and random loading causing elastic-plastic strain in the material. There are some troubles connected with calculation of strain energy density during loading change in the case of random loading by direct integration of the closed and open hysteresis loops.

During schematization of the random loading history, the discrete history of the measured quantity is replaced by set of equivalent range pairs and single ranges. Each distinguished basic or complementary range and each single range is characterized by the amplitude, mean value and time of duration.

Tachankov [29] has developed an incremental approach to estimate the hysteresis energy during the random loading. In his tests, the loading histories included constant amplitude step-up and step-down and random loading with uniformly and Gaussion distribution of stresses. The calculation of dissipated energy under random loading was based on the

von Mises material behavior. He correlated the dissipated hysteresis energy with the fatigue life of type 35 steel specimens. The failure occurred when a critical boundary value for dissipated energy was reached.

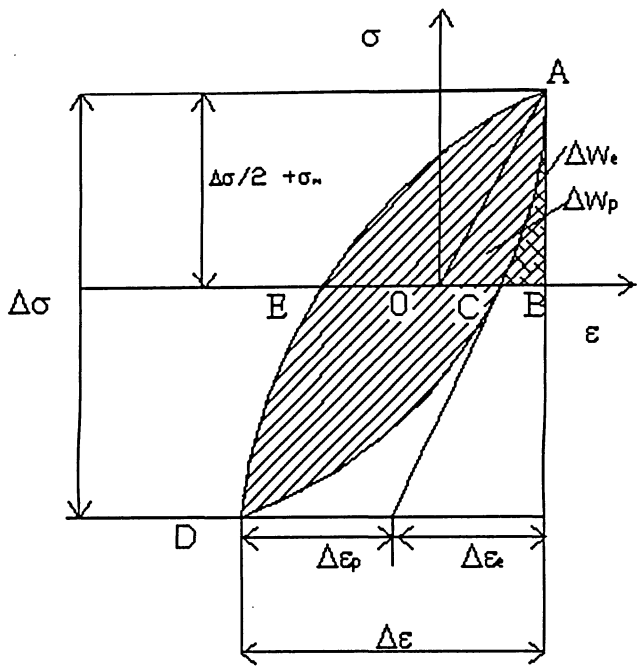

Figure 1.7 Energy Based Approach - Hysteresis Loop [25].

1.2.7 Continuum Damage Mechanics (CDM) Approaches:

This approach is developed based on the original concept of Kachanov and Rabotnov [30] in treating creep damage problems. The success of CDM application in modeling the creep damage process has encouraged many researchers to extend this approach to ductile plastic damage, creep-fatigue interaction, brittle fracture and fatigue damage. Chaboche [31] postulated that fatigue damage evolution per cycle could be generalized by a function of the loading condition under completely reversed strain-controlled condition. By measuring the change in tensile load-carrying capacity and using the effective stress concept, the formulated a nonlinear damage evolution equation as:

$$D = 1 - \left[1 - r^{1/(1-\alpha_c)}\right]^{\frac{1}{(1+\beta_c)}} \tag{1.18}$$

where β_c is a material constant, α_c is a function of the stress state and r is a cycle ratio. This damage model is highly nonlinear and is able to account for the mean stress effect. It is therefore called a nonlinear continuous fatigue damage model. This model has three main advantages. First, it allows for the growth of damage below the initial fatigue limit. Second, the model is able to take into account the influence of initial hardening effect. Third, mean stress effect is directly incorporated in the model. However, since a scalar damage variable is employed and the model is written in its uniaxial form involving the maximum and mean stresses, difficulties will inevitably be present when the model is extended to multiaxial loading conditions.

The CDM-models mentioned were mainly developed for uniaxial fatigue loading. Some difficulties arise when these models are extended to multiaxial loading. To overcome these difficulties chow and Wei [32] have recently attempted a generalized three-dimensional isotropic CDM-model by introducing a damage effect tensor. However, due to complexity of non-proportional multiaxial fatigue problems, a three-dimensional anisotropic CDM model does not yet exist. Though Chaboche great efforts are still needed to obtain an appropriate generalized prediction model for cumulative fatigue damage already proposed the framework.

1.2.8 Critical plane Damage Theories:

Fatigue analysis using the concept of critical plane is very effective because the critical plane concept is based upon the fracture mode or the initiation mechanism of cracks. Brown and Miller [33] defined damage parameter as a combination of maximum shear strain (γ_{max}) and normal strain (ε_n) components on the plane of maximum shear strain:

$$\gamma_{max} + C\varepsilon_n = f(N_f) \tag{1.19}$$

Stulen and Cumming [34] defined damage parameter as combination of normal stress (σ_n) and maximum shear stress (τ_{max}):

$$\tau_{max} + C\sigma_n = f(N_f) \tag{1.20}$$

where C in equation (1.19) and equation (1.20) is a material constant.

Fatemi-Socie [35] came up as combination of maximum strain and maximum normal stress components acting on the critical plane as:

$$\gamma_{max}\left[1+n^{*}\frac{\sigma_n^{max}}{\sigma_y}\right] = f(N_f) \tag{1.21}$$

In equation (1.21), (σ_n^{max}) corresponds to the maximum normal stress acting on the plane of maximum shear strain, (σ_y) is the yield strength of material, and constant n* in Fatemi-Socie parameter unifies shear and tensile fatigue data.

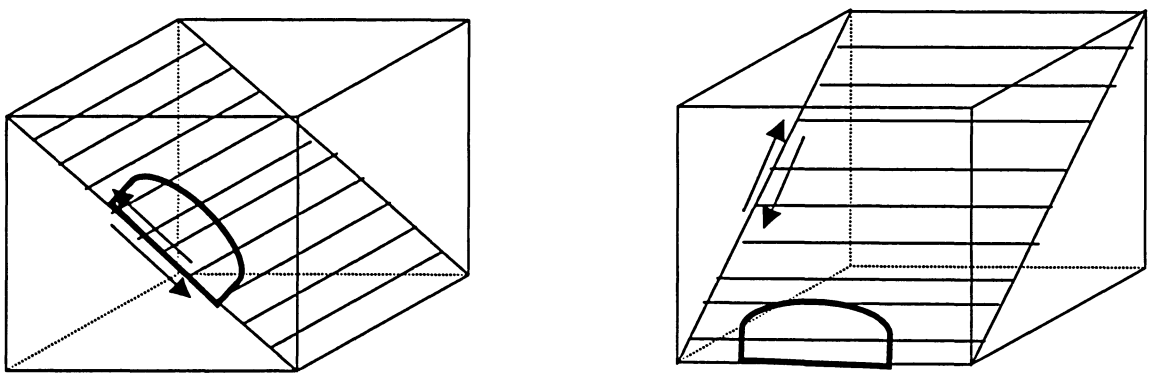

Case A

Case B

Figure 1.8 Schematic presentation of different Critical Planes [33]

The constant is n*= 0.6 for 1045 steel. Most researchers have shown that shear stress is more dominant factor. The different critical planes are shown in the Figure 1.8 to support above-mentioned theory [33].

1.2.9 Energy based-critical plane damage approaches:

Critical plane parameters have been criticized for lack of adherence to rigorous continuum mechanics fundamentals. Some of the below mentioned researchers used the energy criterion in conjunction with the critical plane approach. Energy-critical plane parameters are defined on specific planes and account for states of stress through combinations of the normal and shear strain ranges. These parameters depend upon the choice of the critical plane and the stress and strain ranges acting on that plane. Lagoda, [36] showed a sum of the elastic and plastic strain energy density in the critical plane for description of experimental data obtained from the fatigue test 35NCD16 steel, GGG40 and GG60 cast irons subjected to constant amplitude cyclic tension-compression, torsion and variable-amplitude tension. The parameter of specific work of selected stress on selected strain in the critical plane is an effective parameter, which is used to express the fatigue life of material under a desired loading condition. The critical plane is the plane where the parameter of normal strain energy density reaches its maximum. Lagoda [37,38] also accounted for the stress and stress sign during determination of the energy density allowing one to distinguish the strain energy density at the tension and compression path.

Recently, Varvani [39] has developed a fatigue damage approach. The proposed parameter is sum of the normal energy and shear energy range calculated for critical plane on which the stress and strain Mohr's circles are largest during the loading and unloading part of a cycle. The normal and shear energies used in this parameter are divided by the tensile and shear fatigue properties. The details of this model are discussed in chapter 2.

The present thesis, will further study Varvani's critical plane-energy based damage parameter including several phenomenological factors, such as load dependence, multiple

damage stages, nonlinear damage evolution, load sequence and interaction effects, and small amplitude cycle below fatigue limit for smooth component subjected to uniaxial variable amplitude fatigue loading condition.

CHAPTER TWO

Variable Amplitude Spectrum and Application

Fatigue damage is one of the most frequent causes of breakdown in operation. Hence the problem of reliable estimation of fatigue strength of either material or machine parts continues to be essential, not only in the development of new devices but also in the assessment of the fatigue strength of the original construction. Some of the common practical applications of fatigue failure in real life situations are described in this chapter.

2.1 Aircraft Industry Application:

One of the typical examples for random fatigue loading is the design of wing loading spectrum in airplanes. Everett [41] has carried out studies on design of spectra for simple block sequence of loads in commercial airplanes. The material used for this study was 2024-T3 aluminum sheet taken from a special stock of material at the NASA Langley research center, which has been used for fatigue and fracture studies over several decades. The alloy 2024 has been used in the lower wing skin of many commercial transport aircraft. The material has yield strength of 52 ksi and an ultimate strength of 72 ksi. The fatigue endurance limit of this material is approximately 18ksi and the nominal thickness is 0.090 in. The study consists of five different flight types for random loading. Flight number one is the most severe and occurs only once in 5000 flights. Flight number two occurs 13 times, flight number three occurs 215 times, and flight number four occurs 1067 times, respectively, in the 5000 cycles sequence. Everett has done this study to account for sequence loading effect in commercial transport. The five loading histories were used to find out the life of component. The loading history was also rearranged in increasing order to evaluate for load sequence effect.

2.2 Automobile Industry Application:

All the moving parts in vehicles are subjected to some kind of fatigue loading. Some of the common examples in automobile industry are suspension load, axle load, bracket vibration which are used by society of automotive engineers. Dowling and Wilison [42] has discussed extensive fatigue testing and analysis program conducted by cumulative damage division of fatigue design and evaluation committee. In this program, two steel specimens, Man-ten and RQC-100 are used. The former is hot-rolled steel having yield strength of about 47 ksi, and the latter is rolled, quenched and tempered steel with a yield strength of 120 ksi. Tests were conducted using three vehicle service load histories for suspension, axle and bracket vibration. For each test, loads were repeatedly applied, with several load levels being investigated for each combination of material and load history. The fatigue failure applications is not limited to automobile but is applied to the entire transportation industry.

2.3 Nuclear Power Plant Application:

To study the behavior of fatigue crack in nuclear power plant the expert organization of Fortnum Nuclear Services Ltd. has given the technical assistance for Loviisa [48]. To understand failure and potential failure mechanism of components is the key issue to collect input data. In order to examine the cracks, ultrasonic and eddy current are used. The result and feedback of measured ultrasonic and eddy current examinations have the key role when assessing the properties of cracked components.

2.4 Civil Engineering Application:

Fatigue damage accumulation in steel structures under random loading is a common phenomenon. Agerskov [47] has determined the fatigue life of welded joints by conducting experiments and fracture mechanics analysis. The fatigue tests and the critical plane-energy method have been carried out using load histories, which is realistic in relation to the types of structures studied, i.e. primarily bridges, offshore structures and chimneys. In general, the test series was carried for constant amplitude and variable

amplitude fatigue. Civil structures such as offshore, highway bridges and chimneys are frequently subjected variable amplitude loading spectra.

2.4.1 Offshore Structures:

In the investigations on offshore structures, five different types of load histories have been used. These load histories are generated by computer program and developed at the Department of Structure Engineering and Materials of the Technical University of Denmark [47]. The program simulates a stationary Gaussian stochastic process in real time. Only the extremes of the process are needed, since the load course between consecutive extremes is considered unimportant. In Agerskov's model [47], the next extreme to be generated will be depending only on the present extreme, and not on the preceding load history, i.e. it has a one-step memory. The load histories used in the investigations on the offshore structures are equally in tension and compression and with irregularity factors, I, varying from 0.745 to 0.987. For narrow band loading, the irregularity factor will be close to unity. Typical load histories for fixed offshore structures will be broader banded, with irregularity factors in the range from ~0.6 to 0.8. These are some of the features, which Agerskov's used in study for offshore structures.

2.4.2 Bridges:

2.4.2.1 Steel bridge Deck:

For steel bridge deck, fatigue design curves have traditionally been obtained from constant amplitude tests. This is not a realistic in relation to traffic loading, which is the variable loading or random on the steel bridge decks. The main aim of Agerskov's[47] study was to carry out test series and analytical investigations for the difference between the fatigue lives under variable amplitude and constant amplitude loading. The variable amplitude loading that is used in the fatigue tests of this investigation has been determined from the strain gauge measurements on the orthotropic steel deck structure of the Faro Bridge in Denmark. Strain gauge measurements were carried out at 10 different locations in the orthotropic deck. The measurement area is placed at a distance of approximately 8m from the simple support of the bridge girder on the nearest bridge pier. The length of the bridge spans was approximately 80m. This location of the strain gauges

means that only local bending effect in the deck structure will be registered, whereas the stresses due to global bending in the bridge girder will be negligible. The 10 strain gauges are placed in two sections between two transverse diaphragms. One of these sections is in the middle of the longitudinal stiffener span, which has a length of 4m, and the other section is placed at a distance of 0.5m from one of the transverse diaphragms. Four of the strain gauges in each section are placed on the bottom of trapezoidal longitudinal stiffener of the deck plate. The fifth gage in each section is placed on the butt weld between the trapezoidal stiffener and the deck plate. In this way variable realistic loading data are compared with constant amplitude data used in other early studies [47].

2.4.2.2 Concrete Bridge:

Many concrete structures such as bridges have experienced fatigue cracks under long cyclic loadings caused by trucks etc. The crack strongly affects the normal use and durability of the structure. Analysis reveals that unreasonable fatigue strength and unreasonable design rule are main reasons [48]. Nowadays, because of the limitation of experimental methods, structures are wholly designed by uniaxial fatigue strength or uniaxial compression fatigue strength under constant amplitude loading. Practice proved that the result is conservative or dangerous. Song [48] has carried out some experiments on uniaxial tensile strength and uniaxial compression strength of plain concrete under constant amplitude cyclic loading. Studies in this area have been carried out by other researches on biaxial compression strength under constant amplitude or variable-amplitude loading, but the experiment and analysis on biaxial tension-compression strength have not been done yet. Analysis proved that Miner's Rule is not wholly suitable to the fatigue crack of concrete material. So there is need for more suitable model, which works for uniaxial and biaxial fatigue loading condition.

2.4.3 Chimneys:

The variable amplitude loading that was used in the investigation of a chimney has been determined from wind tunnel tests. An undamped chimney model, subject to transverse oscillations was studied [47]. Two load histories were used, both determined from the

strain gauge measurements on the model. These load histories are equal in tension and compression and narrow-banded, with an irregularity factor of $I = 0.998$.

2.4.4 Pile Supported Structures:

It is common that piles and pile-supported structures are subjected to cyclic loading. For example, offshore structure (such as ocean petroleum platform) with pile foundation subjected is to cyclic wave loading. Many researchers [48] have worked to accurately predict static and dynamic soil-pile-superstructure response through various numerical analyses. Only the static/constant loading tests are carried out because of a limited series of field and complexity of tests. For piles of ocean petroleum platform, another problem is seawater-pile interaction. The Seawater-pile interaction is commonly considered using water-damping method. It goes under continues cyclic loading due to waves in seawater.

2.4.5 Ice and Offshore Structures:

The moving ice induces offshore structures strong vibrations. In order to evaluate fatigue life of the structure under ice force, it necessary to estimate the distribution of ice thickness, ice velocity as well as impacting frequency at least one year. This needs sea ice observation and simulation in long term. Systematic sea ice observations have been conducted in Bohai Bay of China and large amount of data has been accumulated. Short term ice simulation in small-scale has been carried. Some calculation parameters and the viscous-plastic constitutive laws of the ice are modified [48].

CHAPTER THREE

Fatigue Damage Analysis and Modeling

3.1 Introduction:

Reliable estimate of fatigue life at every stage in the construction of a structure is necessary because it is operationally difficult, uneconomic and time-consuming to test each component or the entire structure experimentally in the laboratory or directly during operation. The results of useful life estimation are not always satisfactory. This is due to the fact that none hypothesis is sufficiently general to consider the effects of all the interacting factors in fatigue life evaluation. Most service loading histories have variable amplitudes and can be quite complex. Several methods have been developed to deal with variable amplitude loading using the baseline data generated from constant amplitude tests.

The total fatigue life of a component may be divided into two different regimes: crack initiation and crack propagation. A general mechanism for crack initiation is based on coarse slip processes. Coarse slip occurs on the favorably oriented crystallographic planes with single grains of material. Cyclic loading causes reversed slip and the formation of persistent slip bands. Materials displaced in local regions forming intrusion, extrusions and ultimately de-cohesion occurs, forming a microcrack. The applied shear stress and resulting shear strains are the dominant parameters for this initiation process. The definition of the crack initiation is usually taken as the formation of an "engineering size" crack (usually between 0.1 to 5 μm in surface length). The analysis developed in this chapter deals with fatigue damage assessment of engineering component subjected to constant and variable amplitude uniaxial loading conditions based on Varvani's energy based-critical plane approach [39]. According to this approach, the proposed parameter is

sum of the normal energy and shear energy range calculated for critical plane on which the stress and strain Mohr's circles are largest during the loading and unloading part of a cycle. The normal and shear energies used in this parameter are divided by the tensile and shear fatigue properties.

3.2 Elements of Fatigue Damage Assessment based on Varvani's Approach [38]:

Figure 3.1 presents a thin walled tubular specimen subjected to combined axial and torsional fatigue. The tensorial stress and strain components for an infinitesimal element on the tube can be presented by:

$$\Delta\varepsilon_{ij} = \begin{pmatrix} -\nu_{eff}\Delta\varepsilon_{ap} & \Delta\left(\frac{\gamma_{ap}}{2}\right) & 0 \\ \Delta\left(\frac{\gamma_{ap}}{2}\right) & \Delta\varepsilon_{ap} & 0 \\ 0 & 0 & -\nu_{eff}\Delta\varepsilon_{ap} \end{pmatrix} \tag{3.1}$$

$$\Delta\sigma_{ij} = \begin{pmatrix} 0 & \Delta\tau_a & 0 \\ \Delta\tau_a & \Delta\sigma_a & 0 \\ 0 & 0 & 0 \end{pmatrix} \tag{3.2}$$

where axial and shear strain ranges $\Delta\varepsilon_n$ and $\Delta\left(\frac{\gamma_{max}}{2}\right)$ respectively are given by the following equations:

$$\Delta\varepsilon_{ap} = \Delta\varepsilon_a \sin\theta \tag{3.3}$$

$$\Delta\left(\frac{\gamma_{ap}}{2}\right) = \Delta\left(\frac{\gamma_a}{2}\right)\sin(\theta - \phi) \tag{3.4}$$

where ε_{ap} and $\frac{\gamma_{ap}}{2}$ are the applied axial and shear amplitude strains, respectively. The angle θ is the angle during a cycle of straining at which the Mohr's circle is the largest and has the maximum value of shear strain. Angle ϕ corresponds to the phase delay between strains on the axial and torsional axes. In equation (3.2) $\Delta\sigma_a$ and $\Delta\tau_a$ are the ranges of axial and shear stresses, respectively.

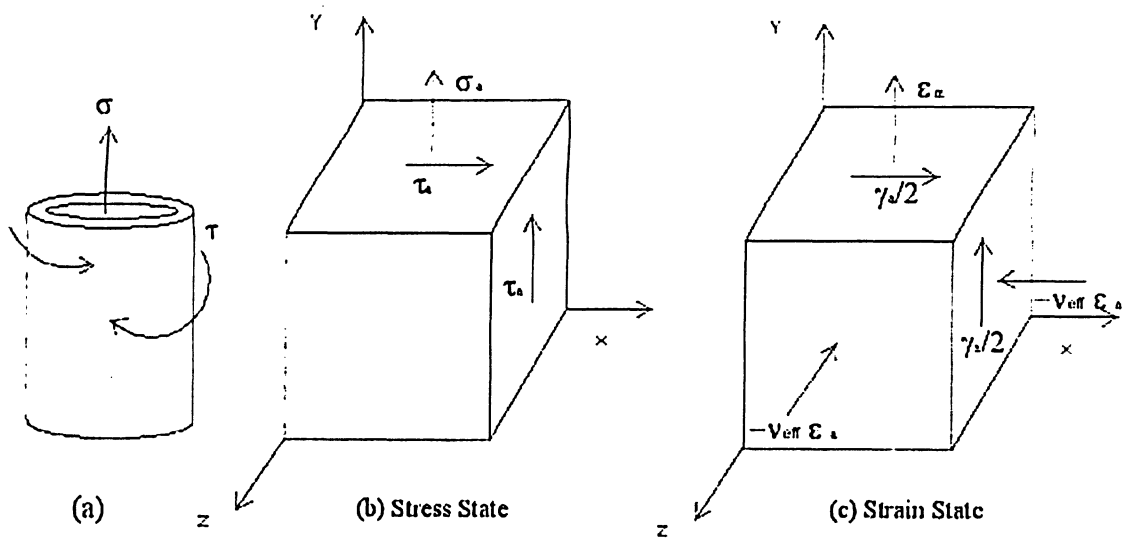

Figure 3.1 3D presentation of stress and strain state for multiaxial loading [38].

Principal strain values $\varepsilon_1, \varepsilon_2, \varepsilon_3$ $(\varepsilon_1 > \varepsilon_2 > \varepsilon_3)$ are given as:

$$\varepsilon_1 = (1-\nu_{eff})\frac{\varepsilon_{app}}{2} + 1/2\left[\varepsilon_{ap}{}^2(1+\nu_{eff})^2 + (\frac{\gamma_{ap}}{2})^2\right]^{1/2} \tag{3.5}$$

$$\varepsilon_2 = -\nu_{eff}\varepsilon_{ap} \tag{3.6}$$

$$\varepsilon_3 = (1-\nu_{eff})\frac{\varepsilon_{app}}{2} - 1/2\left[\varepsilon_{ap}{}^2(1+\nu_{eff})^2 + (\frac{\gamma_{ap}}{2})^2\right]^{1/2} \tag{3.7}$$

Where ε_{ap} is applied axial strain, γ_{ap} is applied shear strain and ν_{eff} is the effective Poisson's ratio, which is given by:

$$\nu_{eff} = \frac{\nu_e \varepsilon_e + \nu_p \varepsilon_p}{\varepsilon_e + \varepsilon_p} \quad (3.8) .$$

Where $\nu_e = 0.3$ is the elastic Poisson's ratio and $\nu_p = 0.5$ is the plastic Poisson's ratio. The unknown axial elastic and plastic strain are calculated, respectively:

$$\varepsilon_e = \frac{\sigma_a}{E} \quad (3.9)$$

$$\varepsilon_p = \varepsilon_{ay} - \frac{\sigma_a}{E} \quad (3.10)$$

Where ε_e is axial elastic strain, ε_p is axial plastic strain, ε_{ay} is axial total strain along Y-axis, E is Modulus of elasticity, σ_a is axial total stress. The range of maximum shear strain $\Delta\left(\frac{\gamma_{max}}{2}\right)$ and the corresponding normal strain range ($\Delta\varepsilon_n$) on the critical plane at which both strain and stress Mohr's circles are the largest during loading (at the angle θ_1) and unloading (at the angle θ_2) of a cycle (see Figure 3.2) are calculate as:

$$\Delta\left(\frac{\gamma_{max}}{2}\right) = \left(\frac{\varepsilon_1 - \varepsilon_3}{2}\right)_{\theta_1} - \left(\frac{\varepsilon_1 - \varepsilon_3}{2}\right)_{\theta 2} \quad (3.11)$$

$$\Delta(\varepsilon_n)=\left(\frac{\varepsilon_1+\varepsilon_3}{2}\right)_{\theta_1}-\left(\frac{\varepsilon_1+\varepsilon_3}{2}\right)_{\theta 2} \tag{3.12}$$

Similarly, the range of maximum shear stress ($\Delta\tau_{max}$) and the corresponding normal stress range ($\Delta\sigma_n$) are calculated from the largest stress Mohr's circle during loading (at the angle θ_1) and unloading (at the angle θ_2) of a cycle are calculate as shown in Figure 3.2:

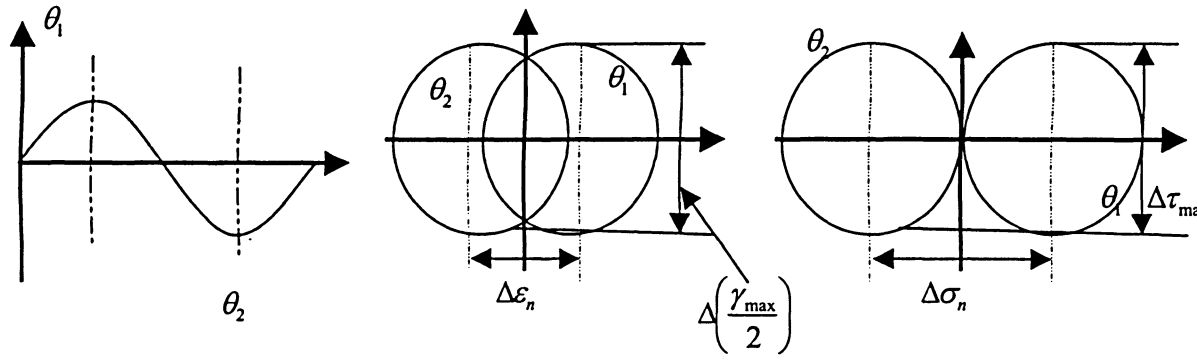

(a) Strain History (b) Strain Mohr's Circle (c) Stress Mohr's Circle

Figure 3.2 Strain history, strain Mohr's circle, and stress Mohr's circle for uniaxial loading condition [38].

$$\Delta\tau_{max}=\left[\frac{\sigma_1-\sigma_3}{2}\right]_{\theta 1}-\left[\frac{\sigma_1-\sigma_3}{2}\right]_{\theta 2} \tag{3.13}$$

$$\Delta\sigma_n=\left[\frac{\sigma_1+\sigma_3}{2}\right]_{\theta 1}-\left[\frac{\sigma_1+\sigma_3}{2}\right]_{\theta 2} \tag{3.14}$$

where $\sigma_1,\sigma_2,\sigma_3$ are the principal stress values ($\sigma_1>\sigma_2>\sigma_3$) and are calculated as:

$$\sigma_1 = \frac{\sigma_a}{2} + 1/2\left[\sigma_a{}^2 + 4\tau_a{}^2\right]^{1/2} \tag{3.15}$$

$$\sigma_2 = 0 \qquad \text{(Plane stress condition)} \tag{3.16}$$

$$\sigma_3 = \frac{\sigma_a}{2} - 1/2\left[\sigma_a{}^2 + 4\tau_a{}^2\right]^{1/2} \tag{3.17}$$

The range of maximum shear stress $\Delta\tau_{max}$ and shear strain $\Delta\left(\frac{\gamma_{max}}{2}\right)$ obtained from the largest stress and strain Mohr's circles during the loading and unloading parts of a cycle and the corresponding normal stress range $\Delta\sigma_n$ and normal strain range $\Delta\varepsilon_n$ on that plane are the components of the Varvani's approach. In this approach both the normal and shear strain energies were weighted by the axial and shear fatigue properties, respectively.

$$\frac{1}{\sigma_f'\varepsilon_f'}\Delta\sigma_n\Delta\varepsilon_n + \frac{1}{\tau_f'\gamma_f'}\Delta\tau_{max}\Delta\left(\frac{\gamma_{max}}{2}\right) = f(N_f) \tag{3.18}$$

Considering the effect of axial mean stress, a mean stress correction factor of the form $(1+\sigma_n{}^m/\sigma_f')$ in equation (3.19) was employed, and the damage equation with mean stress effect yielded as:

$$\frac{1}{\sigma_f'\varepsilon_f'}\Delta\sigma_n\Delta\varepsilon_n + \frac{\left(1+\frac{\sigma_n{}^m}{\sigma_f'}\right)}{\tau_f'\gamma_f'}\Delta\tau_{max}\Delta\left(\frac{\gamma_{max}}{2}\right) = f(N_f) \tag{3.19}$$

Where the normal mean stress $\sigma_n{}^m$ acting on the critical plane is given by:

$$\sigma_n{}^m = \frac{1}{2}(\sigma_n{}^{max} + \sigma_n{}^{min}) \tag{3.20}$$

In equation (3.20), σ_n^{max} and σ_n^{min} are the maximum and minimum normal stresses which are calculated from the stress Mohr's circles. In fatigue damage assessment under variable amplitude loading condition, the effects of following phenomenological factors are studied:

3.3 Sequence loading.

3.4 Memory effect.

3.5 Small cycles.

A schematic view of the model and damage analysis is shown in Figure 3.3, which shows the detail steps involved in the life prediction presented in this study.

3.3 Effect of sequence loading:

3.3.1 Background:

The order in which cycles are applied has a significant effect in random loading. Due to sequence effect these strain-time histories will yield a very different stress-strain response. According to Kliman [40] under a given amplitude frequency in a loading block, the effect of the loading history can be seen in the different values of the energy to fracture and its dependence on the arrangement of the amplitude. This means that the arrangement of amplitudes in the loading block will significantly influence the energy for blocks with a large number of amplitudes and levels. Golos and Ellyin [25] examined the cumulative damage and the effect of loading sequence. Tests were performed with two, three and four stage loading. A schematic diagram of block loading is as shown in the Figure 3.4.

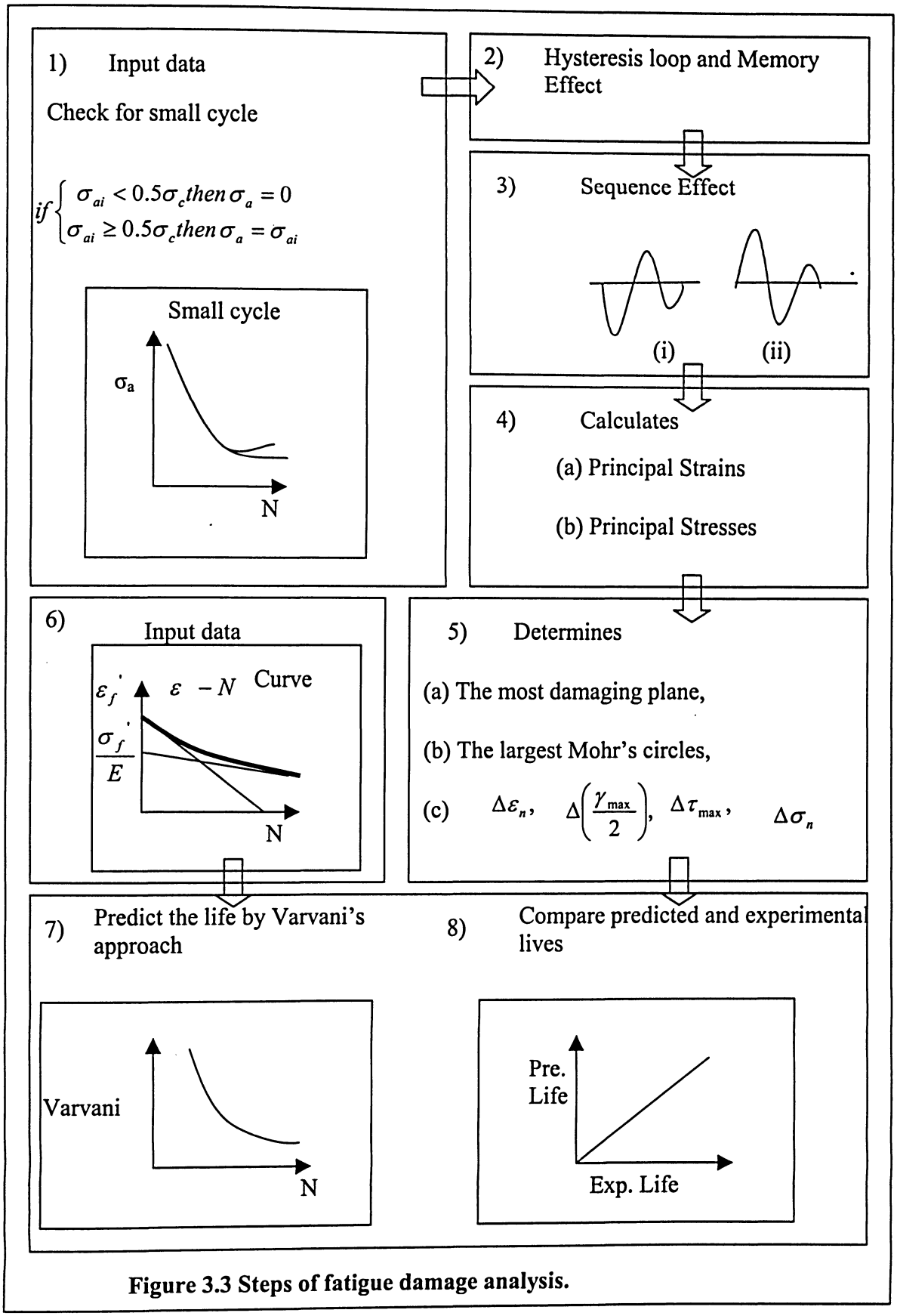

Figure 3.3 Steps of fatigue damage analysis.

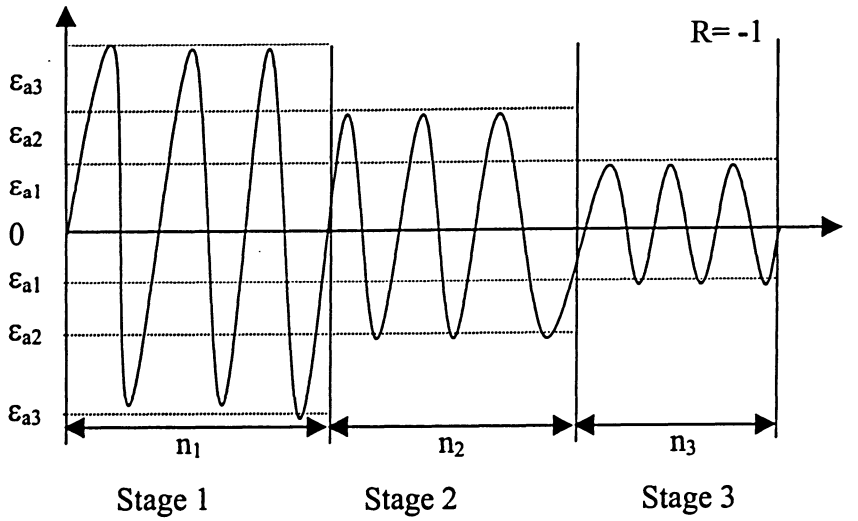

Figure 3.4 A schematic diagram of block/step loading condition [25].

These tests show that changing the loading sequence significantly influences the energies obtained from different loading stages. Hence loading sequence has a significant relationship with damage magnitude.

Everett [41] has done studies to evaluate the loading sequence effects that could exist in commercial fixed-wing fatigue loading spectra. To evaluate this effect, a typical commercial wing spectrum was re-arranged from the smallest load range until the largest load range. Tests on open hole test specimens made of 2024-T3 aluminum alloys were conducted on the normal sequence loading as well as on re-arranged loading. sequence. The test results showed no significant difference between the fatigue lives of normal loading sequence and rearranged loading sequence.

3.3.2 Description:

The above discussed sequence effect can be explained with the help of Figure 3.5. The Case 1, Figure 3.5a starts with initial tensile overload followed by a compressive overload and then normal loading condition. The Case 2, Figure 3.5b consists of initial compressive overload followed by a tensile overload and then normal loading condition.

If Cases 1 and 2 are compared, then it is noticed that the only difference between Figures 3.5(a) and (b) is sequence of stresses applied. In Case 1, the hysteresis loops start with stress value 540 MPa and then followed by another positive stress value as 340 MPa, but in Case 2 loop start with stress value 340 MPa and followed by another positive stress value of 540 MPa. Therefore, in both cases the total stress value remains same and according to Miner's rule as discussed in section 1.1, the strain response should be the same for both above cases. However, when actual strain response is checked, it is found that strains are entirely different.

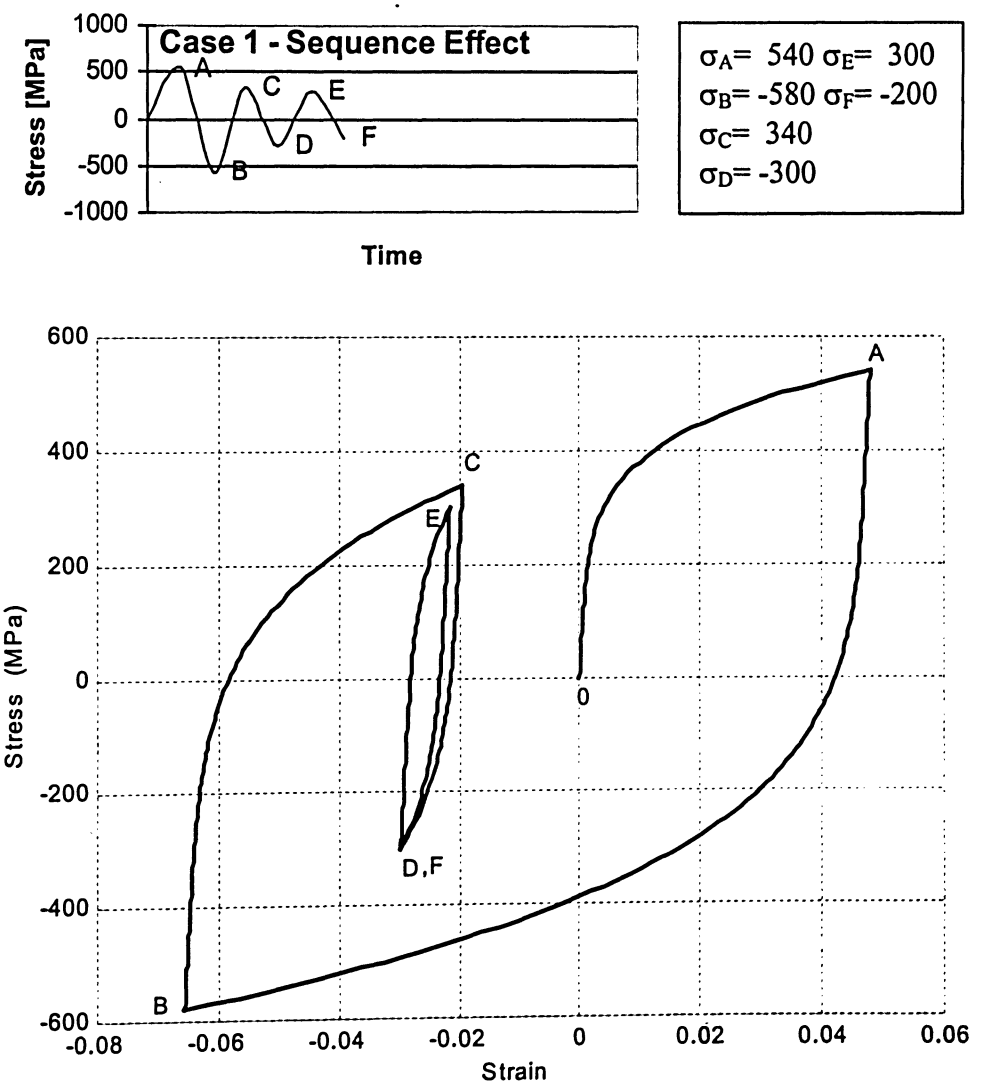

(a) Case 1

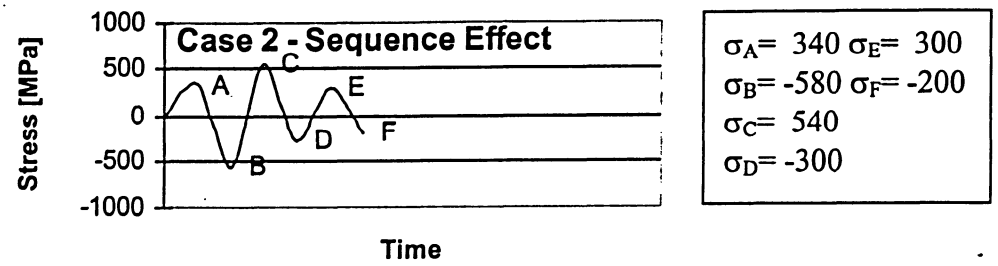

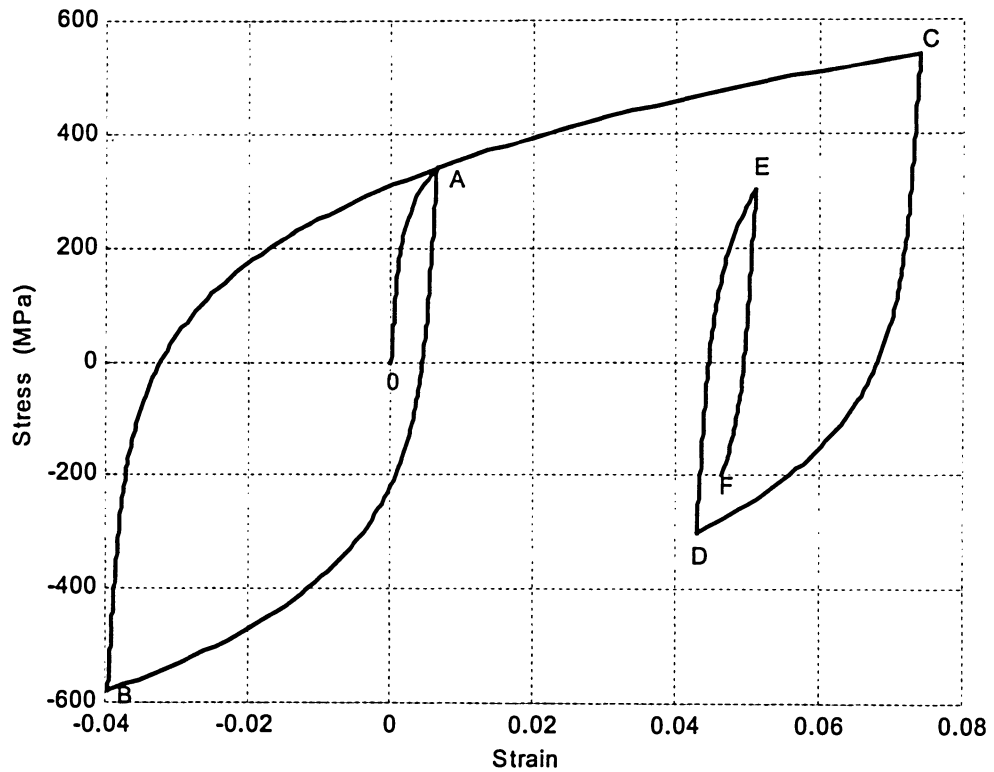

(b) Case 2

Figure 3.5 Schematic Representation of Sequence Effect.

For Case 1 strain value at D is -0.01 and for Case 2 strain value at D is 0.0125. This shows that sequence effect studied above results in different material damage and deformation, which has to be considered for variable amplitude loading conditions.

3.3.3 Implementation:

In order to incorporate above effect, the equations (3.21 - 3.23) are used. Referring to Figure 3.5, the first 0-A portion of curve is developed by general Ramberg-Osgood equation (3.21) with instantaneous stress values σ_i, strain for 0-A is calculated with Ramberg-Osgood equation as:

$$\varepsilon_1 or \varepsilon_A = \left(\frac{\sigma_i}{E}\right) + \left(\frac{\sigma_i}{K}\right)^{1/n_1} \tag{3.21}$$

Where E is Modulus of elasticity, K is cyclic strength coefficient, and n_1 is cyclic hardening exponent. From all the possible strain values maximum strain value obtained from the equation (3.21) is used to calculate principal strains for 0-A portion of curve Principal strains and principal stress, effective Poisson's ratio, elastic strain and plastic strain are calculated using maximum strain value obtained from equation (3.21). The previously calculated maximum strain ε_1 at point A is then used in equation (3.22) to calculate minimum strain for A-B portion, the principal strain and principal stress are calculated for A-B portion of the hysteresis loops. Once two set of principal stresses and strains are available then maximum shear strain range and normal strain range are calculated from these principal strains and principal stresses. After calculating normal and shear ranges the damage is calculated and stored in one variable. Strain ε_2 is calculated for unloading part of cycle (A-B) using Ramberg-Osgood equation as:

$$\varepsilon_2 or \varepsilon_B = \varepsilon_A - \left[\left(\sigma_A - \frac{\sigma_i}{E}\right) - 2\left(\sigma_A - \frac{\sigma_i}{2k}\right)^{1/n}\right] \tag{3.22}$$

The B-C portion of curve (reloading part) is developed by increasing Ramberg-Osgood equation (3.23), which is developed in the similar manner like 0-A portion except it uses previously calculated minimum strain ε_2 (3.22) as the starting point. Then plastic strain, elastic strain, passions ratio, principal strain and principal stress are accordingly

calculated. For reloading portion of cyclic stress-strain loop (B-C portion), ε_3 is calculated using Ramberg-Osgood equation as:

$$\varepsilon_3 or \varepsilon_c = \left[\left(-\sigma_B + \frac{\sigma_i}{E}\right) + 2\left(-\sigma_B + \frac{\sigma_i}{2k}\right)^{1/n}\right] + \varepsilon_B \qquad (3.23)$$

Where, ε_B is minimum strain at point B, σ_B is minimum stress at point B. The fourth C-D portion of curve is calculated using Ramberg-Osgood equation and follows the same unloading Ramberg-Osgood equation as calculated for A-B portion. This chain of loading (equation (3.22)) and reloading (equation (3.23)) will continue till the failure of component occurs. Thus, the sequence effect is incorporated in model through the latest value of strain calculated from equations (3.21 -3.23), and thereafter using them in the next equation. The above mentioned equation also takes care of overload and underload histories because sequence effect uses the last damage quantity in the calculation.

In same regards Macha [36] has introduced sign effect, which is supportive to the above discussion. It is noticed that the negative and positive signs are provided in the bracket, in such a way that the values will always remain positive inside the bracket. In case of loading, the value will be added and in case of unloading, the value will be deducted. The negative value outside the bracket takes care of negative sign (during the unloading cycle). Hence, in sequence effect unloading and reloading (Ramberg-Osgood) equations, the sign effect proposed by Macha was already incorporated as a built-in feature.

3.4 Memory Effect:

3.4.1 Background:

Dowling and Wilson [42] characterized the memory effect by two rules:

(a) According to Figure 3.6, when the strain next reaches a value (D' in Figure 3.6) at which the direction of straining was previously reversed, a stress - strain hysteresis loop

is closed, and the stress- strain path beyond this point is the same as if the direction of straining had not been removed.

(b) Once a strain excursion forms a closed loop, this excursion does not affect the subsequent behavior. The above two rules for the memory effect may be used to estimate the entire stress-strain response for any repeating strain history. The repeating history should be considered to begin and end at most extreme strain peak in either directions. The co-ordinates of this most extreme and first peak may then be estimated by assuming that from zero stress and strain the stress- strain path follows the cyclic stress-strain curve.

3.4.2 Description:

The above stated rule can be explained by figure 3.6. Looking at this figure it is noticed that an initially maximum stress value of 600 MPa is attained by the hysteresis loop at point A, then minimum stress value of –600 MPa at point B, again a maximum value of 600 MPa at point C. However at point D stress value goes up to –300 MPa and raises to a positive stress value of 300 MPa, thereafter it goes to minimum value of –600. As it can be seen, DED' forms a small close loop inside a big loop, and once the small loop is constructed it follows the bigger loop path as if the direction of straining was never changed. If the hysteresis loop is plotted according to the sequence effect, the latest stress/strain value will not form a closed loop. Hence, memory effect concept has been carefully monitored and programmed to correspond to the closed hyestersis loop.

3.4.3 Implementation:

The above mentioned memory concept is used to develop the close hysteresis loop for random and variable loading. In order to close the loop, the developed computer program should be capable of knowing the limits (i.e. maximum and minimum values are stored from the input data), and these maximum and minimum values are used as restricted boundaries for the loop generated by interpolating σ_i values in equations (3.21-3.23), which gives respective ε_i values. As the above-mentioned sequence effect is implemented in the program the values generated are not strain controlled. Therefore, Memory effect

concept has been carefully monitored and programmed to correspond to the closed hysteresis loop in each block loading history.

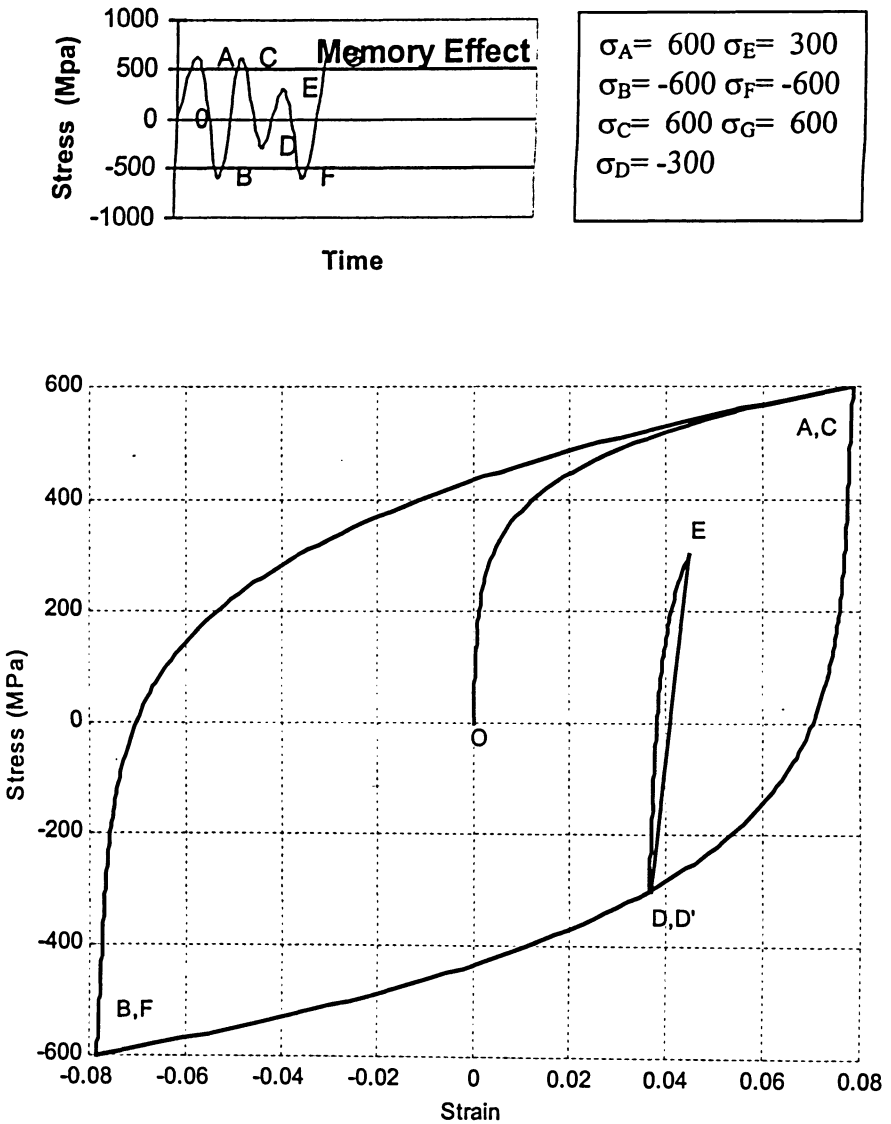

Figure 3.6 Schematic Representation of Memory Effect.

3.5 Effect due to small cycles below endurance limit:

3.5.1 Background:

The Palgrim-Miner hypothesis does not take into account the effect of amplitude below the fatigue limit. The suggested hypothesis is valid provided; the value of maximum stress amplitude (σ_a) is not below the fatigue limit (σ_c). Kilman [40] calculated the effect of amplitude below the fatigue limit and above the fatigue limit. At high stresses (where there are no instantaneous stress amplitude σ_{ai} less than σ_c in the loading block) the curve are identical. As the stress decreases (i.e. with an increasing number of amplitude σ_{ai} less than σ_c in the loading block), the inclusion of the σ_{ai} amplitude in the calculation leads to shorter lives. Pompetzki and Topper [43] conducted extensive studies on overload (OL) and underload (UL) fatigue loading. They demonstrated that when tensile, compressive or single cycle OL's were inserted periodically within a small cycle below the fatigue endurance limit, the small-stress cycles following those events contribute significantly damage accumulation. Pompetzki and Topper assumed that when an OL/UL was applied periodically in an otherwise small-stress cycle background, that event worked to reduce the crack closure stress and hence enhanced the effective crack driving force. This would persist until the OL/UL effect was diminished and steady state condition was resumed, whereas if the small-stress cycle would instead, be intermittently added into an otherwise larger regular loading pattern. In this case, the larger cycle would not represent OLs but rather they could be regarded as service loads whereas the small-stress cycles would constitute minor loads caused by machine vibration, or other low amplitude external loads.

Ngiau [44] showed the damage contribution from small amplitude cycles in both LCF and HCF regimes for 2024-T351aluminum. Block loads that contain intermittent small-stress amplitude cycle are applied to the regular LCF or HCF loading scheme using two patterns: block to constant (B-C) or constant to block (C-B), i.e. where the blocks precede or follow the regular constant amplitude cycles, respectively. These two patterns are chosen in order to study the contribution of small-stress amplitude cycles in both crack initiation and propagation life. In general, the small stress cycles would affect the initiation life more than the propagation life in the B-C sequence, while the opposite

effect might prevail in the C-B sequence. He showed that having intermittent small cycles with amplitude as low as 50% the endurance limit with regular low cycle fatigue (LCF) or high cycle fatigue (HCF) service loading conditions can indeed be very damaging for both initiation and propagation life. In his study, he has compared damage between 100% endurance to 50% endurance limit for HCF and LCF. He found that even 50% of fatigue limit cycles are also creating significant damage. From above study, it is noted that small cycle up to 50% of fatigue limit are damaging.

3.5.2 Description:

The above discussed effect can be explained from Figure 3.7. This figure shows the relation between stress value with number of cycles to failure. Curve A (A-B) consist of stress values above the endurance limit (it means that value below fatigue limit are neglected) and Curve B (A-C) consists of values above and below the fatigue limit. It is observed that the Curve A has longer life than Curve B; hence it implies that Curve B has something in addition to Curve A that has significant effect on life of component. Another part of the study is how much percentage of stress below the fatigue limit is damaging and whether the intensity of that stress below and above fatigue limit is same or not. From the above references, it was found that 50% of fatigue limit is significantly damaging the life of component, and the intensity is definitely dependent on stress and strain amplitudes. If the amplitude is more then damage will be more, hence the cycles below the fatigue limit are damaging but not in the same amount as damage caused by cycles above the fatigue limit.

3.5.3 Implementation:

In order to implement the above effect, it is important to identify a limit below which the stresses do not have significant damaging effect. It is found that cycles below 50% fatigue limit do not effect significantly. Keeping this point in mind, an equation is developed to implement the above effect:

$$if \begin{cases} \sigma_{ai} < 0.5\sigma_c \; then \;\; \sigma_a = 0 \\ \sigma_{ai} \geq 0.5\sigma_c \; then \;\; \sigma_a = \sigma_{ai} \end{cases} \tag{3.24}$$

Here σ_{ai} is instantaneous stress amplitude, σ_a is stress amplitude and σ_c is endurance limit or fatigue limit. This equation explains that if the stress value is above 50% of endurance limit then instantaneous value will be considered as stress amplitude otherwise if the stress value is below 50% of fatigue limit the value becomes zero. In the same regards, Figures (3.81-3.84) prove that the model is working as per equation (3.24). In Figure 3.8 stresses above the fatigue limit are taken and corresponding number of cycles are obtained for constant as well as variable amplitude loading. Similarly stresses at fatigue limit, stresses at 50% of fatigue limit, and stresses at 20% of fatigue are shown in Figures 3.8 to 3.11. Hence the effect of cycles below 50% fatigue limit on damage accumulation is negligible.

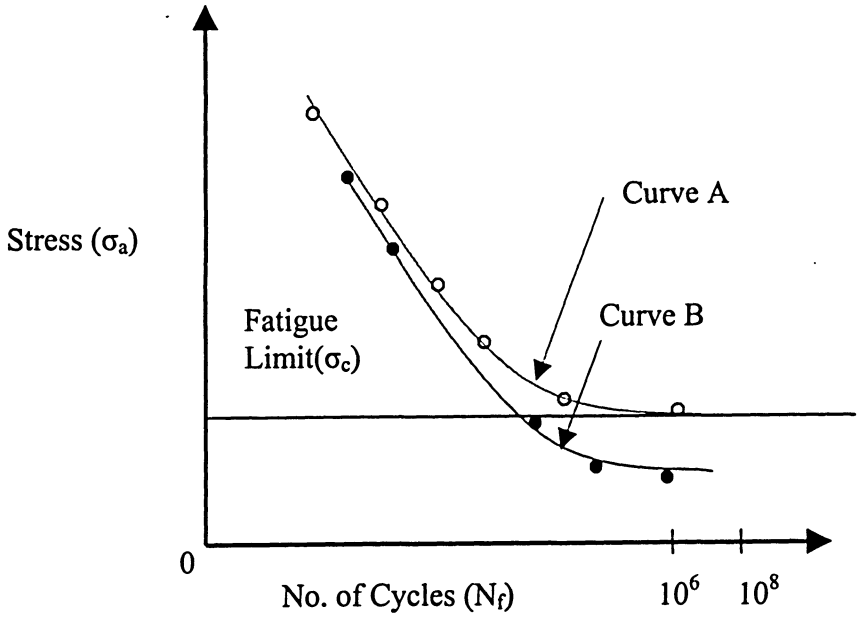

Figure 3.7 Effect of small cycles below fatigue limit [44].

All the above-mentioned phenomenological factors are incorporated in the new proposed model using a computer algorithm developed in this study. The details about computer algorithm are explained in the next chapter.

a) Constant amplitude loading:

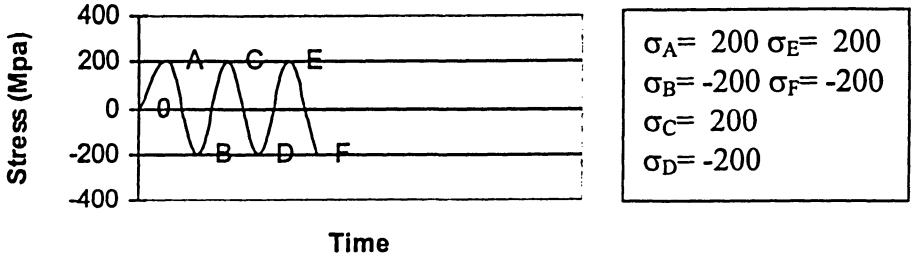

The Number of Cycles required for above stress history: 148000.

b) Variable amplitude loading:

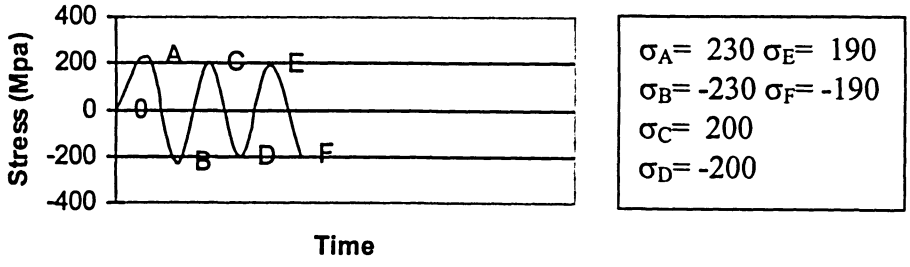

The Number of Cycles required for above stress history: 148000.

Figure 3.8 Stress value above endurance limit (175MPa).

a) Constant amplitude loading:

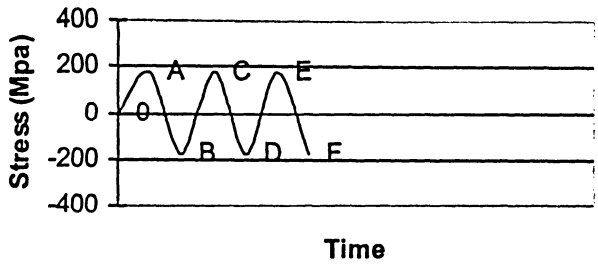

σ_A= 175 σ_E= 175
σ_B= -175 σ_F= -175
σ_C= 175
σ_D= -175

The Number of Cycles required for above stress history: 238000.

b) Variable amplitude loading:

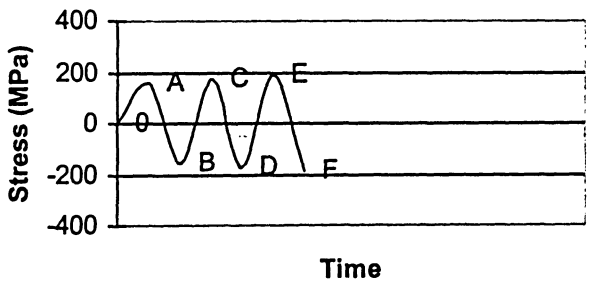

σ_A= 160 σ_E= 190
σ_B= -160 σ_F= -190
σ_C= 175
σ_D= -175

The Number of Cycles required for above stress history: 266500.

Figure 3.9 Stress value at endurance limit (at 175MPa).

a) Constant amplitude loading:

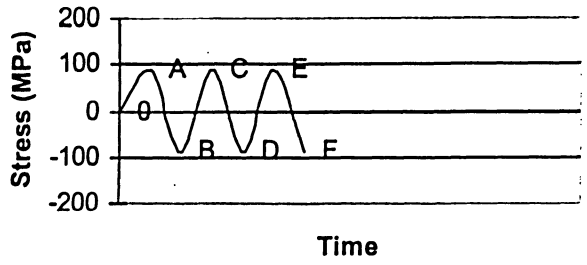

σ_A= 89 σ_E= 89
σ_B= -89 σ_F= -89
σ_C= 89
σ_D= -89

The Number of Cycles required for above stress history: 549000.

b) Variable amplitude loading:

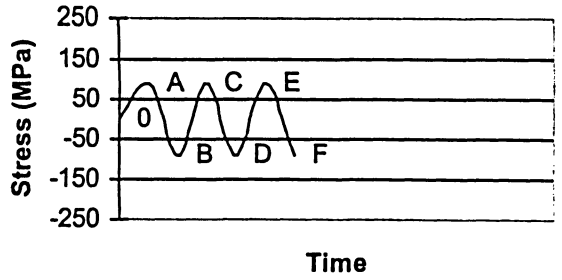

σ_A= 90 σ_E= 92
σ_B= -90 σ_F= -92
σ_C= 89
σ_D= -89

The Number of Cycles required for above stress history: 517500.

Figure 3.10 Stress value 50% below endurance limit.

a) Constant amplitude loading:

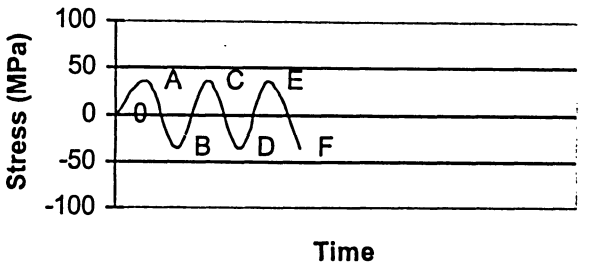

σ_A= 35 σ_E= 35
σ_B= -35 σ_F= -35
σ_C= 35
σ_D= -35

The Number of Cycles required for above stress history: 549000.

b) Variable amplitude loading:

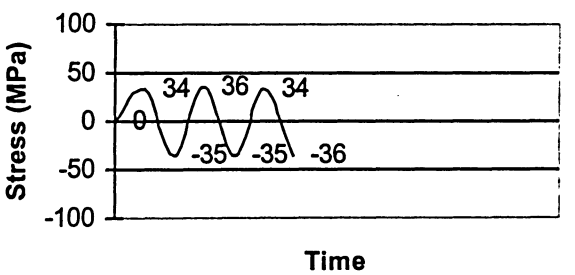

σ_A= 34 σ_E= 34
σ_B= -35 σ_F= -36
σ_C= 36
σ_D= -35

The Number of Cycles required for above stress history: 549000.

Figure 3.11 Stress value 20% below endurance limit.

CHAPTER FOUR

Algorithm of Fatigue Damage Analysis

4.1 Description of Algorithm:

A computer algorithm and program is developed as shown in Figure 4.1 and 4.2 to find the life of any metallic components subject to fatigue cyclic loading. The program runs at four different stages. Each stage represents loading and unloading alternatively. First two stages run only once at initial time and third and fourth stages run in a loop till the last input is used. The program starts with initialization of axial and shear strength coefficient, axial and shear ductility coefficients, modulus of elasticity, cyclic plastic coefficient, cyclic elastic and plastic exponents, axial and shear stress ranges, axial and shear strain ranges, shear modulus, fatigue limit or endurance limit, maximum stress and minimum stress. The program then asks for first input data from hardware. Stress values derived from experimental is divided into equal intervals as to draw a hysteresis loop. All the stress values between zero and first data are applied in to Ramberg-Osgood equation 3.21 to obtain corresponding total strain values, which will complete the 0-A section of Figure 3.5. The cyclic stress is used to calculate elastic strain by dividing cyclic stress amplitude by modulus of elasticity. The difference between total strain and elastic strain will give plastic strain value. Effective Poisson's ratio is calculated by utilizing elastic and plastic strain and known elastic and plastic Poisson's ratio. Once these values are obtained three principal strains are calculated from the equations 3.5 to 3.7. These three principal strain values will form three strain Mohr's circles. According to the definition of the critical plane, largest Mohr's circles during loading and unloading reversals will be considered for calculation. Next step is to calculate the principal stresses from input data.

These three principal stresses will give three stress Mohr's circles and the largest one is considered for calculation. The program now asks hard drive for next available value. The difference between this value and last value obtained from hardware is divided into equal intervals to plot hysteresis for A-B section of Figure 3.5. These stress values will be plugged into unloading Ramberg-Osgood equation (3.22) to calculate strain values. The maximum value obtained by general Ramberg-Osgood equation, from stage 1, is used in un-loading Ramberg-Osgood equation in stage 2. From this equation, total strain value is obtained. The above mentioned steps are then utilized to calculate elastic strain, plastic strain, effective Poisson's ratio and finally loading and unloading largest Mohr's circles. The stage one represents loading and unloading. So at this stage largest strain Mohr's circle for loading and unloading are used to calculate normal strain range and shear strain range. The normal strain range ($\Delta\sigma_n$) is shown in Figure 3.2. It is the horizontal distance between maximum point on loading to minimum point on unloading. The maximum shear strain range ($\Delta\varepsilon_n$) is shown in Figure 3.2. It is the vertical distance between maximum point on loading Mohr's circle to minimum point on unloading Mohr's circle.

Next step is to calculate mean stress by taking an average of two data. The calculated value is substituted into equation (3.19) to calculate the damage function from all the four ranges so far calculated and four known coefficient. This damage function is added to imaginary function in order to get the addition of all the damage function. Now program asks for third input data. This input data is checked for 50% endurance limit. If the data is less then 50% endurance limit, then it will ask for next data otherwise it will pass on the data to next step. At this point, stage three and four are calculated in the same manner as one and two. Except in stage one, original Ramberg-Osgood equation is used whereas in stage three, loading Ramberg-Osgood is used. Therefore, damage function is calculated from stage three and stage four value is added to previous damage function with the help of imaginary function initialized in the beginning. Remaining values are calculated as stage three and four from repeated loop are added to the previous damage function until all the input is used. The damage function is then equated to Coffin-Manson equation to estimate the number of cycles.

4.2 Conceptual Flow Chart:

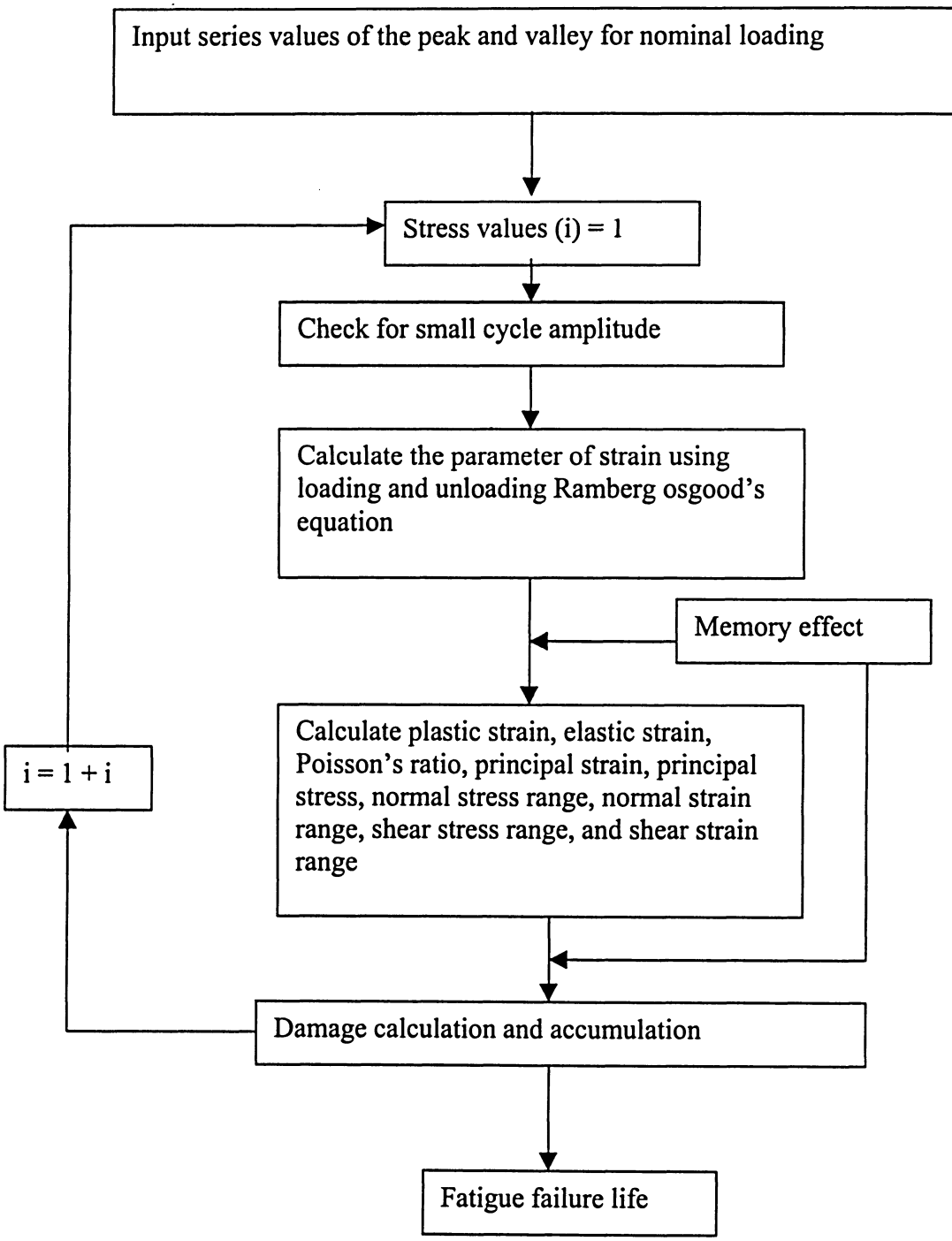

Figure 4.1 Conceptual Flow Chart.

4.3 Computer Program Flow chart (Appendix-B):

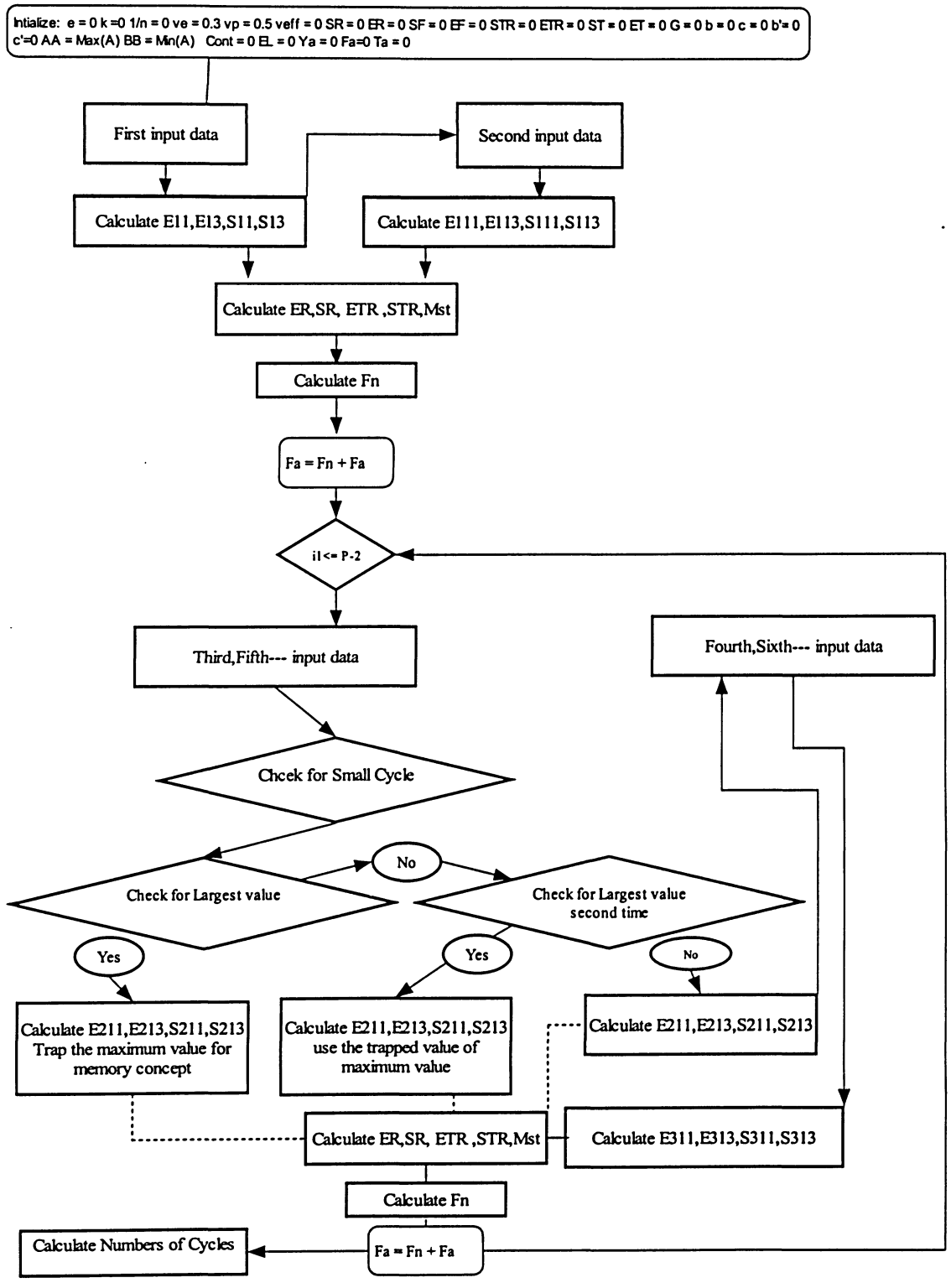

Figure 4.2 Computer Flow Chart.

CHAPTER FIVE

Fatigue Damage Model Evaluation and Results

This chapter deals with evaluation of fatigue damage model by different experimental data available in literature. Data are first converted to terms required in the model and accordingly the values are substituted in the model. This chapter evaluates the model initially with constant amplitude loading, then with step loading and finally with variable amplitude loading conditions.

5.1 Constant loading History:

To evaluate fatigue damage model for constant amplitude loading, the experimental data of Ngiau [44] for uniaxial constant and step loading have been used. Ngiau has tested 2024-T351 aluminum alloy, which is one of the alloys that the automotive industry has considered to be a plausible lightweight substitute for steel. Specimens were machined from 19.05 mm diameter bars. The specimens conform to ASTM E466-82 standards and have a gauge diameter of 12.7 mm, continuous radius of 152.4 mm, a grip cross sectional diameter of 19.05mm and a total length of 228.6mm. Testing was conducted using a MTS 810 uniaxial test frame. All tests were fully reversed and load-controlled. The load history applied to the model is shown in the Figure 5.1.1, the mechanical and cyclic properties used for uniaxial constant amplitude loading are listed in Table A-1. Constant amplitude tests were performed to determine the stress amplitude versus fatigue life (S-N) diagram for the material investigated. The S-N diagram is obtained as shown in Figures 5.1.2. From this Figures it can be noticed that during shorter life, the model shows conservative life up to 10^3, then in the intermediate life 10^3 to 10^4, the model

shows non-conservative and then again the life is conservative in longer life. In the same figure Miner's rule is included to compare different approaches.

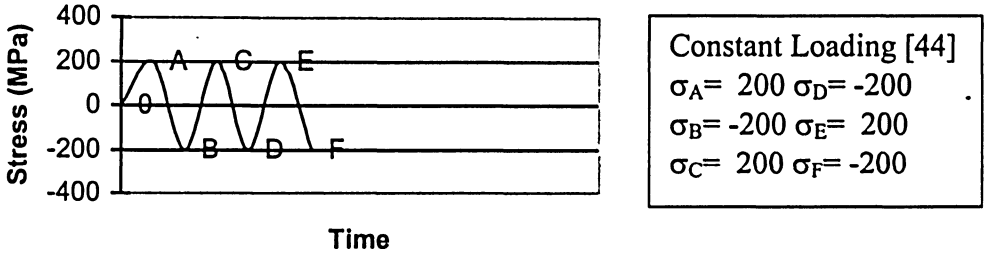

Figure 5.1 Constant amplitude loading History by Ngiau [44].

Figure 5.2 shows four different cases, Case 'a' shows predicted data without any phenomenological factors included. Case 'b' represents predicted data including the sequence effect. Case 'c' describes predicted data with sequence and memory effects. Case'd' presents predicted data including sequence effect, memory effect and small cycle effect.

It can be seen from the figures presented that there is no difference between all four cases. This is so because; in constant loading there is no effect of sequence, memory and small cycle effects. Figure 5.3 shows a comparison between the proposed model and experimental data. The proposed fatigue analysis shows a good agreement with experimental data for uniaxial constant loading. The diagonal dashed line in figure 5.3 represents a comparison line and solid lines indicate a ratio of variation between predicted and experimental lives as compared with the dashed line. The maximum variation is 3.95 in this case.

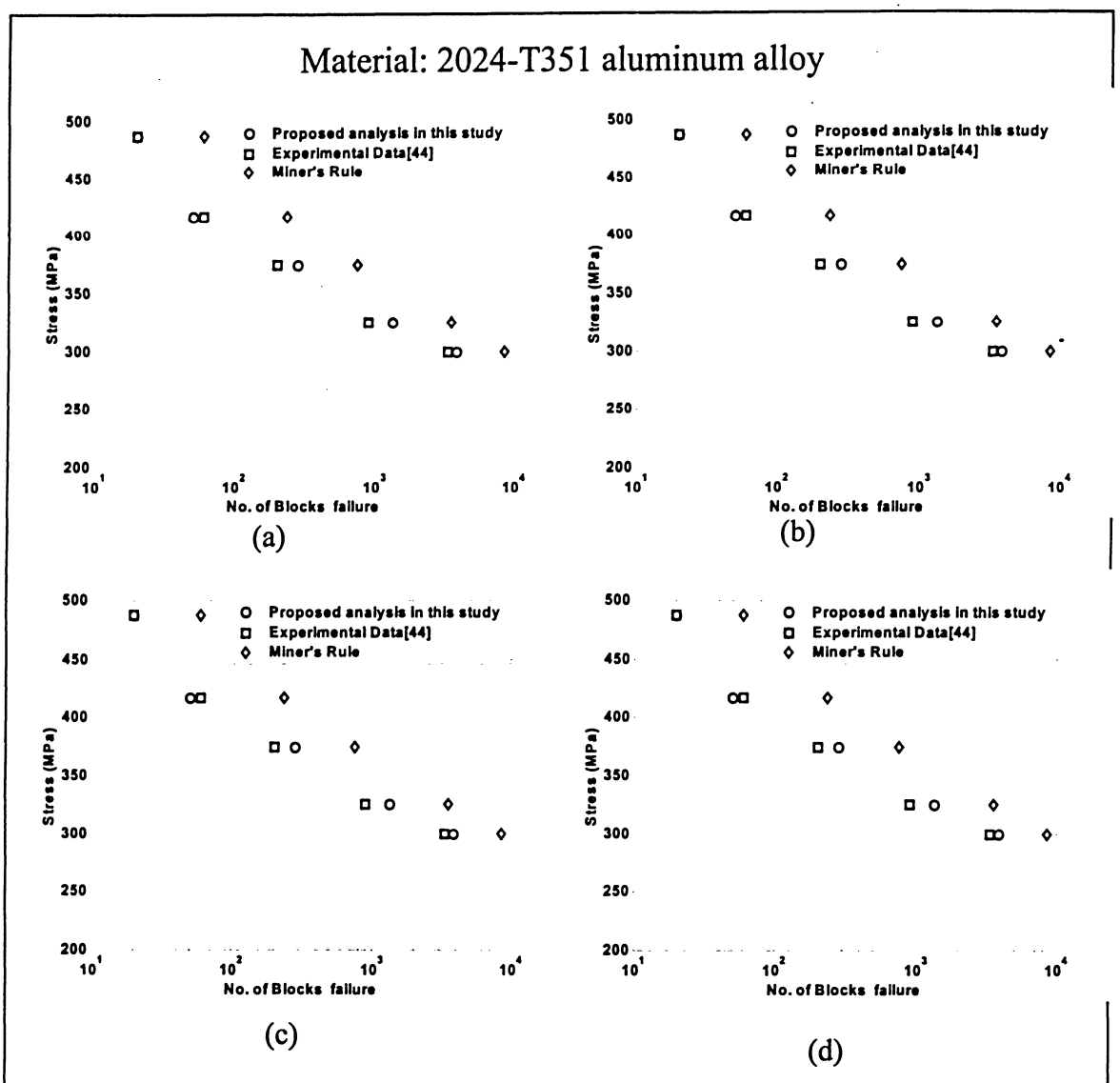

Case	Sequence Effect	Memory Effect	Small cycle Effect	Ratio of Pred. Life to Exp Life	
				Max.	Min.
a	—	—	—	3.95	1.4
b	✓	—	—	3.95	1.4
c	✓	✓	—	3.95	1.4
d	✓	✓	✓	3.95	1.4

Figure 5.2 Comparison of proposed fatigue damage approach and Miner's rule with experimental fatigue life data of 2024-T351 aluminum alloy.

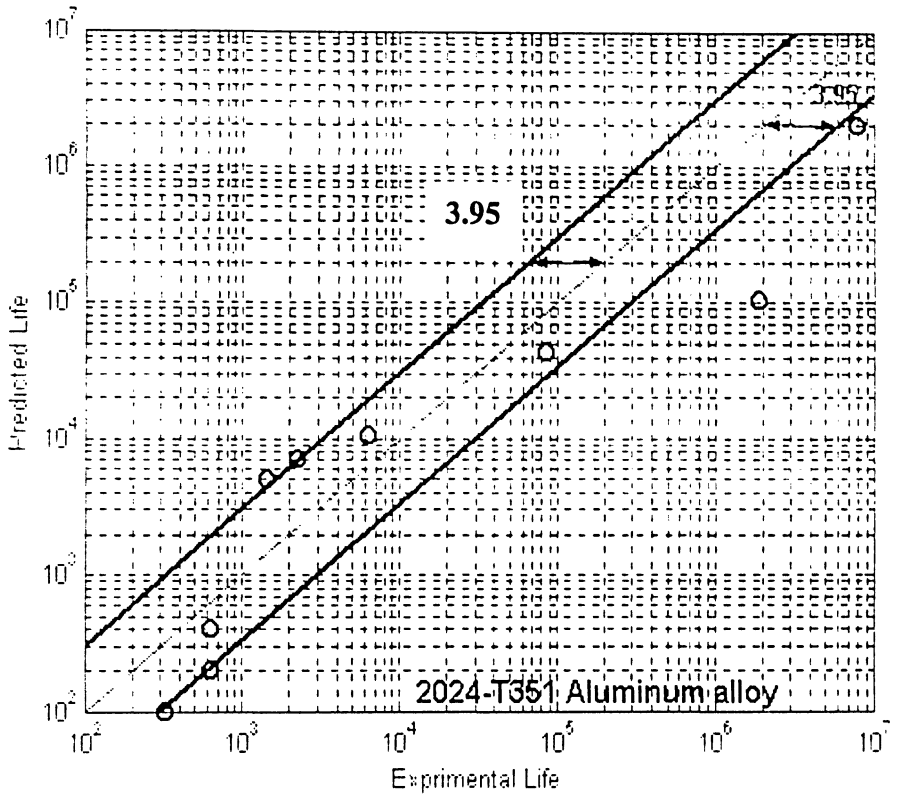

Figure 5.3 Experimental and predicted fatigue lives in Al 2024-T351alloy.

5.2 Step Loading History:

The step loading history used to evaluate the proposed approach in this thesis is shown in figures 5.4 and 5.5. The figure 5.4 shows that initially five LCF cycles of 420 MPa is followed by 1000 constant amplitude cycles (with amplitude of 175 MPa). When the above mentioned history is applied to the proposed approach it gives little conservative life of 4250 cycles. Another case is 100 HCF cycles of 220 MPa is followed by 1000 constant amplitude cycles (with amplitude of 175 MPa). The experimental results from these type of loading is 100,000 cycles and the predicted life using the proposed approach found to be 134,670 cycles.

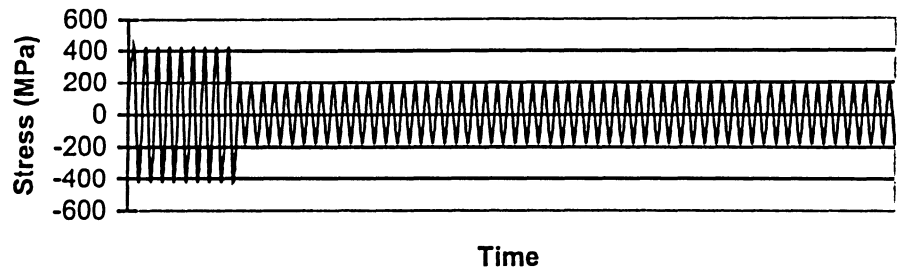

Figure 5.4 LCF cycles loading history by Ngiau [44].

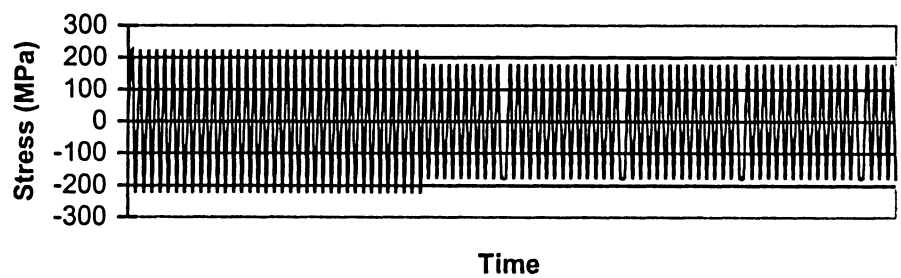

Figure 5.5 HCF cycles loading history by Ngiau [44].

5.3.Variable Amplitude Loading History :

The entire service loads are generally variable or random in nature. This section will evaluate the capability of the fatigue damage approach presented in this thesis for variable amplitude loading condition. The variable loading histories and life data by Kilman [40] conducted on cylindrical specimens of low carbon steel (0.4 wt%c) used in this study to evaluate the damage model in this thesis. The test specimens were loaded in the stress-controlled mode using an MTS computer controlled fatigue system. The loading block was made up of 113 randomly arranged cycles. In order to use the experimental data provided by Kilman, variable loading history has been transformed as per maximum stress value in S-N curve. Figure 5.6 shows the loading history applied by Kilman [40].

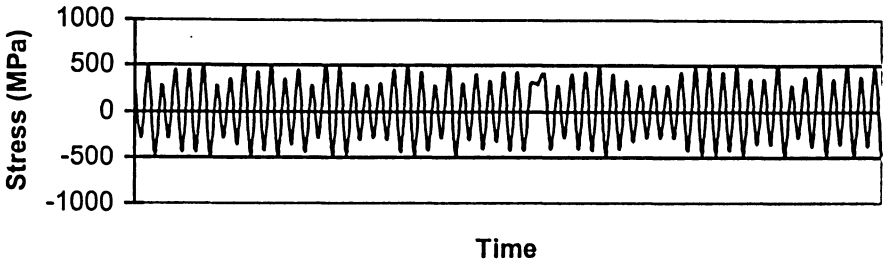

Figure 5.6 Variable loading history by Kilman [40].

Figure 5.7 shows four different cases, Case 'a' shows predicted data without including any phenomenological factors. Case 'b' represents predicted data with sequence effect. Case 'c' describes predicted data with sequence effect and memory effect. Case 'd' presents predicted data with sequence effect, memory effect and small cycle effect. It can be observed from the table given in the Figure 5.3.2 that maximum variation is calculated as the maximum difference between experimental data to data obtained from proposed analysis and minimum variation is calculated as minimum difference between experimental data and data obtained from proposed analysis at any given time between experimental and predicted life data. For Case 'a' the maximum variation is 3.14 and minimum variation is 1.5. By introducing sequence effect the maximum variation reduces to 2.96 and the minimum variation reduces to 1.5. Maximum variation further reduces to 1.48 and 1.36 with introduction of memory and small cycle effects. Hence it can be deduced from the table that introducing phenomenological factors in the study has provided more favorable results.

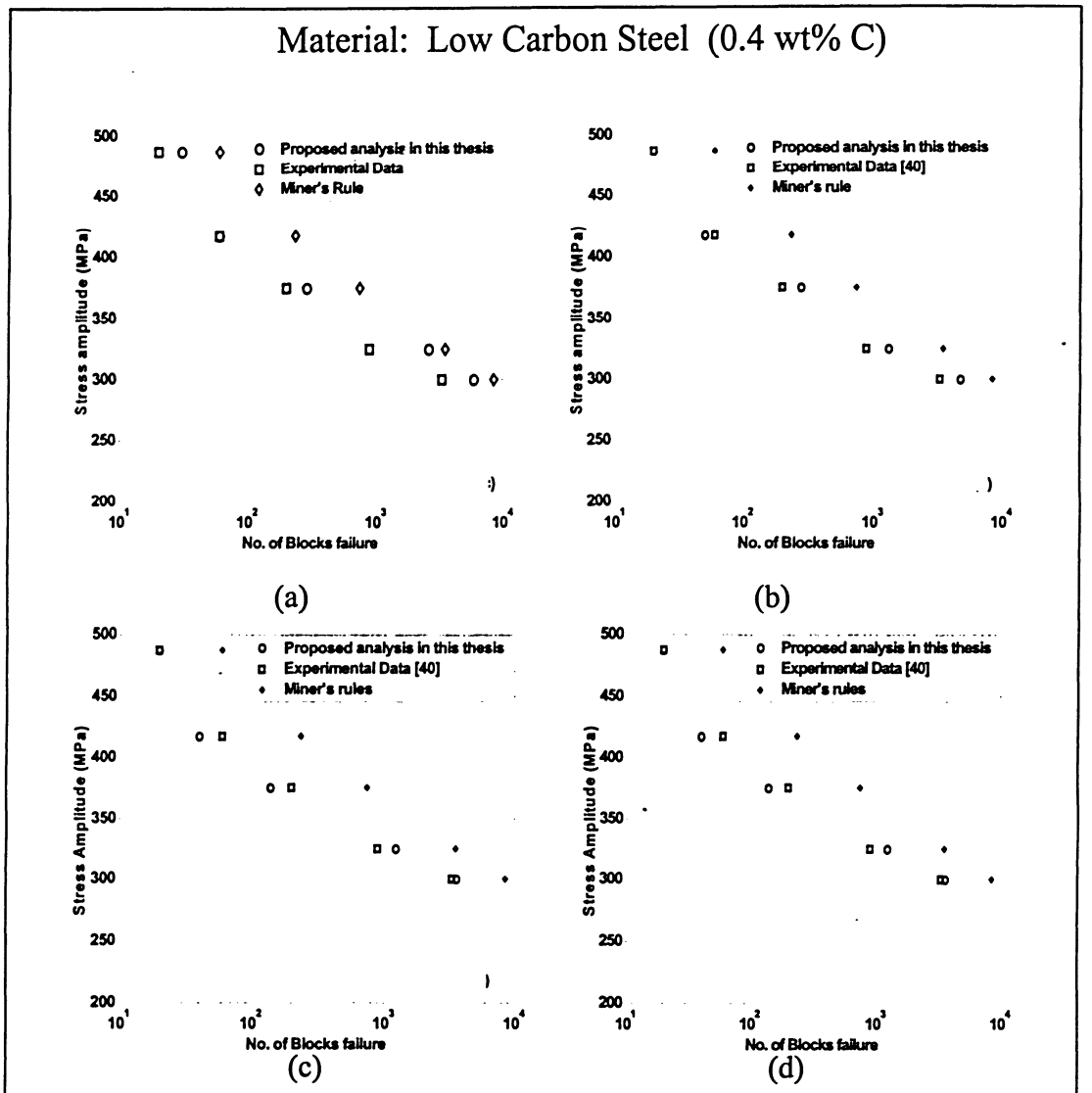

Case	Sequence Effect	Memory Effect	Small cycle Effect	Variation of Pred. Life	
				Max.	Min.
a	—	—	—	3.14	1.5
b	✓	—	—	2.92	1.5
c	✓	✓	—	1.48	1
d	✓	✓	✓	1.36	1

(e)

Figure 5.7 Comparison of proposed fatigue damage approach and Miner's rule with experimental fatigue life data of Low carbon steel.

Figure 5.7 shows relationship between the alternating stress and number of cycle. It also shows good relationship between experimental and predicted life data from proposed model. Figure 5.8 shows that experimental life data agrees with predicted life calculated from proposed damage analysis and maximum variation in this case is 1.36.

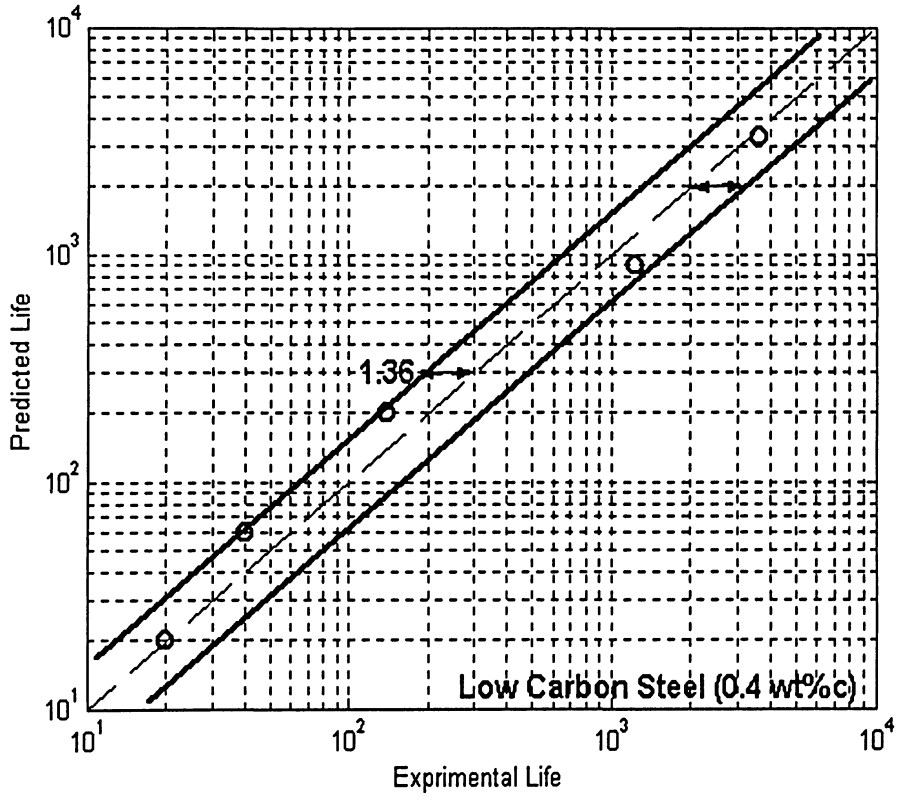

Figure 5.8 Experimental and calculated fatigue lives for low carbon steel

Wu et al. [49] has carried out experiments on 7075-T761 aluminum alloy and specimens were made in accordance to ASTM E606 standard. The material has a yield stress of 503 MPa, ultimate strength of 647 MPa and Young's modulus 74 GPa. An MTS axial-

torsional servo-hydraulic test machine was used to perform fatigue tests. Figure 5.9 presents variable amplitude loading spectrum used by Wu et al. [48].

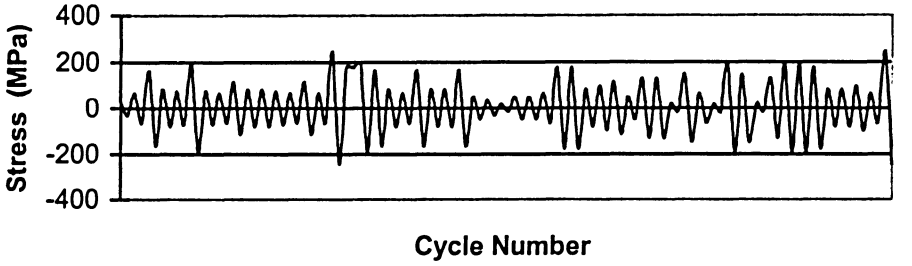

Figure 5.9 Variable amplitude loading history byWu et al. [48].

Figure 5.10 shows four different cases. In this figure, Case a shows predicted data without considering the effect of any phenomenological factors. Case b represents predicted data including loading sequence effect. Case c presents predicted data including sequence and memory effects. Case d presents predicted data with sequence effect, memory effect and small cycle effect. The table compares experimental and predicted life data. The maximum variation is calculated as maximum difference between experimental and predicted life data. The maximum variation is 3.56. This gradually reduces to 2.46 with introducing the sequence effect. It further reduces to 1.48 with including the memory effect. Finally when small cycle effect is introduced it further gives better results by reducing the value to 1.36.

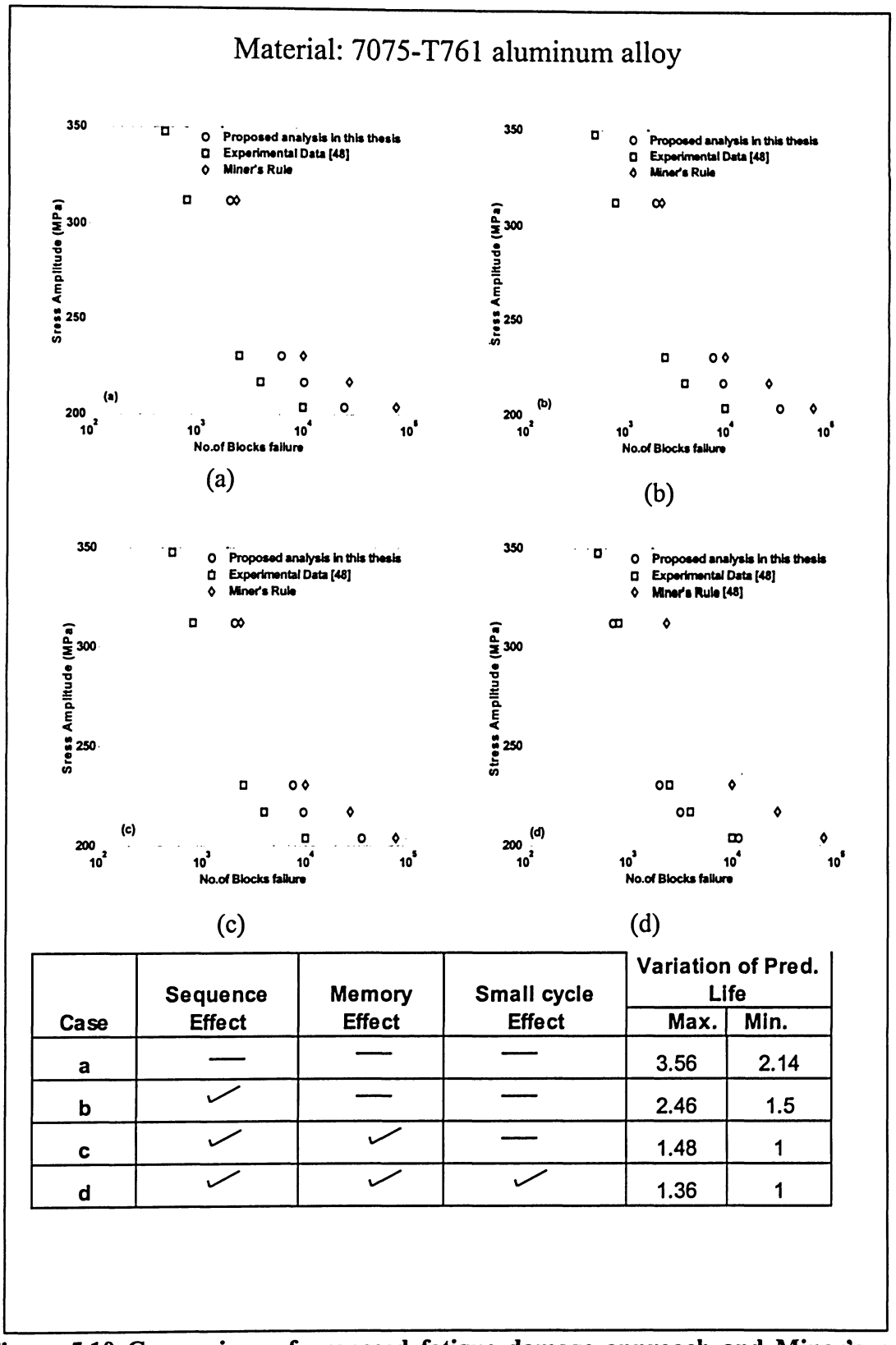

Case	Sequence Effect	Memory Effect	Small cycle Effect	Variation of Pred. Life	
				Max.	Min.
a	—	—	—	3.56	2.14
b	✓	—	—	2.46	1.5
c	✓	✓	—	1.48	1
d	✓	✓	✓	1.36	1

Figure 5.10 Comparison of proposed fatigue damage approach and Miner's rule with experimental fatigue life data of 7075-T761 aluminum alloy.

Figure 5.11 shows good relationship between experimental and predicted fatigue life values.

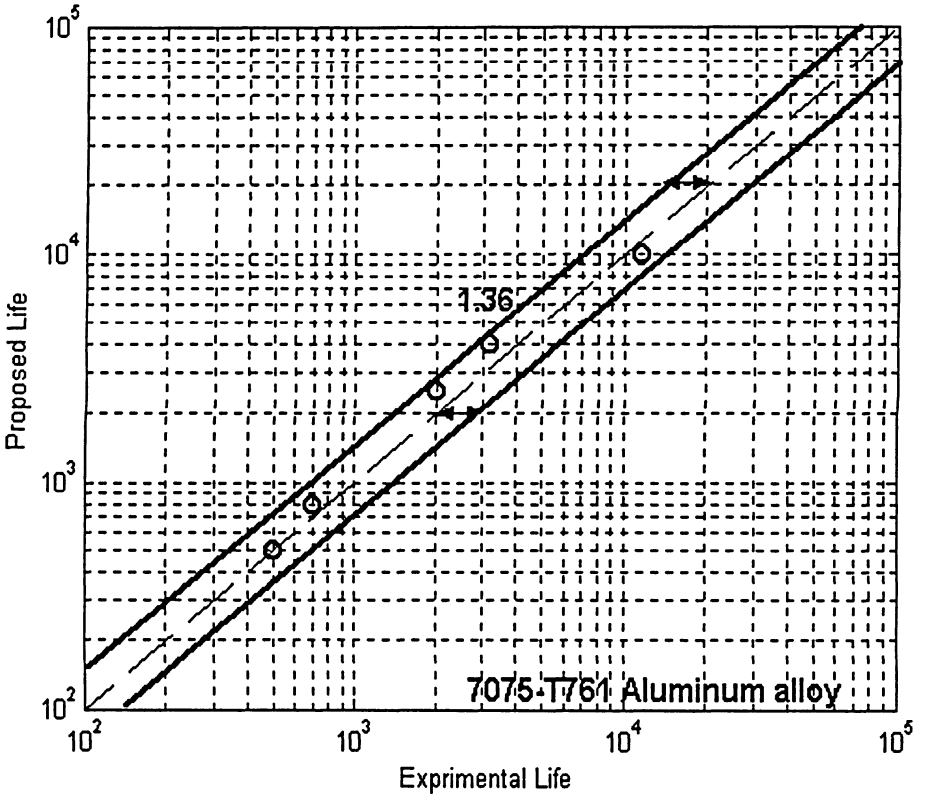

Figure 5.11 Experimental and calculated lives data for Al 7075-T 761 alloy.

Everett [41] has carried out studies on typical commercial transport design spectra for simple block sequence of loads. The material used for this study was 2024-T3 aluminum sheet taken from a special stock of material at the NASA Langley research center, which has been used for fatigue and fracture studies over several decades. The alloy 2024 has been used in the lower wing skin of many commercial transport aircraft. The material has yields strength of 52 ksi and an ultimate strength of 72 ksi. The fatigue endurance limit of this material is 18ksi and the nominal thickness is 0.090 in. the study consists of five different flight types for random loading. Flight number one is the most severe and occurs only once in 5000 flights. Flight number two occurs 13 times, flight number three

occurs 215 times, and flight number four occurs 1067 times, respectively, in the 5000 cycles sequence. Figure 5.12 presents variable loading history reported by Everett [41].

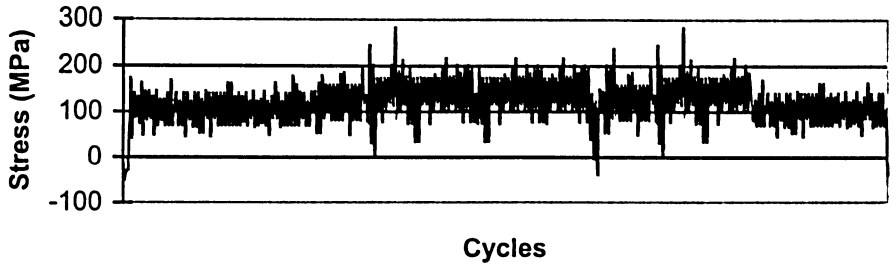

Figure 5.12 Variable amplitude loading history by Everett [41].

In figure 5.13, Case 'a' presents predicted data with no phenomenological factors. Case 'b' represents predicted data with sequence effect. Case 'c' describes predicted data with sequence and memory effects. Case 'd' presents predicted data with sequence , memory effect and small cycle effect. For Case 'a' the maximum variation is 3.95 and minimum variation is 1.5. By introducing sequence effect the maximum variation reduces to 3.45 and minimum to 1.34. Maximum variation further reduces to 1.75 and 1.67 with introduction of memory and small cycle effect. Hence it can be deduced from the table that introducing phenomenological factors in the study has provided more favorable results.

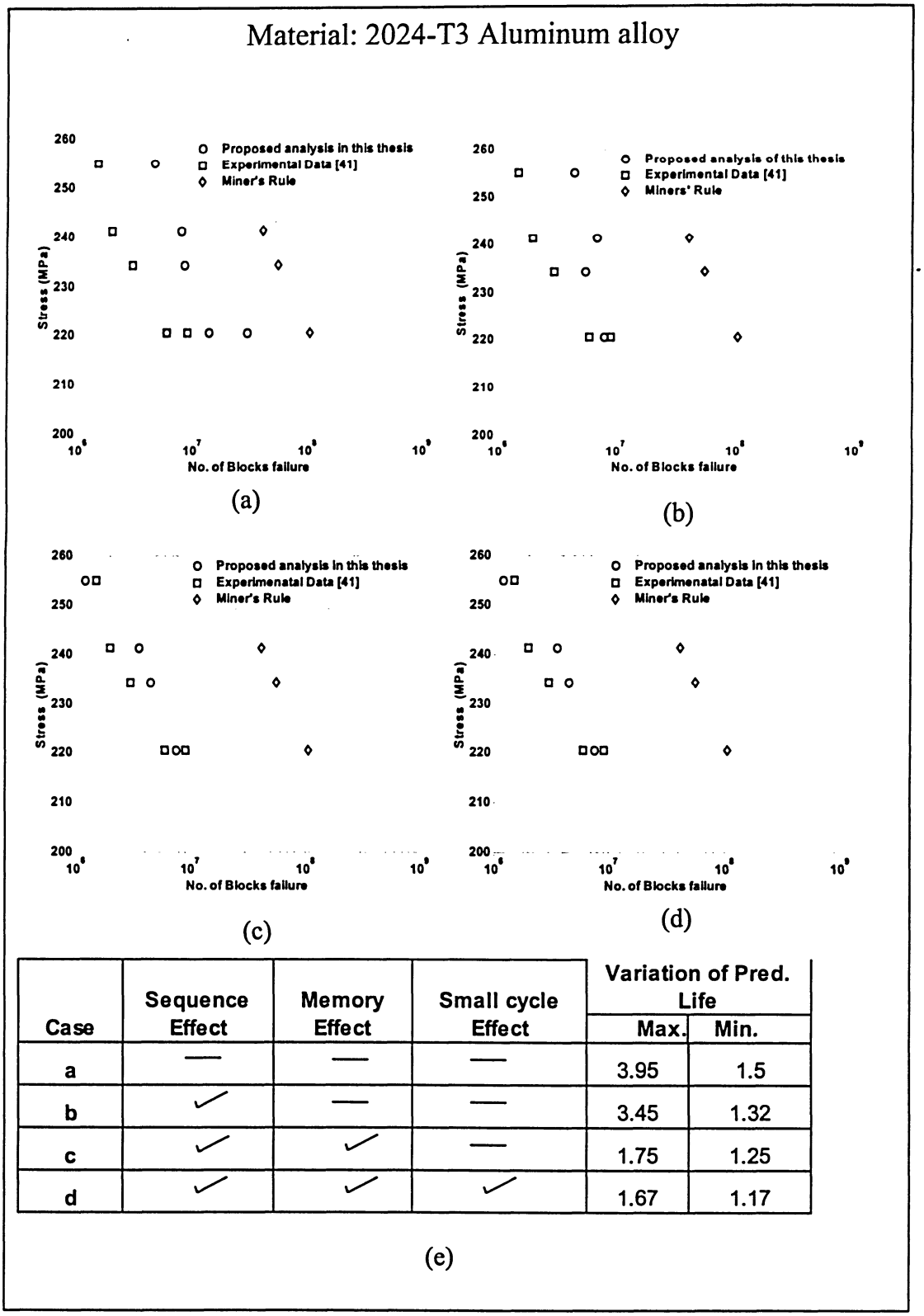

Case	Sequence Effect	Memory Effect	Small cycle Effect	Variation of Pred. Life	
				Max.	Min.
a	—	—	—	3.95	1.5
b	✓	—	—	3.45	1.32
c	✓	✓	—	1.75	1.25
d	✓	✓	✓	1.67	1.17

(e)

Figure 5.13 Comparison of proposed fatigue damage approach and Miner's rule with experimental fatigue life data of 2024-T3 aluminum alloy.

Everett has done this study to account for sequence loading effect in commercial transport. The five loading histories were used to find out the life of component. Figure 5.14 shows the first and most severe loading for fatigue damage analysis. It can be seen from the Figure that experimental fatigue life data and calculated life results fall within the maximum variation of 1.67.

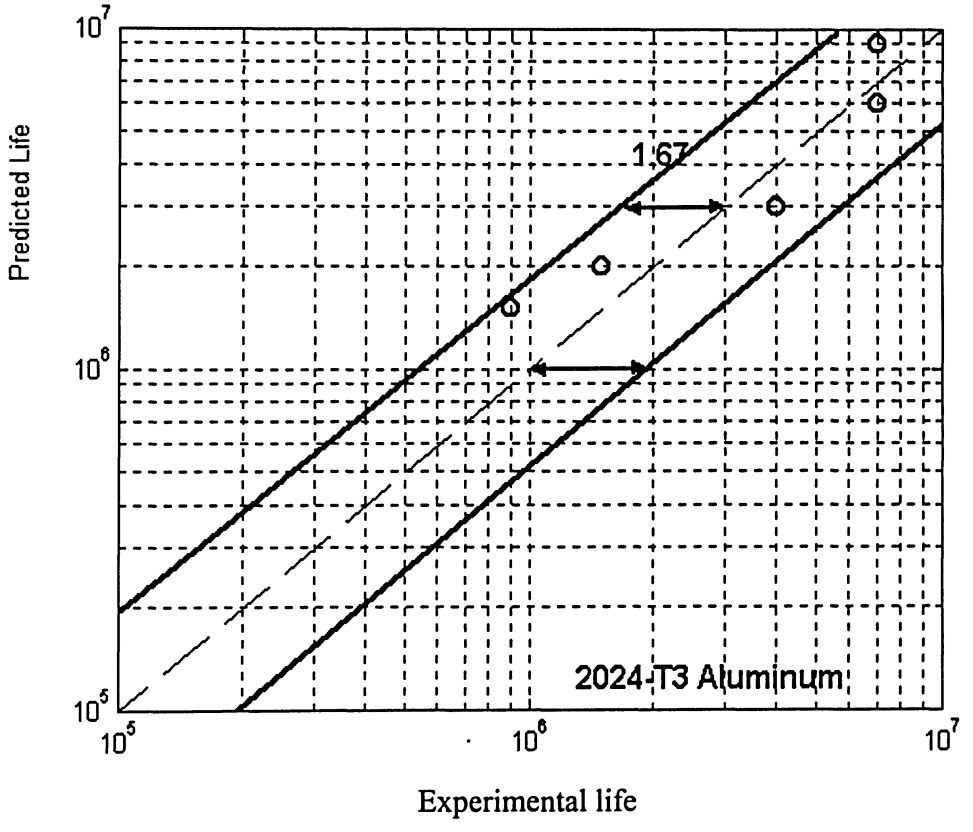

Figure 5.14 Experimental and calculated lives data for Al 2024 T3 alloy.

For steel bridge deck, Agerskov [47] has done investigation by strain gauge measurements on the orthotropic steel deck structure of the Faro Bridge in Denmark. Strain gauge measurements were carried out at 10 different locations in the orthotropic deck. The measurement area is placed at a distance of approximately 8m from the simple support of the bridge girder on the nearest bridge pier. The length of the bridge spans is approximately 80m. This location of the strain gauges means that only local bending

effect in the deck structure will be registered, whereas the stresses due to global bending in the bridge girder will be negligible. Ten strain gauges are placed in two sections between two transverse diaphragms. One of these sections is in the middle of the longitudinal stiffener span, which has a length of 4m, and the other section is placed at a distance of 0.5m from one of the transverse diaphragms. Four of the strain gauges in each section are placed on the bottom of trapezoidal longitudinal stiffener of the deck plate. The fifth gauge in each section is placed on the butt weld between the trapezoidal stiffener and the deck plate. In this way variable realistic loading data is compared with constant amplitude data used in early studies. Figure 5.15 presents variable loading history used by Agerskov [47].

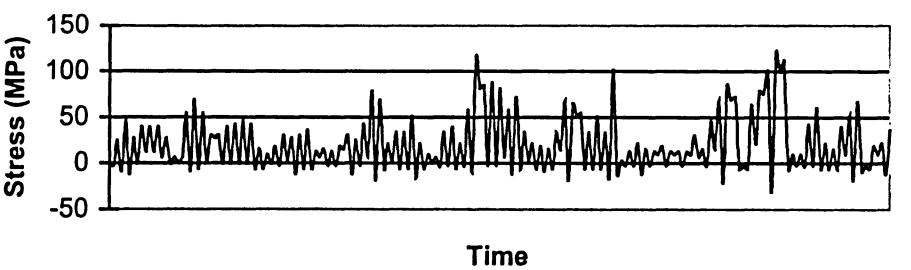

Figure 5.15 Variable amplitude loading history [47].

In figure 5.16, Case 'a' shows predicted data without any phenomenological factors. Case 'b' represents predicted data with sequence effect. Case 'c' describes predicted data with sequence and memory effects. Case 'd' presents predicted data with sequence effect, memory effect and small cycle effect. The maximum variation is 2.77; this gradually reduces to 2.00 with the introduction of sequence effect. It further reduces to 1.92 with introduction of memory effect and finally when small cycle effect is introduced it further gives better results by reducing the value to 1.33.

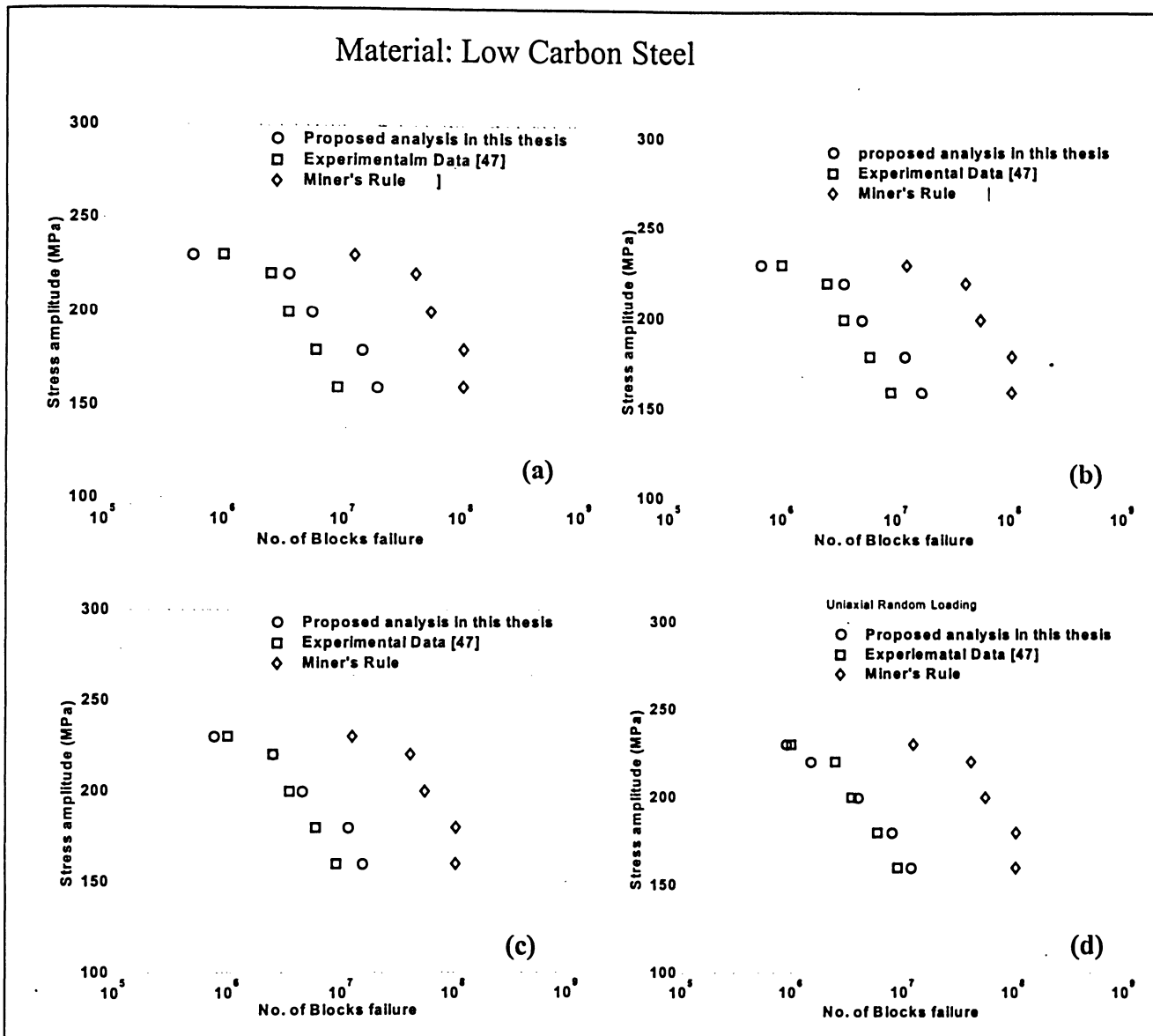

Case	Sequence Effect	Memory Effect	Small cycle Effect	Variation of Pred. Life	
				Max.	Min.
a	—	—	—	2.77	1.14
b	✓	—	—	2.00	1.4
c	✓	✓	—	1.92	1
d	✓	✓	✓	1.33	1.11

Figure 5.16: Comparison of proposed fatigue damage approach and Miner's rule with experimental fatigue life data of low carbon steel

It can be seen from the figure that experimental data are from high cycle zone and observe data shows initially conservative and then non-conservative lives and maximum variation is 1.33 as shown in Figure 5.17.

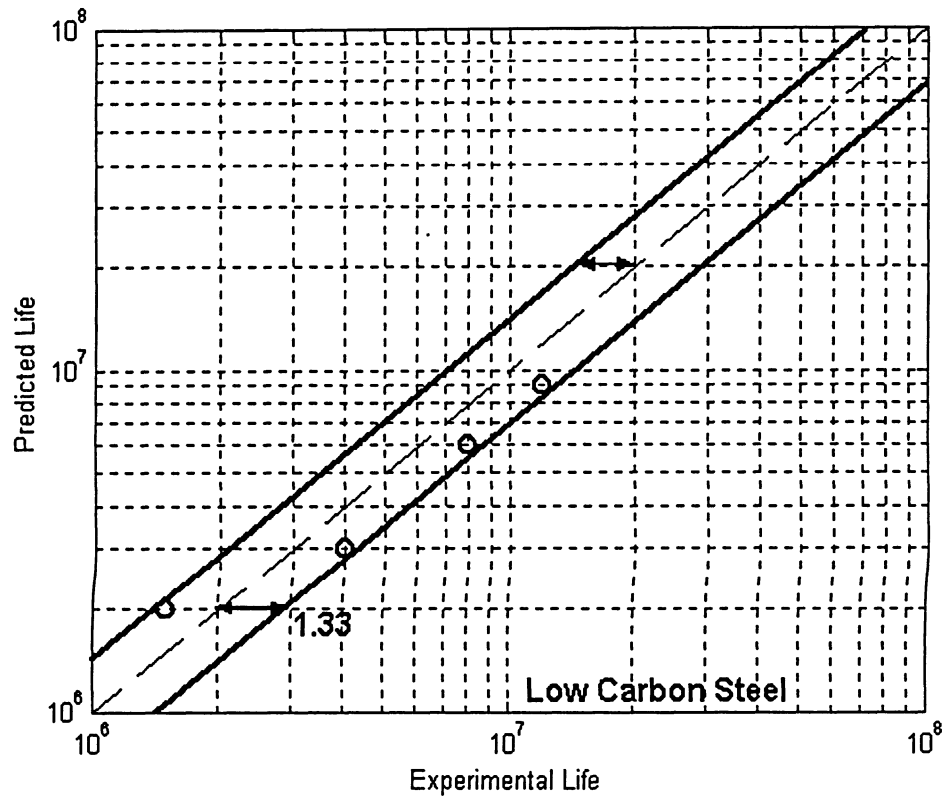

Figure 5.17 Experimental and calculated lives data for low carbon steel.

CHAPTER SIX

Discussion

Fatigue analysis using the concept of a critical plane of maximum shear strain is very effective because the critical plane concept is based on the fracture mode or initiation mechanism of cracks. In the critical plane concept, after determining the maximum shear strain plane, Brown and Miller [33] defined fatigue parameter as combination of normal and shear strain. Stulen and Cummings [34] defined fatigue parameter as combination of normal and shear stress. Fatemi and Socie [35] presented fatigue parameter as combination of normal stress and shear strain. Critical plane defined by Liu's parameter [49], on the other hand, is associated with two different physical modes of failure and the parameter consists of Mode I and Mode II energy components. Liu's parameter does not account for the effect of mean stress but it predicts fatigue life better, regardless of temperature, materials, and load ratio. Chu et al. [50] formulated normal and shear energy components based on the Smith-Waston-Topper parameter. They determined the critical plane and the largest damage parameter from the transformation of strains and stress onto planes spaced at equal increments using a generalized Mroz model. This parameter is based on the maximum value of the damage parameter rather than being defined on planes of maximum stress or strain. Glinka et al. [51] proposed a multiaxial fatigue life parameter based on the summation of the product of normal and shear strains and stresses on the critical plane, which is assumed to be the plane of maximum shear strain. The parameters discussed here are defined on specific planes and state of stress through combination of normal and shear strain and stress ranges. These parameters depend upon the choice of the critical plane and the stress and strain ranges acting on that plane.

Varvani's approach is used as basis to develop a new approach for variable amplitude loading in this thesis. In this approach, critical plane is defined by the largest strain and stress Mohr's circles during loading and unloading. This approach does not require any empirical fitting factor; it takes care of mean stress and additional hardening, phenomenological factors such as sequence loading, memory effect, and small cycles. The effect due to sequence loading is studied for variable loading. It is found that the loading sequence has a great influence in the stress-strain response of hysteresis loops. Memory effect concept has been used to close hysteresis loops in each block loading history. The small amplitude cycles corresponds to 50% to 100% of the endurance limit are also studied. Results indicate that small cycles exceeding 50% of the fatigue endurance limit contribute to the accumulated damage.

The present proposed analysis considers the evaluation of different materials of low carbon steel, 2024T351, and 7075-T761 aluminum alloys. It is found that steel under variable loading has shown better results than aluminum alloys However, the overall results verifies that fatigue life prediction of different materials fall within an acceptable limits.

Macha [36] has introduced sign effect, which supports the sign changes during unloading and reloading. It is noticed that the negative and positive signs are provided in the bracket, in such a way that the values will always remain positive inside the bracket. In case of loading, the value will be added and in case of unloading, the value will be deducted. The negative value outside the bracket takes care of negative sign (during unloading cycle). Hence, in loading, unloading and reloading Ramberg-Osgood equations, the sign effect proposed by Macha was already incorporated as a built-in feature.

It can be observed from Figures 5.2, 5.7, 5.10, 5.13 and 5.16 that life prediction values agree with experimental life data as Case 'a' to Case 'd' by introducing sequence effect, memory effect and small cycle effect gradually. Hence it can be deduced that introducing

phenomenological factors in the study has provided a favorable results for assessing fatigue lives of components under variable loading conditions.

A comparison of the predicted lives with experimental lives for a number of materials and variable loading conditions showed that life data to be skewed from the line of comparison with conservative at longer lives and non-conservative at shorter lives. Figures (6.1.3- 6.5.3) compared the results of damage analysis in this thesis with the widely accepted Miner's rule and available experimental data in the literature. The proposed parameter successfully correlated uniaxial fatigue lives within a factor that varied with materials from 1.5 to a maximum value of 3.0. The poorest correlation of factor 3.0, in fatigue life of 2024-T351 aluminum alloy may be due to such factors as environmental effect, heat treatment impact, geometry of fatigue specimens and finally human errors while carrying out experiments. Other materials like low carbon steel and 7075-T761 showed good correlation of life data and the proposed fatigue parameter.

CHAPTER SEVEN

Conclusions and Recommendations

7.1 Conclusions:

Many fatigue theories developed after 1980 were examined from the viewpoints of: empirical formulas, modifications of coffin-Manson equation, application of stress or strain invariant, use of space averages of stress or strain invariants, critical plane approaches, use of energy and finally energy based-critical plane damage approaches. Considering all the above-mentioned methods, this thesis attempts to further extend Varvani's fatigue damage approach for variable amplitude and uniaxial loading condition. This approach integrates the normal energy range and the shear energy range calculated for the critical plane on which the stress and strain Mohr's circles are largest during peaks and valleys of block loading histories. The normal and shear energies in this parameter have been weighted by the tensile and shear fatigue properties. In this thesis further phenomenological factor extends the applicability of Varvani's equation to be applied for variable amplitude loading conditions. Through the study carried out, the following conclusions can be drawn:

1. An algorithm for calculating fatigue damage for uniaxial loading is proposed which uses Varvani's approach as a foundation and takes care of phenomenological factors such as sequence effect, memory effect and small cycle effect.
2. It is found that the loading sequence has a great influence in the stress-strain response of hysteresis loops. Memory effect concept has been used to close hysteresis loops in each block loading history. The small amplitude cycles of 50%

to 100% of the endurance limit were also studied. Results indicate that small cycles exceeding 50% of the fatigue endurance limit contributes to the accumulated fatigue damage. The effect of small cycles has also been considered on fatigue damage analysis procedure.

3. Fatigue life predictions based on proposed approach for both CAL and VAL were found in good agreement with experimental fatigue life values of different materials extracted from literatures.

7.2 Recommendations:

For many components the most frequent cause of failure is fatigue phenomenon. This problem is very important, and for more than 100 years investigators have sought to alleviate and quantify the effects of fatigue damage. Estimation of fatigue life of a material subjected to variable amplitude loading needs a suitable algorithm and damage analysis methodology. This study has put an effort to develop such algorithm for uniaxial variable amplitude loading by taking Varvani's approach as a basis. The following points need further study to extend the applicability of the proposed model. Due to the rarely available experimental data in the literature, further experimental investigations are required to more accurately evaluate the fatigue damage under variable amplitude loading conditions. This fatigue damage approach is developed for a uniaxial state but it can be extended for multiaxial random loading by considering some more parameters. It is also worthwhile to conduct multiaxial fatigue tests under variable amplitude loading conditions where most engineering structures experience such loading complexity. Availability of such experimental data is required to evaluate and extend the damage model for variable multiaxial loading conditions using the proposed damage approach.

REFERENCES

[1] Bannatine, J. A., Comes, J. J., Handrock, J. L., Fundamentals of metal fatigue analysis, Prentice-Hall,Inc., 1990.

[2] Grifffith A. A., *Philos. Trans. R. Soc. London*, **A221**, 1920, p. 163-165.

[3] Irwin G. R., Fracturing of Metals, *American Society for Metals, Cleveland, Ohio*, **20**, 1949, p.147.

[4] Irwin G. R., "Analysis of Stresses and Strains near the End of a Crack Traversing a Plate," *Trans. ASME, J. Appl. Mech.*, **E24**, 1957, p.361-364.

[5] Palmgren A., "Durability of ball Bearings," *ZVDI*, **68**, No. 14, 1924, p. 339-341 (in German).

[6] Miner M. A., "Cumulative damage in fatigue, " *J. Appl. Mech.*,**12**, *Trans. ASME*, **67**, 1945, p. A159-A164.

[7] Marco, S. M. and Starkey, W. L., A concept of fatigue damages. *Transaction of the ASME*, 1954, **76**, p. 627-632.

[8] Kommers, J. B., The effect of overstress in fatigue on the endurance life of steel, *ASTM*, 1945, **45**, p. 532-541.

[9] Bennett, J. A., A study of damaging effect of fatigue stressing on X4130 steel. Processings, *ASME*, 1946, **46**, p. 693-714.

[10] Splitzer, R.and Corten, H.T., Effect of loading sequence on cumulative fatigue damage of 7071-T6 aluminum alloy. *ASTM*, 1961, **61**, p. 719-731.

[11] Freudenthal, A.M. and Heller, R.A., On the stress interaction in fatigue and a cumulative damage rule, *Journal of the Aerospace Science*, 1959, **26**(7), p. 431-442.

[12] Manson, S.S, Nachigall, A.J. and Freche, J. C., A proposed new relation for cumulative fatigue damage in bending, *ASTM*, 1961, **61**, p. 679-703.

[13] Marrow, J. D., The effect of selected sub-cycle sequences in fatigue loading histories, *ASME Publication,* 1986, **72**, p. 43-60.

[14] Grover, H.J., An observation concerning the cycle ratio in cumulative damage. *ASTM*, PA, 1960, **5**, p. 120-124.

[15] Mason, S.S., Interface between fatigue, creep and fracture. *International Journal of Fracture Mechanics*, 1966, **2**, p. 328-363.

[16] Mason, S.S. and Halford, G. R., Practical implementation of the double linear damage rule and damage rule and damage curve approach for treating cumulative fatigue damage, *International Journal of fatigue*, 1981, **17**(2), p. 169-192.

[17] Mason, S.S. and Halford, G. R., complexities of high-temperature metal fatigue: some steps toward understanding. *Israel Journal of Technology*, 1983, **21**, p. 29-53.

[18] Bui–Quoc-T., An interaction effect consideration in cumulative damage on a mild steel under torsion loading. *Proceedings of the 5th International Conference on Fracture*, 1981, **5**, p. 2625-2633.

[19] Wheeler, O E., Spectrum loading and crack growth. *ASME*, 1972, **D94** (1), p. 181-186.

[20] Willenburg, J., Eagle, R. M. and Wood, H. A., A crack growth retardation model using an effective stress concept, *AFFDL TM-71-1-FBR*, 1971,**14**, p. 67-75.

[21] Miller, K. J. and Zachariah, K. P., Cumulative damage laws for fatigue crack initiation and stage I propagation. *Journal of Strain Analysis*, 1977, **12**(4), p. 262-270.

[22] Ibrahim, M. F.E and Miller, K. J., Determination of fatigue cracks initiation life. *Fatigue of Engineering Material and Structure*, 1980, **2**, p. 351-360.

[23] Miller, K J, Mohamed, H J and de los Rios, E R., Fatigue damage accumulation above and below the fatigue limit, *Mechanical Engineering Publication*, **2**, 1986, p. 491-511.

[24] Garud, Y.S.,Proc.Symp., On Methods for predicting materials life in fatigue, *ASME*, 1979,**103**, p.247-251.

[25] Golos, K. and Ellyin, F., A total strain energy density theory for cumulative fatigue damage. *ASME Journal of Pressure Vessel Technology*, 1988, **110**, p.36-41.

[26] Ellyin, F., cyclic strain energy density as a criterion for multiaxial fatigue failure. *Mechanical Engineering Publications*, Suffolk, UK, 1989, **89**, p. 571-583.

[27] Ellyin, F. and Golos, K., Plastic strain energy in fatigue failure. *Trans. ASME, J. Engng Mater. Technol.* 1988, **110**, p.63-69.

[28] Lachowicz, C T., Calculation of the elastic-plastic strain energy density under cyclic and random loading. *International Journal of fatigue*, 2000, **23**, p. 643-652.

[29] Tachankov, D S and Vesselinov, K V., Fatigue life prediction under random loading using total hysteresis energy, *I J of Pressure Vessels and Piping*, 1998, **75**, p.955-960.

[30] Kachanov, K M. and Rabotnov, Y. N., Time to the rupture process under creep condition, Izvestiia, *AN SSSR*, 1984, (**8**), p. 26-31.

[31] Chaboche, J L., Fracture mechanics and damage mechanics: complementarily of approaches. *In Numerical Method in fracture Mechanics Fourth International Conference*, ed.,Swansea, 1987, p. 309-324.

[32] Chow, C L and Wei, Y A., Model of continuum damage mechanics for fatigue failure. *International Journal of fatigue*, 1991, **50**, p. 301-316.

[33] Brown, M.W. and Miller, K.J.,Proc., *Conf. Of the fatigue of metals, the institute of mechanical Engineerings*, **46**, 1973, p.746-752.

[34] Stulen, F.B. and Cummings, H.N., *Proc. ASME*, 1954, **54**, p.822-827.

[35] Fatemi, A. and Socie, D.F., Fatigue fracture of engineering materials and structures, 1988, **11**, p. 149-154.

[36] Lagoda, T and Macha, E., Energy approach to fatigue life estimation under combined tensile with torsion, *VII Summer School of fracture Mechanics*, 2001, **6**, p.18-22.

[37] Lagoda, T., Energy model for fatigue life estimates under uniaxial random loading I, *International journal of fatigue*, 2001, **23**, p.467-480.

[38] Lagoda, T., Energy model for fatigue life estimate under uniaxial random loading II: Verification of model, *International journal of fatigue*, 2001, **21**, p.481-489.

[39] Varvani-Farahani, A., A new critical plane parameter for fatigue life assessment of various metallic materials subjected to in-phase and out-of-phase multiaxial fatigue loading conditions, *International journal of fatigue*, 2000, **22**, p.295-305.

[40] Kilman, V., Fatigue life prediction for a material under programmable loading using the cyclic stress-strain properties. *Material Science and Engineering*, 1983, **68**, p.1-10.

[41] Everett, R. A., The effect of load sequencing on the fatigue life of 2024-T3 aluminum alloy. *International journal of fatigue*, 1997, **19**, p.289-293.

[42] Dowling, N. E. and Wilson W. K., Notch member fatigue life prediction by local strain approach, Westinghouse research labs, the American Society of Automotive Engineer, 1977, **32**, p.55-106.

[43] Pompetzki, M. A. and Topper, T. H., Effect of compressive underloads and tensile overloads on fatigue damage accumulation in 2024-T351 aluminum, *J Testing Eval, JTEVA*, 1990; **18**(1), p. 53-61.

[44] Naigu, C. Sequence effect of small amplitude cycles on fatigue crack initiation and propagation in 2024-T351 aluminum, *International journal of fatigue*, 2001, **23**, p.807-815.

[45] Elber, W., Fatigue crack closure. *J Engng Fracture Mechanics*. 1970; **2**(1), p. 37-45.

[46] Fatemi A, Socie DF. A critical plane approach to multiaxial fatigue damage including out of phase loading. *Fatigue Fract. Eng Mater Struct* 1988; **11**, p. 49-65.

[47] Agerskov, H., fatigue in steel structures under random loading. *Journal of Constructional Steel Research*, 2000, **53**, p. 283-305.

[48] Wu.W.F, Liou.H.Y and Tsse.H.C., Estimation of fatigue damage and fatigue life of components under random loading.

[49] Song, Y., Fatigue test and analysis of concrete under biaxial cyclic load. *Journal of Constructional concrete Research*, 1999, **51**, p. 223-235.

[50] Chu, C.C.,Conle, F.A., and Bonnen J.F., Multiaxial stress-strain modeling and fatigue life prediction of SAE axle shaft, ASTM STP 1191, 1993, **30**, 37-54.

[51] Glinka, G., Shen, G., Plumtree, A., A multiaxial fatigue strain energy density parameter related to the critical plane. Fatigue Fract Eng Mater Struct 1995, **18**, 37-46.

Appendix A

(a) Fatigue properties of Low Carbon Steel

Cyclic Strength Coefficient	K'= 549.5 MPa
Cyclic Strain hardening exponent	n'= 0.193
Fatigue Strength Coefficient	σ'_f= 842 MPa
Fatigue Strength Exponent	b = -0.102
Fatigue Ductility Coefficient	ε'_f= 0.204
Fatigue Ductility Exponent	c = -0.499
Modulus of Elasticity	E = 204 GPa

Peak and valley stress data (in MPa) of low carbon steel reported by Kilman [40]

277.18	270.53	202.90	131.88	79.13
-277.18	-270.53	-202.90	-131.88	-79.13
464.58	453.43	340.07	221.05	132.63
-464.58	-453.43	-340.07	-221.05	-132.63
277.18	270.53	202.90	131.88	79.13
-277.18	-270.53	-202.90	-131.88	-79.13
441.15	430.56	322.92	209.90	125.94
-441.15	-430.56	-322.92	-209.90	-125.94
441.15	430.56	322.92	209.90	125.94
-441.15	-430.56	-322.92	-209.90	-125.94
488.00	476.29	357.22	232.19	139.31
-488.00	-476.29	-357.22	-232.19	-139.31
277.18	270.53	202.90	131.88	79.13
-277.18	-270.53	-202.90	-131.88	-79.13
347.46	339.12	254.34	165.32	99.19
-347.46	-339.12	-254.34	-165.32	-99.19
488.00	476.29	357.22	232.19	139.31
-488.00	-476.29	-357.22	-232.19	-139.31
417.73	407.70	305.78	198.76	119.25
-417.73	-407.70	-305.78	-198.76	-119.25
488.00	476.29	357.22	232.19	139.31
-488.00	-476.29	-357.22	-232.19	-139.31
347.46	339.12	254.34	165.32	99.19
-347.46	-339.12	-254.34	-165.32	-99.19
441.15	430.56	322.92	209.90	125.94
-441.15	-430.56	-322.92	-209.90	-125.94
277.18	270.53	202.90	131.88	79.13
-277.18	-270.53	-202.90	-131.88	-79.13
488.00	476.29	357.22	232.19	139.31
-488.00	-476.29	-357.22	-232.19	-139.31
464.58	453.43	340.07	221.05	132.63

-464.58	-453.43	-340.07	-221.05	-132.63
300.61	293.39	220.05	143.03	85.82
-300.61	-293.39	-220.05	-143.03	-85.82
277.18	270.53	202.90	131.88	79.13
-277.18	-270.53	-202.90	-131.88	-79.13
300.61	293.39	220.05	143.03	85.82
-300.61	-293.39	-220.05	-143.03	-85.82
441.15	430.56	322.92	209.90	125.94
-441.15	-430.56	-322.92	-209.90	-125.94
488.00	476.29	357.22	232.19	139.31
-488.00	-476.29	-357.22	-232.19	-139.31
417.73	407.70	305.78	198.76	119.25
-417.73	-407.70	-305.78	-198.76	-119.25
277.18	270.53	202.90	131.88	79.13
-277.18	-270.53	-202.90	-131.88	-79.13
488.00	476.29	357.22	232.19	139.31
-488.00	-476.29	-357.22	-232.19	-139.31
300.61	293.39	220.05	143.03	85.82
-300.61	-293.39	-220.05	-143.03	-85.82
394.30	384.84	288.63	187.61	112.57
-394.30	-384.84	-288.63	-187.61	-112.57
324.03	316.26	237.19	154.17	92.50
-324.03	-316.26	-237.19	-154.17	-92.50
417.73	407.70	305.78	198.76	119.25
-417.73	-407.70	-305.78	-198.76	-119.25
417.73	407.70	305.78	198.76	119.25
-417.73	-407.70	-305.78	-198.76	-119.25
300.61	293.39	220.05	143.03	85.82
300.61	293.39	220.05	143.03	85.82
394.30	384.84	288.63	187.61	112.57
-394.30	-384.84	-288.63	-187.61	-112.57
277.18	270.53	202.90	131.88	79.13
-277.18	-270.53	-202.90	-131.88	-79.13
394.30	384.84	288.63	187.61	112.57
-394.30	-384.84	-288.63	-187.61	-112.57
417.73	407.70	305.78	198.76	119.25
-417.73	-407.70	-305.78	-198.76	-119.25
488.00	476.29	357.22	232.19	139.31
-488.00	-476.29	-357.22	-232.19	-139.31
394.30	384.84	288.63	187.61	112.57
-394.30	-384.84	-288.63	-187.61	-112.57
324.03	316.26	237.19	154.17	92.50
-324.03	-316.26	-237.19	-154.17	-92.50
277.18	270.53	202.90	131.88	79.13
-277.18	-270.53	-202.90	-131.88	-79.13
277.18	270.53	202.90	131.88	79.13
-277.18	-270.53	-202.90	-131.88	-79.13
277.18	270.53	202.90	131.88	79.13

-277.18	-270.53	-202.90	-131.88	-79.13
417.73	407.70	305.78	198.76	119.25
-417.73	-407.70	-305.78	-198.76	-119.25
464.58	453.43	340.07	221.05	132.63
-464.58	-453.43	-340.07	-221.05	-132.63
464.58	453.43	340.07	221.05	132.63
-464.58	-453.43	-340.07	-221.05	-132.63
417.73	407.70	305.78	198.76	119.25
-417.73	-407.70	-305.78	-198.76	-119.25
464.58	453.43	340.07	221.05	132.63
-464.58	-453.43	-340.07	-221.05	-132.63
347.46	339.12	254.34	165.32	99.19
-347.46	-339.12	-254.34	-165.32	-99.19
347.46	339.12	254.34	165.32	99.19
-347.46	-339.12	-254.34	-165.32	-99.19
488.00	476.29	357.22	232.19	139.31
-488.00	-476.29	-357.22	-232.19	-139.31
277.18	270.53	202.90	131.88	79.13
-277.18	-270.53	-202.90	-131.88	-79.13
370.88	361.98	271.48	176.46	105.88
-370.88	-361.98	-271.48	-176.46	-105.88
464.58	453.43	340.07	221.05	132.63
-464.58	-453.43	-340.07	-221.05	-132.63
347.46	339.12	254.34	165.32	99.19
-347.46	-339.12	-254.34	-165.32	-99.19
488.00	476.29	357.22	232.19	139.31
-488.00	-476.29	-357.22	-232.19	-139.31
370.88	361.98	271.48	176.46	105.88
-370.88	-361.98	-271.48	-176.46	-105.88
464.58	453.43	340.07	221.05	132.63
-464.58	-453.43	-340.07	-221.05	-132.63
488.00	476.29	357.22	232.19	139.31
-488.00	-476.29	-357.22	-232.19	-139.31
347.46	339.12	254.34	165.32	99.19
-347.46	-339.12	-254.34	-165.32	-99.19
394.30	384.84	288.63	187.61	112.57
-394.30	-384.84	-288.63	-187.61	-112.57
464.58	453.43	340.07	221.05	132.63
-464.58	-453.43	-340.07	-221.05	-132.63
417.73	407.70	305.78	198.76	119.25
-417.73	-407.70	-305.78	-198.76	-119.25
277.18	270.53	202.90	131.88	79.13
-277.18	-270.53	-202.90	-131.88	-79.13
370.88	361.98	271.48	176.46	105.88
-370.88	-361.98	-271.48	-176.46	-105.88
324.03	316.26	237.19	154.17	92.50
-324.03	-316.26	-237.19	-154.17	-92.50
488.00	476.29	357.22	232.19	139.31

-488.00	-476.29	-357.22	-232.19	-139.31
464.58	453.43	340.07	221.05	132.63
-464.58	-453.43	-340.07	-221.05	-132.63
488.00	476.29	357.22	232.19	139.31
-488.00	-476.29	-357.22	-232.19	-139.31
324.03	316.26	237.19	154.17	92.50
-324.03	-316.26	-237.19	-154.17	-92.50
324.03	316.26	237.19	154.17	92.50
-324.03	-316.26	-237.19	-154.17	-92.50
394.30	384.84	288.63	187.61	112.57
-394.30	-384.84	-288.63	-187.61	-112.57
324.03	316.26	237.19	154.17	92.50
-324.03	-316.26	-237.19	-154.17	-92.50
277.18	270.53	202.90	131.88	79.13
-277.18	-270.53	-202.90	-131.88	-79.13
300.61	293.39	220.05	143.03	85.82
-300.61	-293.39	-220.05	-143.03	-85.82
394.30	384.84	288.63	187.61	112.57
-394.30	-384.84	-288.63	-187.61	-112.57
324.03	316.26	237.19	154.17	92.50
-324.03	-316.26	-237.19	-154.17	-92.50
488.00	476.29	357.22	232.19	139.31
-488.00	-476.29	-357.22	-232.19	-139.31
277.18	270.53	202.90	131.88	79.13
-277.18	-270.53	-202.90	-131.88	-79.13
488.00	476.29	357.22	232.19	139.31
-488.00	-476.29	-357.22	-232.19	-139.31
464.58	453.43	340.07	221.05	132.63
-464.58	-453.43	-340.07	-221.05	-132.63
347.46	339.12	254.34	165.32	99.19
-347.46	-339.12	-254.34	-165.32	-99.19
300.61	293.39	220.05	143.03	85.82
-300.61	-293.39	-220.05	-143.03	-85.82
394.30	384.84	288.63	187.61	112.57
-394.30	-384.84	-288.63	-187.61	-112.57
488.00	476.29	357.22	232.19	139.31
-488.00	-476.29	-357.22	-232.19	-139.31
394.30	384.84	288.63	187.61	112.57
-394.30	-384.84	-288.63	-187.61	-112.57
324.03	316.26	237.19	154.17	92.50
-324.03	-316.26	-237.19	-154.17	-92.50
300.61	293.39	220.05	143.03	85.82
-300.61	-293.39	-220.05	-143.03	-85.82
417.73	407.70	305.78	198.76	119.25
-417.73	-407.70	-305.78	-198.76	-119.25
347.46	339.12	254.34	165.32	99.19
-347.46	-339.12	-254.34	-165.32	-99.19
347.46	339.12	254.34	165.32	99.19

-347.46	-339.12	-254.34	-165.32	-99.19
324.03	316.26	237.19	154.17	92.50
-324.03	-316.26	-237.19	-154.17	-92.50
394.30	384.84	288.63	187.61	112.57
-394.30	-384.84	-288.63	-187.61	-112.57
488.00	476.29	357.22	232.19	139.31
-488.00	-476.29	-357.22	-232.19	-139.31
277.18	270.53	202.90	131.88	79.13
-277.18	-270.53	-202.90	-131.88	-79.13
300.61	293.39	220.05	143.03	85.82
-300.61	-293.39	-220.05	-143.03	-85.82
324.03	316.26	237.19	154.17	92.50
-324.03	-316.26	-237.19	-154.17	-92.50
370.88	361.98	271.48	176.46	105.88
-370.88	-361.98	-271.48	-176.46	-105.88
394.30	384.84	288.63	187.61	112.57
-394.30	-384.84	-288.63	-187.61	-112.57
300.61	293.39	220.05	143.03	85.82
-300.61	-293.39	-220.05	-143.03	-85.82
488.00	476.29	357.22	232.19	139.31
-488.00	-476.29	-357.22	-232.19	-139.31
488.00	476.29	357.22	232.19	139.31
-488.00	-476.29	-357.22	-232.19	-139.31
324.03	316.26	237.19	154.17	92.50
-324.03	-316.26	-237.19	-154.17	-92.50
488.00	476.29	357.22	232.19	139.31
-488.00	-476.29	-357.22	-232.19	-139.31
394.30	384.84	288.63	187.61	112.57
-394.30	-384.84	-288.63	-187.61	-112.57
277.18	270.53	202.90	131.88	79.13
-277.18	-270.53	-202.90	-131.88	-79.13
417.73	407.70	305.78	198.76	119.25
-417.73	-407.70	-305.78	-198.76	-119.25
417.73	407.70	305.78	198.76	119.25
-417.73	-407.70	-305.78	-198.76	-119.25
488.00	476.29	357.22	232.19	139.31
-488.00	-476.29	-357.22	-232.19	-139.31
324.03	316.26	237.19	154.17	92.50
-324.03	-316.26	-237.19	-154.17	-92.50
277.18	270.53	202.90	131.88	79.13
-277.18	-270.53	-202.90	-131.88	-79.13
347.46	339.12	254.34	165.32	99.19
-347.46	-339.12	-254.34	-165.32	-99.19
464.58	453.43	340.07	221.05	132.63
-464.58	-453.43	-340.07	-221.05	-132.63
324.03	316.26	237.19	154.17	92.50
-324.03	-316.26	-237.19	-154.17	-92.50
277.18	270.53	202.90	131.88	79.13

-277.18	-270.53	-202.90	-131.88	-79.13
370.88	361.98	271.48	176.46	105.88
-370.88	-361.98	-271.48	-176.46	-105.88

(b) Fatigue properties of 7075-T761 Aluminum alloy

Cyclic Strength Coefficient	K' = 852 MPa
Cyclic Strain hardening exponent	n' = 0.074
Fatigue Strength Coefficient	σ'_f=1231 MPa
Fatigue Strength Exponent	b = -0.122
Fatigue Ductility Coefficient	ε'_f= 0.263
Fatigue Ductility Exponent	c = -0.806
Modulus of Elasticity	E = 700 GPa

Peak and valley stress data (in MPa) of 7075-T761 Aluminum alloy reported by Wu [49]

42.88	41.36	30.57	28.77	26.98
-42.88	-41.36	-30.57	-28.77	-26.98
85.76	82.72	61.14	57.55	53.95
-85.76	-82.72	-61.14	-57.55	-53.95
215.74	208.10	153.81	144.77	135.72
-215.74	-208.10	-153.81	-144.77	-135.72
108.54	104.70	77.39	72.83	68.28
-108.54	-104.70	-77.39	-72.83	-68.28
93.8	90.48	66.88	62.94	59.01
-93.8	-90.48	-66.88	-62.94	-59.01
259.96	250.76	185.34	174.44	163.54
-259.96	-250.76	-185.34	-174.44	-163.54
93.8	90.48	66.88	62.94	59.01
-93.8	-90.48	-66.88	-62.94	-59.01
85.76	82.72	61.14	57.55	53.95
-85.76	-82.72	-61.14	-57.55	-53.95
151.42	146.06	107.96	101.61	95.26
-151.42	-146.06	-107.96	-101.61	-95.26
108.54	104.70	77.39	72.83	68.28
-108.54	-104.70	-77.39	-72.83	-68.28
108.54	104.70	77.39	72.83	68.28
-108.54	-104.70	-77.39	-72.83	-68.28
93.8	90.48	66.88	62.94	59.01
-93.8	-90.48	-66.88	-62.94	-59.01
85.76	82.72	61.14	57.55	53.95
-85.76	-82.72	-61.14	-57.55	-53.95
151.42	146.06	107.96	101.61	95.26
-151.42	-146.06	-107.96	-101.61	-95.26
85.76	82.72	61.14	57.55	53.95
-85.76	-82.72	-61.14	-57.55	-53.95
324.28	312.80	231.20	217.60	204.00
-324.28	-312.80	-231.20	-217.60	-204.00

237.18	228.78	169.10	159.15	149.21
237.18	228.78	169.10	159.15	149.21
259.96	250.76	185.34	174.44	163.54
-259.96	-250.76	-185.34	-174.44	-163.54
219.76	211.98	156.68	147.46	138.25
-219.76	-211.98	-156.68	-147.46	-138.25
108.54	104.70	77.39	72.83	68.28
-108.54	-104.70	-77.39	-72.83	-68.28
85.76	82.72	61.14	57.55	53.95
-85.76	-82.72	-61.14	-57.55	-53.95
219.76	211.98	156.68	147.46	138.25
-219.76	-211.98	-156.68	-147.46	-138.25
108.54	104.70	77.39	72.83	68.28
-108.54	-104.70	-77.39	-72.83	-68.28
108.54	104.70	77.39	72.83	68.28
-108.54	-104.70	-77.39	-72.83	-68.28
219.76	211.98	156.68	147.46	138.25
-219.76	-211.98	-156.68	-147.46	-138.25
64.32	62.04	45.86	43.16	40.46
-64.32	-62.04	-45.86	-43.16	-40.46
42.88	41.36	30.57	28.77	26.98
-42.88	-41.36	-30.57	-28.77	-26.98
21.44	20.68	15.29	14.39	13.49
-21.44	-20.68	-15.29	-14.39	-13.49
64.32	62.04	45.86	43.16	40.46
-64.32	-62.04	-45.86	-43.16	-40.46
64.32	62.04	45.86	43.16	40.46
-64.32	-62.04	-45.86	-43.16	-40.46
85.76	82.72	61.14	57.55	53.95
-85.76	-82.72	-61.14	-57.55	-53.95
237.18	228.78	169.10	159.15	149.21
-237.18	-228.78	-169.10	-159.15	-149.21
237.18	228.78	169.10	159.15	149.21
-237.18	-228.78	-169.10	-159.15	-149.21
108.54	104.70	77.39	72.83	68.28
-108.54	-104.70	-77.39	-72.83	-68.28
129.98	125.38	92.67	87.22	81.77
-129.98	-125.38	-92.67	-87.22	-81.77
151.42	146.06	107.96	101.61	95.26
-151.42	-146.06	-107.96	-101.61	-95.26
64.32	62.04	45.86	43.16	40.46
-64.32	-62.04	-45.86	-43.16	-40.46
172.86	166.74	123.24	115.99	108.74
-172.86	-166.74	-123.24	-115.99	-108.74
172.86	166.74	123.24	115.99	108.74
-172.86	-166.74	-123.24	-115.99	-108.74
21.44	20.68	15.29	14.39	13.49
-21.44	-20.68	-15.29	-14.39	-13.49

194.3	187.42	138.53	130.38	122.23
-194.3	-187.42	-138.53	-130.38	-122.23
85.76	82.72	61.14	57.55	53.95
-85.76	-82.72	-61.14	-57.55	-53.95
21.44	20.68	15.29	14.39	13.49
-21.44	-20.68	-15.29	-14.39	-13.49
259.96	250.76	185.34	174.44	163.54
-259.96	-250.76	-185.34	-174.44	-163.54
194.3	187.42	138.53	130.38	122.23
-194.3	-187.42	-138.53	-130.38	-122.23
21.44	20.68	15.29	14.39	13.49
-21.44	-20.68	-15.29	-14.39	-13.49
172.86	166.74	123.24	115.99	108.74
-172.86	-166.74	-123.24	-115.99	-108.74
259.96	250.76	185.34	174.44	163.54
-259.96	-250.76	-185.34	-174.44	-163.54
259.96	250.76	185.34	174.44	163.54
-259.96	-250.76	-185.34	-174.44	-163.54
237.18	228.78	169.10	159.15	149.21
-237.18	-228.78	-169.10	-159.15	-149.21
108.54	104.70	77.39	72.83	68.28
-108.54	-104.70	-77.39	-72.83	-68.28
108.54	104.70	77.39	72.83	68.28
-108.54	-104.70	-77.39	-72.83	-68.28
129.98	125.38	92.67	87.22	81.77
-129.98	-125.38	-92.67	-87.22	-81.77
85.76	82.72	61.14	57.55	53.95
-85.76	-82.72	-61.14	-57.55	-53.95
324.28	312.80	231.20	217.60	204.00
-324.28	-312.80	-231.20	-217.60	-204.00

(c) Fatigue properties of 2024-T3 aluminum

Cyclic Strength Coefficient	K'= 852 MPa
Cyclic Strain hardening exponent	n'= 0.074
Fatigue Strength Coefficient	σ'_f =1231 MPa
Fatigue Strength Exponent	b = -0.122
Fatigue Ductility Coefficient	ε'_f = 0.263
Fatigue Ductility Exponent	c = -0.806
Modulus of Elasticity	E = 700 GPa

Peak and valley stress data (in MPa) of 2024-T3 aluminum reported by Everett [41]

4.55	4.31	4.19	3.94
-50.10	-47.40	-46.04	-43.33
-31.88	-30.16	-29.30	-27.58
-27.33	-25.85	-25.11	-23.64
173.09	163.73	159.05	149.70
40.99	38.78	37.67	35.45
141.20	133.57	129.75	122.12
86.54	81.87	79.53	74.85
131.40	124.30	120.75	113.65
73.43	69.46	67.48	63.51
162.32	153.55	149.16	140.39
50.24	47.53	46.17	43.45
143.00	135.27	131.40	123.67
81.16	76.77	74.58	70.19
143.00	135.27	131.40	123.67
85.03	80.43	78.13	73.54
131.40	124.30	120.75	113.65
50.24	47.53	46.17	43.45
143.00	135.27	131.40	123.67
69.57	65.81	63.93	60.17
127.54	120.65	117.20	110.30
81.16	76.77	74.58	70.19
127.54	120.65	117.20	110.30
69.57	65.81	63.93	60.17
139.13	131.61	127.85	120.33
69.57	65.81	63.93	60.17
166.19	157.20	152.71	143.73
69.57	65.81	63.93	60.17
123.67	116.99	113.65	106.96
139.13	131.61	127.85	120.33
69.57	65.81	63.93	60.17
123.67	116.99	113.65	106.96
69.57	65.81	63.93	60.17
139.13	131.61	127.85	120.33
46.38	43.87	42.62	40.11
139.13	131.61	127.85	120.33

81.16	76.77	74.58	70.19
123.67	116.99	113.65	106.96
65.70	62.15	60.37	56.82
139.13	131.61	127.85	120.33
65.70	62.15	60.37	56.82
139.13	131.61	127.85	120.33
54.11	51.18	49.72	46.80
127.54	120.65	117.20	110.30
54.11	51.18	49.72	46.80
143.00	135.27	131.40	123.67
85.03	80.43	78.13	73.54
139.13	131.61	127.85	120.33
46.38	43.87	42.62	40.11
139.13	131.61	127.85	120.33
85.03	80.43	78.13	73.54
139.13	131.61	127.85	120.33
69.57	65.81	63.93	60.17
139.13	131.61	127.85	120.33
69.57	65.81	63.93	60.17
139.13	131.61	127.85	120.33
69.57	65.81	63.93	60.17
162.32	153.55	149.16	140.39
69.57	65.81	63.93	60.17
162.32	153.55	149.16	140.39
69.57	65.81	63.93	60.17
131.40	124.30	120.75	113.65
69.57	65.81	63.93	60.17
139.13	131.61	127.85	120.33
69.57	65.81	63.93	60.17
131.40	124.30	120.75	113.65
77.30	73.12	71.03	66.85
139.13	131.61	127.85	120.33
69.57	65.81	63.93	60.17
123.67	116.99	113.65	106.96
85.03	80.43	78.13	73.54
143.00	135.27	131.40	123.67
65.70	62.15	60.37	56.82
123.67	116.99	113.65	106.96
69.57	65.81	63.93	60.17
127.54	120.65	117.20	110.30
73.43	69.46	67.48	63.51
143.00	135.27	131.40	123.67
69.57	65.81	63.93	60.17
123.67	116.99	113.65	106.96
50.24	47.53	46.17	43.45
131.40	124.30	120.75	113.65
85.03	80.43	78.13	73.54
162.32	153.55	149.16	140.39

85.03	80.43	78.13	73.54
139.13	131.61	127.85	120.33
65.70	62.15	60.37	56.82
123.67	116.99	113.65	106.96
69.57	65.81	63.93	60.17
139.13	131.61	127.85	120.33
69.57	65.81	63.93	60.17
139.13	131.61	127.85	120.33
69.57	65.81	63.93	60.17
177.78	168.17	163.37	153.76
69.57	65.81	63.93	60.17
158.46	149.89	145.61	137.04
69.57	65.81	63.93	60.17
143.00	135.27	131.40	123.67
85.03	80.43	78.13	73.54
139.13	131.61	127.85	120.33
69.57	65.81	63.93	60.17
123.67	116.99	113.65	106.96
69.57	65.81	63.93	60.17
143.00	135.27	131.40	123.67
96.62	91.40	88.79	83.56
143.00	135.27	131.40	123.67
54.11	51.18	49.72	46.80
162.32	153.55	149.16	140.39
54.11	51.18	49.72	46.80
177.78	168.17	163.37	153.76
85.03	80.43	78.13	73.54
158.46	149.89	145.61	137.04
96.62	91.40	88.79	83.56
158.46	149.89	145.61	137.04
81.16	76.77	74.58	70.19
158.46	149.89	145.61	137.04
81.16	76.77	74.58	70.19
158.46	149.89	145.61	137.04
81.16	76.77	74.58	70.19
181.65	171.83	166.92	157.10
81.16	76.77	74.58	70.19
185.51	175.48	170.47	160.44
100.49	95.05	92.34	86.91
158.46	149.89	145.61	137.04
50.24	47.53	46.17	43.45
158.46	149.89	145.61	137.04
81.16	76.77	74.58	70.19
158.46	149.89	145.61	137.04
81.16	76.77	74.58	70.19
158.46	149.89	145.61	137.04
81.16	76.77	74.58	70.19
193.24	182.80	177.57	167.13

119.81	113.33	110.10	103.62
135.27	127.96	124.30	116.99
81.16	76.77	74.58	70.19
243.48	230.32	223.74	210.58
30.92	29.25	28.41	26.74
200.97	190.11	184.68	173.81
3.86	3.66	3.55	3.34
173.92	164.52	159.82	150.41
100.49	95.05	92.34	86.91
173.92	164.52	159.82	150.41
77.30	73.12	71.03	66.85
173.92	164.52	159.82	150.41
104.35	98.71	95.89	90.25
173.92	164.52	159.82	150.41
119.81	113.33	110.10	103.62
200.97	190.11	184.68	173.81
112.08	106.02	102.99	96.93
282.13	266.88	259.26	244.01
100.49	95.05	92.34	86.91
189.38	179.14	174.02	163.78
100.49	95.05	92.34	86.91
212.57	201.08	195.33	183.84
115.94	109.68	106.54	100.28
177.78	168.17	163.37	153.76
73.43	69.46	67.48	63.51
193.24	182.80	177.57	167.13
73.43	69.46	67.48	63.51
173.92	164.52	159.82	150.41
34.78	32.90	31.96	30.08
173.92	164.52	159.82	150.41
34.78	32.90	31.96	30.08
173.92	164.52	159.82	150.41
115.94	109.68	106.54	100.28
173.92	164.52	159.82	150.41
115.94	109.68	106.54	100.28
173.92	164.52	159.82	150.41
73.43	69.46	67.48	63.51
173.92	164.52	159.82	150.41
100.49	95.05	92.34	86.91
181.65	171.83	166.92	157.10
119.81	113.33	110.10	103.62
173.92	164.52	159.82	150.41
100.49	95.05	92.34	86.91
193.24	182.80	177.57	167.13
100.49	95.05	92.34	86.91
216.43	204.73	198.88	187.18
100.49	95.05	92.34	86.91
177.78	168.17	163.37	153.76

115.94	109.68	106.54	100.28
177.78	168.17	163.37	153.76
100.49	95.05	92.34	86.91
200.97	190.11	184.68	173.81
100.49	95.05	92.34	86.91
185.51	175.48	170.47	160.44
77.30	73.12	71.03	66.85
193.24	182.80	177.57	167.13
104.35	98.71	95.89	90.25
200.97	190.11	184.68	173.81
77.30	73.12	71.03	66.85
197.11	186.45	181.12	170.47
77.30	73.12	71.03	66.85
139.13	131.61	127.85	120.33
69.57	65.81	63.93	60.17
123.67	116.99	113.65	106.96
69.57	65.81	63.93	60.17
143.00	135.27	131.40	123.67
96.62	91.40	88.79	83.56
143.00	135.27	131.40	123.67
54.11	51.18	49.72	46.80
162.32	153.55	149.16	140.39
54.11	51.18	49.72	46.80
177.78	168.17	163.37	153.76
85.03	80.43	78.13	73.54
158.46	149.89	145.61	137.04
96.62	91.40	88.79	83.56
158.46	149.89	145.61	137.04
81.16	76.77	74.58	70.19
158.46	149.89	145.61	137.04
81.16	76.77	74.58	70.19
158.46	149.89	145.61	137.04
81.16	76.77	74.58	70.19
181.65	171.83	166.92	157.10
81.16	76.77	74.58	70.19
185.51	175.48	170.47	160.44
100.49	95.05	92.34	86.91
158.46	149.89	145.61	137.04
50.24	47.53	46.17	43.45
158.46	149.89	145.61	137.04
81.16	76.77	74.58	70.19
158.46	149.89	145.61	137.04
81.16	76.77	74.58	70.19
158.46	149.89	145.61	137.04
81.16	76.77	74.58	70.19
193.24	182.80	177.57	167.13
119.81	113.33	110.10	103.62
135.27	127.96	124.30	116.99

81.16	76.77	74.58	70.19
243.48	230.32	223.74	210.58
30.92	29.25	28.41	26.74
200.97	190.11	184.68	173.81
3.86	3.66	3.55	3.34
173.92	164.52	159.82	150.41
100.49	95.05	92.34	86.91
173.92	164.52	159.82	150.41
77.30	73.12	71.03	66.85
173.92	164.52	159.82	150.41
104.35	98.71	95.89	90.25
173.92	164.52	159.82	150.41
119.81	113.33	110.10	103.62
200.97	190.11	184.68	173.81
112.08	106.02	102.99	96.93
251.21	237.63	230.84	217.27
100.49	95.05	92.34	86.91
189.38	179.14	174.02	163.78
100.49	95.05	92.34	86.91
212.57	201.08	195.33	183.84
115.94	109.68	106.54	100.28
177.78	168.17	163.37	153.76
73.43	69.46	67.48	63.51
193.24	182.80	177.57	167.13
73.43	69.46	67.48	63.51
173.92	164.52	159.82	150.41
34.78	32.90	31.96	30.08
173.92	164.52	159.82	150.41
34.78	32.90	31.96	30.08
173.92	164.52	159.82	150.41
115.94	109.68	106.54	100.28
173.92	164.52	159.82	150.41
115.94	109.68	106.54	100.28
173.92	164.52	159.82	150.41
73.43	69.46	67.48	63.51
173.92	164.52	159.82	150.41
100.49	95.05	92.34	86.91
181.65	171.83	166.92	157.10
119.81	113.33	110.10	103.62
173.92	164.52	159.82	150.41
100.49	95.05	92.34	86.91
193.24	182.80	177.57	167.13
100.49	95.05	92.34	86.91
216.43	204.73	198.88	187.18
100.49	95.05	92.34	86.91
177.78	168.17	163.37	153.76
115.94	109.68	106.54	100.28
177.78	168.17	163.37	153.76

100.49	95.05	92.34	86.91
200.97	190.11	184.68	173.81
100.49	95.05	92.34	86.91
185.51	175.48	170.47	160.44
77.30	73.12	71.03	66.85
193.24	182.80	177.57	167.13
104.35	98.71	95.89	90.25
200.97	190.11	184.68	173.81
77.30	73.12	71.03	66.85
197.11	186.45	181.12	170.47
77.30	73.12	71.03	66.85
173.92	164.52	159.82	150.41
73.43	69.46	67.48	63.51
173.92	164.52	159.82	150.41
100.49	95.05	92.34	86.91
181.65	171.83	166.92	157.10
119.81	113.33	110.10	103.62
173.92	164.52	159.82	150.41
100.49	95.05	92.34	86.91
193.24	182.80	177.57	167.13
100.49	95.05	92.34	86.91
216.43	204.73	198.88	187.18
100.49	95.05	92.34	86.91
177.78	168.17	163.37	153.76
115.94	109.68	106.54	100.28
177.78	168.17	163.37	153.76
100.49	95.05	92.34	86.91
200.97	190.11	184.68	173.81
100.49	95.05	92.34	86.91
185.51	175.48	170.47	160.44
77.30	73.12	71.03	66.85
193.24	182.80	177.57	167.13
104.35	98.71	95.89	90.25
200.97	190.11	184.68	173.81
77.30	73.12	71.03	66.85
197.11	186.45	181.12	170.47
38.65	36.56	35.51	33.43
139.13	131.61	127.85	120.33
-3.86	-3.66	-3.55	-3.34
123.67	116.99	113.65	106.96
-38.65	-36.56	-35.51	-33.43
143.00	135.27	131.40	123.67
96.62	91.40	88.79	83.56
143.00	135.27	131.40	123.67
54.11	51.18	49.72	46.80
200.97	190.11	184.68	173.81
54.11	51.18	49.72	46.80
200.97	190.11	184.68	173.81

85.03	80.43	78.13	73.54
235.75	223.01	216.64	203.90
96.62	91.40	88.79	83.56
158.46	149.89	145.61	137.04
81.16	76.77	74.58	70.19
158.46	149.89	145.61	137.04
81.16	76.77	74.58	70.19
158.46	149.89	145.61	137.04
81.16	76.77	74.58	70.19
181.65	171.83	166.92	157.10
81.16	76.77	74.58	70.19
185.51	175.48	170.47	160.44
100.49	95.05	92.34	86.91
158.46	149.89	145.61	137.04
50.24	47.53	46.17	43.45
158.46	149.89	145.61	137.04
81.16	76.77	74.58	70.19
158.46	149.89	145.61	137.04
81.16	76.77	74.58	70.19
158.46	149.89	145.61	137.04
81.16	76.77	74.58	70.19
193.24	182.80	177.57	167.13
119.81	113.33	110.10	103.62
135.27	127.96	124.30	116.99
81.16	76.77	74.58	70.19
243.48	230.32	223.74	210.58
30.92	29.25	28.41	26.74
200.97	190.11	184.68	173.81
3.86	3.66	3.55	3.34
173.92	164.52	159.82	150.41
100.49	95.05	92.34	86.91
173.92	164.52	159.82	150.41
77.30	73.12	71.03	66.85
173.92	164.52	159.82	150.41
104.35	98.71	95.89	90.25
173.92	164.52	159.82	150.41
119.81	113.33	110.10	103.62
200.97	190.11	184.68	173.81
112.08	106.02	102.99	96.93
282.13	266.88	259.26	244.01
100.49	95.05	92.34	86.91
189.38	179.14	174.02	163.78
100.49	95.05	92.34	86.91
212.57	201.08	195.33	183.84
115.94	109.68	106.54	100.28
177.78	168.17	163.37	153.76
73.43	69.46	67.48	63.51
193.24	182.80	177.57	167.13

73.43	69.46	67.48	63.51
173.92	164.52	159.82	150.41
34.78	32.90	31.96	30.08
173.92	164.52	159.82	150.41
34.78	32.90	31.96	30.08
173.92	164.52	159.82	150.41
115.94	109.68	106.54	100.28
173.92	164.52	159.82	150.41
115.94	109.68	106.54	100.28
173.92	164.52	159.82	150.41
73.43	69.46	67.48	63.51
173.92	164.52	159.82	150.41
100.49	95.05	92.34	86.91
181.65	171.83	166.92	157.10
119.81	113.33	110.10	103.62
173.92	164.52	159.82	150.41
100.49	95.05	92.34	86.91
193.24	182.80	177.57	167.13
100.49	95.05	92.34	86.91
216.43	204.73	198.88	187.18
100.49	95.05	92.34	86.91
177.78	168.17	163.37	153.76
115.94	109.68	106.54	100.28
177.78	168.17	163.37	153.76
100.49	95.05	92.34	86.91
200.97	190.11	184.68	173.81
100.49	95.05	92.34	86.91
185.51	175.48	170.47	160.44
127.54	120.65	117.20	110.30
81.16	76.77	74.58	70.19
127.54	120.65	117.20	110.30
69.57	65.81	63.93	60.17
139.13	131.61	127.85	120.33
69.57	65.81	63.93	60.17
166.19	157.20	152.71	143.73
69.57	65.81	63.93	60.17
123.67	116.99	113.65	106.96
139.13	131.61	127.85	120.33
69.57	65.81	63.93	60.17
123.67	116.99	113.65	106.96
69.57	65.81	63.93	60.17
139.13	131.61	127.85	120.33
46.38	43.87	42.62	40.11
139.13	131.61	127.85	120.33
81.16	76.77	74.58	70.19
123.67	116.99	113.65	106.96
65.70	62.15	60.37	56.82
139.13	131.61	127.85	120.33

65.70	62.15	60.37	56.82
139.13	131.61	127.85	120.33
54.11	51.18	49.72	46.80
127.54	120.65	117.20	110.30
54.11	51.18	49.72	46.80
143.00	135.27	131.40	123.67
85.03	80.43	78.13	73.54
139.13	131.61	127.85	120.33
46.38	43.87	42.62	40.11
139.13	131.61	127.85	120.33
85.03	80.43	78.13	73.54
139.13	131.61	127.85	120.33
69.57	65.81	63.93	60.17
139.13	131.61	127.85	120.33
69.57	65.81	63.93	60.17
139.13	131.61	127.85	120.33
69.57	65.81	63.93	60.17
162.32	153.55	149.16	140.39
69.57	65.81	63.93	60.17
162.32	153.55	149.16	140.39
69.57	65.81	63.93	60.17
131.40	124.30	120.75	113.65
69.57	65.81	63.93	60.17
139.13	131.61	127.85	120.33
69.57	65.81	63.93	60.17
131.40	124.30	120.75	113.65
77.30	73.12	71.03	66.85
139.13	131.61	127.85	120.33
69.57	65.81	63.93	60.17
123.67	116.99	113.65	106.96
85.03	80.43	78.13	73.54
143.00	135.27	131.40	123.67
65.70	62.15	60.37	56.82
123.67	116.99	113.65	106.96
69.57	65.81	63.93	60.17
127.54	120.65	117.20	110.30
73.43	69.46	67.48	63.51
143.00	135.27	131.40	123.67
69.57	65.81	63.93	60.17
123.67	116.99	113.65	106.96
50.24	47.53	46.17	43.45
131.40	124.30	120.75	113.65
85.03	80.43	78.13	73.54
162.32	153.55	149.16	140.39
85.03	80.43	78.13	73.54
139.13	131.61	127.85	120.33
65.70	62.15	60.37	56.82
123.67	116.99	113.65	106.96

69.57	65.81	63.93	60.17
139.13	131.61	127.85	120.33
69.57	65.81	63.93	60.17
139.13	131.61	127.85	120.33
69.57	65.81	63.93	60.17

(d) Fatigue properties of Low carbon steel

Cyclic Strength Coefficient	K'= 549.5 MPa
Cyclic Strain hardening exponent	n'= 0.193
Fatigue Strength Coefficient	σ'_f = 842 MPa
Fatigue Strength Exponent	b= -0.102
Fatigue Ductility Coefficient	ε'_f = 0.204
Fatigue Ductility Exponent	c = -0.499
Modulus of Elasticity	E = 204 GPa

Peak and valley stress data (in MPa) of low carbon steel reported by Agerskov [47]

.92	2.09	1.67	1.5	1.33
-5.75	-6.27	-5.00	-4.5	-4.00
46.00	50.18	40.00	36	32.00
-17.25	-18.82	-15.00	-13.5	-12.00
86.25	94.09	75.00	67.5	60.00
-23.00	-25.09	-20.00	-18	-16.00
51.75	56.45	45.00	40.5	36.00
-1.92	-2.09	-1.67	-1.5	-1.33
74.75	81.55	65.00	58.5	52.00
23.00	25.09	20.00	18	16.00
74.75	81.55	65.00	58.5	52.00
23.00	25.09	20.00	18	16.00
74.75	81.55	65.00	58.5	52.00
11.50	12.55	10.00	9	8.00
51.75	56.45	45.00	40.5	36.00
-1.92	-2.09	-1.67	-1.5	-1.33
11.50	12.55	10.00	9	8.00
1.92	2.09	1.67	1.5	1.33
11.50	12.55	10.00	9	8.00
103.50	112.91	90.00	81	72.00
-17.25	-18.82	-15.00	-13.5	-12.00
132.25	144.27	115.00	103.5	92.00
-11.50	-12.55	-10.00	-9	-8.00
103.50	112.91	90.00	81	72.00
1.92	2.09	1.67	1.5	1.33
57.50	62.73	50.00	45	40.00
51.75	56.45	45.00	40.5	36.00
57.50	62.73	50.00	45	40.00
-1.92	-2.09	-1.67	-1.5	-1.33
74.75	81.55	65.00	58.5	52.00
-1.92	-2.09	-1.67	-1.5	-1.33
80.50	87.82	70.00	63	56.00
-1.92	-2.09	-1.67	-1.5	-1.33
86.25	94.09	75.00	67.5	60.00

-1.92	-2.09	-1.67	-1.5	-1.33
80.50	87.82	70.00	63	56.00
-11.50	-12.55	-10.00	-9	-8.00
28.75	31.36	25.00	22.5	20.00
-11.50	-12.55	-10.00	-9	-8.00
17.25	18.82	15.00	13.5	12.00
-1.92	-2.09	-1.67	-1.5	-1.33
34.50	37.64	30.00	27	24.00
-5.75	-6.27	-5.00	-4.5	-4.00
57.50	62.73	50.00	45	40.00
5.75	6.27	5.00	4.5	4.00
51.75	56.45	45.00	40.5	36.00
-23.00	-25.09	-20.00	-18	-16.00
57.50	62.73	50.00	45	40.00
-11.50	-12.55	-10.00	-9	-8.00
69.00	75.27	60.00	54	48.00
-11.50	-12.55	-10.00	-9	-8.00
23.00	25.09	20.00	18	16.00
11.50	12.55	10.00	9	8.00
28.75	31.36	25.00	22.5	20.00
-5.75	-6.27	-5.00	-4.5	-4.00
23.00	25.09	20.00	18	16.00
-5.75	-6.27	-5.00	-4.5	-4.00
34.50	37.64	30.00	27	24.00
28.75	31.36	25.00	22.5	20.00
57.50	62.73	50.00	45	40.00
-23.00	-25.09	-20.00	-18	-16.00
46.00	50.18	40.00	36	32.00
-5.75	-6.27	-5.00	-4.5	-4.00
80.50	87.82	70.00	63	56.00
11.50	12.55	10.00	9	8.00
149.50	163.09	130.00	117	104.00
-34.50	-37.64	-30.00	-27	-24.00
132.25	144.27	115.00	103.5	92.00
-11.50	-12.55	-10.00	-9	-8.00
40.25	43.91	35.00	31.5	28.00
1.92	2.09	1.67	1.5	1.33
63.25	69.00	55.00	49.5	44.00
-11.50	-12.55	-10.00	-9	-8.00
63.25	69.00	55.00	49.5	44.00
-11.50	-12.55	-10.00	-9	-8.00
97.75	106.64	85.00	76.5	68.00
-28.75	-31.36	-25.00	-22.5	-20.00
40.25	43.91	35.00	31.5	28.00
-11.50	-12.55	-10.00	-9	-8.00
17.25	18.82	15.00	13.5	12.00
1.92	2.09	1.67	1.5	1.33
11.50	12.55	10.00	9	8.00

-5.75	-6.27	-5.00	-4.5	-4.00
63.25	69.00	55.00	49.5	44.00
-5.75	-6.27	-5.00	-4.5	-4.00
74.75	81.55	65.00	58.5	52.00
-11.50	-12.55	-10.00	-9	-8.00
40.25	43.91	35.00	31.5	28.00
-5.75	-6.27	-5.00	-4.5	-4.00
109.25	119.18	95.00	85.5	76.00
-17.25	-18.82	-15.00	-13.5	-12.00
218.50	238.36	190.00	171	152.00
155.25	169.36	135.00	121.5	108.00
161.00	175.64	140.00	126	112.00
-5.75	-6.27	-5.00	-4.5	-4.00
166.75	181.91	145.00	130.5	116.00
-5.75	-6.27	-5.00	-4.5	-4.00
155.25	169.36	135.00	121.5	108.00
11.50	12.55	10.00	9	8.00
109.25	119.18	95.00	85.5	76.00
-23.00	-25.09	-20.00	-18	-16.00
138.00	150.55	120.00	108	96.00
-11.50	-12.55	-10.00	-9	-8.00
63.25	69.00	55.00	49.5	44.00
5.75	6.27	5.00	4.5	4.00
40.25	43.91	35.00	31.5	28.00
-11.50	-12.55	-10.00	-9	-8.00
34.50	37.64	30.00	27	24.00
-17.25	-18.82	-15.00	-13.5	-12.00
28.75	31.36	25.00	22.5	20.00
-11.50	-12.55	-10.00	-9	-8.00
63.25	69.00	55.00	49.5	44.00
28.75	31.36	25.00	22.5	20.00
126.50	138.00	110.00	99	88.00
-34.50	-37.64	-30.00	-27	-24.00
120.75	131.73	105.00	94.5	84.00
97.75	106.64	85.00	76.5	68.00
103.50	112.91	90.00	81	72.00
-11.50	-12.55	-10.00	-9	-8.00
63.25	69.00	55.00	49.5	44.00
-11.50	-12.55	-10.00	-9	-8.00
97.75	106.64	85.00	76.5	68.00
-11.50	-12.55	-10.00	-9	-8.00
63.25	69.00	55.00	49.5	44.00
-28.75	-31.36	-25.00	-22.5	-20.00
195.50	213.27	170.00	153	136.00
-23.00	-25.09	-20.00	-18	-16.00
5.75	6.27	5.00	4.5	4.00
-5.75	-6.27	-5.00	-4.5	-4.00
23.00	25.09	20.00	18	16.00

-5.75	-6.27	-5.00	-4.5	-4.00
40.25	43.91	35.00	31.5	28.00
-23.00	-25.09	-20.00	-18	-16.00
28.75	31.36	25.00	22.5	20.00
-5.75	-6.27	-5.00	-4.5	-4.00
23.00	25.09	20.00	18	16.00
17.25	18.82	15.00	13.5	12.00
34.50	37.64	30.00	27	24.00
-5.75	-6.27	-5.00	-4.5	-4.00
23.00	25.09	20.00	18	16.00
17.25	18.82	15.00	13.5	12.00
23.00	25.09	20.00	18	16.00
-5.75	-6.27	-5.00	-4.5	-4.00
23.00	25.09	20.00	18	16.00
17.25	18.82	15.00	13.5	12.00
57.50	62.73	50.00	45	40.00
11.50	12.55	10.00	9	8.00
28.75	31.36	25.00	22.5	20.00
-5.75	-6.27	-5.00	-4.5	-4.00
86.25	94.09	75.00	67.5	60.00
28.75	31.36	25.00	22.5	20.00
126.50	138.00	110.00	99	88.00
-40.25	-43.91	-35.00	-31.5	-28.00
161.00	175.64	140.00	126	112.00
132.25	144.27	115.00	103.5	92.00
138.00	150.55	120.00	108	96.00
-11.50	-12.55	-10.00	-9	-8.00
-5.75	-6.27	-5.00	-4.5	-4.00
-11.50	-12.55	-10.00	-9	-8.00
120.75	131.73	105.00	94.5	84.00
40.25	43.91	35.00	31.5	28.00
149.50	163.09	130.00	117	104.00
143.75	156.82	125.00	112.5	100.00
189.75	207.00	165.00	148.5	132.00
-57.50	-62.73	-50.00	-45	-40.00
230.00	250.91	200.00	180	160.00
189.75	207.00	165.00	148.5	132.00
212.75	232.09	185.00	166.5	148.00
-11.50	-12.55	-10.00	-9	-8.00
17.25	18.82	15.00	13.5	12.00
-5.75	-6.27	-5.00	-4.5	-4.00
17.25	18.82	15.00	13.5	12.00
-5.75	-6.27	-5.00	-4.5	-4.00
80.50	87.82	70.00	63	56.00
-5.75	-6.27	-5.00	-4.5	-4.00
115.00	125.45	100.00	90	80.00
-11.50	-12.55	-10.00	-9	-8.00
40.25	43.91	35.00	31.5	28.00

-11.50	-12.55	-10.00	-9	-8.00
28.75	31.36	25.00	22.5	20.00
-11.50	-12.55	-10.00	-9	-8.00
74.75	81.55	65.00	58.5	52.00
17.25	18.82	15.00	13.5	12.00
97.75	106.64	85.00	76.5	68.00
-34.50	-37.64	-30.00	-27	-24.00
126.50	138.00	110.00	99	88.00
-17.25	-18.82	-15.00	-13.5	-12.00
-5.75	-6.27	-5.00	-4.5	-4.00
-11.50	-12.55	-10.00	-9	-8.00
34.50	37.64	30.00	27	24.00
17.25	18.82	15.00	13.5	12.00
40.25	43.91	35.00	31.5	28.00
-23.00	-25.09	-20.00	-18	-16.00
69.00	75.27	60.00	54	48.00

Appendix B
Programming Code

Symbols (in Code)	Symbols (in Text)	Variable Description
e	E	Modulus of elasticity
k	K'	Cyclic Strength Coefficient
n	1/n'	Cyclic Strain Hardening Exponent
Ve	ν_e	Elastic Poisson's ratio
Vp	ν_p	Plastic Poisson's ratio
Veff	ν_{eff}	Effective Poisson's ratio
EA	ε_t	Total Strain
EP	ε_p	Plastic Strain
EE	ε_e	Elastic Strain
Ya	$(\frac{\gamma_a}{2})$	Shear Strain
Ta	τ_a	Shear Stress
SF	σ_f'	Fatigue Axial Strength Coefficient
EF	ε_f'	Fatigue Axial Ductility Coefficient
ST	τ_f'	Shear Fatigue Strength Coefficient
ET	γ_f'	Shear Fatigue Ductility Coefficient
G	G	Shear Modulus
b	b	Fatigue Strength Exponent
c	c	Fatigue Ductility Exponent
b1	b'	Fatigue Torsional Strength Exponent
c1	c'	Fatigue Torsional Ductility Exponent
SR	$\Delta\sigma_n$	Normal Axial Stress Range
ER	$\Delta\varepsilon_n$	Normal Axial Strain Range
STR	$\Delta\tau_{max}$	Maximum Shear Stress Range
ETR	$\Delta(\frac{\gamma_{max}}{2})$	Maximum Shear Strain Range

```
clear
%%%%%%%%%%%%%%%%%%%%%%%%%%%%%%%%%%%%%%%%%%%
% Static input data for low carbon steel
%%%%%%%%%%%%%%%%%%%%%%%%%%%%%%%%%%%%%%%%%%%
 e=205000;% E,Modulus of elasticity
 k=1022;% K',Cyclic Strength Coefficient
 n=4.85;% n',Cyclic Strain hardening exponent
 Ve=0.3;% $\nu_e$,Elastic Poisson's ratio
 Vp=0.5;% $\nu_p$,Plastic Poisson's ratio
 Veff=0;% $\nu_{eff}$,Effective Poisson's ratio
 EA=0.0;% $\varepsilon_t$,Total Strain
 EP=0.0;% $\varepsilon_p$,Plastic Strain
 EE=0.0;% $\varepsilon_e$,Elastic Strain
 Ya=0.0;% $(\frac{\gamma_a}{2})$,Shear Strain
 Ta=0.0;% $\tau_a$,Shear Stress
 SF=948;% $\sigma_f'$ , Fatigue Axial Strength Coefficient
 EF=0.26;% $\varepsilon_f$ , Fatigue Axial Ductility Coefficient
 Fa=0;%Iterative variable
 ST = 505;% $\tau_f'$ ,Shear fatigue strength coefficient
 ET = 0.413;% $\gamma_f'$ ,Shear fatigue ductility coefficient
 G = 80000;% G, Shear Modulus
 b = -0.092% b, Fatigue Strength Exponent
 c = -0.445% c, Fatigue Ductility Exponent
 b1 = -0.097% b',Fatigue Torsional Strength Exponent
 c1 = -0.445% c',Fatigue Torsional Ductility Exponent
 SR=0;% $\Delta\sigma_n$,Normal Axial Stress Range
 ER=0;% $\Delta\varepsilon_n$,Normal Axial Strain Range
 STR=0;% $\Delta\tau_{max}$,Maximum Shear Stress Range
 ETR=0;% $\Delta(\frac{\gamma_{max}}{2})$, Maximum Shear Strain Range
 %%%%%%%%%%%%%%%%%%%%%%%%%%%%%%%%%%%%%%%%%%%%%%%%%%%%%%%%%%%%%
%A - Fetch's the input stress data from the hardware drive.
%%%%%%%%%%%%%%%%%%%%%%%%%%%%%%%%%%%%%%%%%%%%%%%%%%%%%%%%%%%%%%
A=load('c:\Input file.txt');
AA=max(A); % AA will select the max. stress from the data.
BB=min(A); % BB will select the min. stress from the data.
real Maxyh %Traps the max. stress value
cont=1 %Counter for trapping max. stress value
cont1=1 %Counter for trapping min. stress value
EL=175 %Endurance Limit or Fatigue Limit
x=A(1); %Inputting first stress value
x1=abs(x*0.10); %Dividing Input stress into equal intervals
p=0:x/x1:x; %$\sigma_a$,p represent stress values from 0 to x
```

```
j=p/e + (p/k).^n %ε_a, j represents strain values with respect to p.
 E1 = length(j) % E1 tells the length of j
 EA = j(E1); % EA traps the last value of E1
 EE=EA/e % Calculate the Elastic strain
 EP = EA-EE; % Calculate the plastic strain from total strain
 Veff=(Ve*EE+Vp*EP)/(EE+EP)% Calculate the effective Poisson's ratio.
 %%%%%%%%%%%%%%%%%%%%%%%%%%%%%%%%%%%%%%%%%%%%%%%%
 % E11,E12,E13 calculate  Principal strains
 %%%%%%%%%%%%%%%%%%%%%%%%%%%%%%%%%%%%%%%%%%%%%%%%
 E11=(1-Veff)*EA/2+0.5*((EA^2)*(1+Veff)+(Ya/2)^2)^0.5
 E12=-Veff*EA
 E13=(1-Veff)*EA/2-0.5*((EA^2)*(1+Veff)+(Ya/2)^2)^0.5
 %%%%%%%%%%%%%%%%%%%%%%%%%%%%%%%%%%%%%%%%%%%%%%%%%%%%%%%%%%%%%%%%%%%%%%%%%%%
 %Logic to get maximum and minimum principal strain values
 %%%%%%%%%%%%%%%%%%%%%%%%%%%%%%%%%%%%%%%%%%%%%%%%%%%%%%%%%%%%%%%%%%%%%%%%%%%
 if (E12 < E13 & E11 > E13)
    E13=E12
    E11=E11
 elseif (E12 > E13 & E11 < E13)
    E11=E12
    E13=E13
 elseif (E12 < E11 & E13 > E11)
    E11=E13
    E13=E12
  else
    E13=E13
    E11=E11
 end

 j1=length(p); % j1 tells the length of p
 J = p(j1); J traps the last value of j1
 %%%%%%%%%%%%%%%%%%%%%%%%%%%%%%%%%%%%%%%%%%%%%%%%
 % S11,S12,S13 calculate  Principal stresses
 %%%%%%%%%%%%%%%%%%%%%%%%%%%%%%%%%%%%%%%%%%%%%%%%
 S11=J/2+0.5*(J^2+4*Ta^2)^0.5
 S12=0
 S13=J/2-0.5*(J^2+4*Ta^2)^0.5
 P = length(A) % P tells the length of A
 %%%%%%%%%%%%%%%%%%%%%%%%%%%%%%%%%%%%%%%%%%%%%%%%
 %second Stress input is taken from the file
 %%%%%%%%%%%%%%%%%%%%%%%%%%%%%%%%%%%%%%%%%%%%%%%%
 y=A(2) %Inputting second stress value
 y1=abs(y*0.10) %Dividing Input stress into equal intervals
 %%%%%%%%%%%%%%%%%%%%%%%%%%%%%%%%%%%%%%%%%%%%%%%%%%%%%%%%%%%%%%%%%%%%%%%%%%%
 % J compares with max. value and y with minimum to trap max. value
 %%%%%%%%%%%%%%%%%%%%%%%%%%%%%%%%%%%%%%%%%%%%%%%%%%%%%%%%%%%%%%%%%%%%%%%%%%%
 if (J == AA & y ~= BB & cont1 == 1)
 q = J:y/y1:y; %σ_a, q represent stress values from J to y
 h = EA-((J-(q))/e)-2*((J-(q))/(2*k)).^n % h is ε_a, strain values
```

```
%%%%%%%%%%%%%%%%%%%%%%%%%%%%%%%%%%%%%%%%%%%%%%%%%%%%
% BB1 Record the min. range from the last data
%%%%%%%%%%%%%%%%%%%%%%%%%%%%%%%%%%%%%%%%%%%%%%%%%%%%

 BB1 = abs(0.1*BB)
y1r= J:BB/BB1:BB; %σa,y1r represent stress values from J to BB
y1i = EA-((J-(y1r))/e)-2*((J-(y1r))/(2*k)).^n
% y1i is εa, strain values
h1 = length(q)
H = q(h1);
E2 = length(h)
EB = h(E2);
EE=EB/e % Calculate the Elastic strain
EP = EB-EE % Calculate the plastic strain from total strain
Veff=(Ve*EE+Vp*EP)/(EE+EP)% Calculate the effective Poisson's ratio
%%%%%%%%%%%%%%%%%%%%%%%%%%%%%%%%%%%%%%%%%%%%%%%%%%%%
% E111,E112,E113 calculate  Principal strains
%%%%%%%%%%%%%%%%%%%%%%%%%%%%%%%%%%%%%%%%%%%%%%%%%%%%
E111=(1-Veff)*EB/2+0.5*((EB^2)*(1+Veff)+(Ya/2)^2)^0.5
E112=-Veff*EB
E113=(1-Veff)*EB/2-0.5*((EB^2)*(1+Veff)+(Ya/2)^2)^0.5
%%%%%%%%%%%%%%%%%%%%%%%%%%%%%%%%%%%%%%%%%%%%%%%%%%%%%%%%%%%%%%%%%%%%%%%%%%%
Logic to get maximum and minimum principal strain values
%%%%%%%%%%%%%%%%%%%%%%%%%%%%%%%%%%%%%%%%%%%%%%%%%%%%%%%%%%%%%%%%%%%%%%%%%%%
if (E112 < E113 & E111 > E113)
   E113=E112
   E111=E111
elseif (E112 > E113 & E111 < E113)
   E111=E112
   E113=E113
elseif (E112 < E111 & E113 > E111)
   E111=E113
   E113=E112
 else
   E113=E113
   E111=E111
End
%%%%%%%%%%%%%%%%%%%%%%%%%%%%%%%%%%%%%%%%%%%%%%%%%%%%
% S111,S112,S113 calculate  Principal stresses
%%%%%%%%%%%%%%%%%%%%%%%%%%%%%%%%%%%%%%%%%%%%%%%%%%%%
S111=H/2+0.5*(H^2+4*Ta^2)^0.5
S112=0
S113=H/2-0.5*(H^2+4*Ta^2)^0.5
cont1 = cont1 +1
else
q = J:y/y1:y; %σa,q represent stress values from J to y
h = EA-((J-(q))/e)-2*((J-(q))/(2*k)).^n % h is εa, strain
h1 = length(q)
H = q(h1);
E2 = length(h)
EB = h(E2);
EE=EB/e % Calculate the Elastic strain
EP = EB-EE % Calculate the plastic strain from total strain
Veff=(Ve*EE+Vp*EP)/(EE+EP) % Calculate the effective Poisson's ratio
```

```
%%%%%%%%%%%%%%%%%%%%%%%%%%%%%%%%%%%%%%%%%%%%%%%%%%%%
% E111,E112,E113 calculate  Principal strains
%%%%%%%%%%%%%%%%%%%%%%%%%%%%%%%%%%%%%%%%%%%%%%%%%%%%

E111=(1-Veff)*EB/2+0.5*((EB^2)*(1+Veff)+(Ya/2)^2)^0.5
E112=-Veff*EB
E113=(1-Veff)*EB/2-0.5*((EB^2)*(1+Veff)+(Ya/2)^2)^0.5
%%%%%%%%%%%%%%%%%%%%%%%%%%%%%%%%%%%%%%%%%%%%%%%%%%%%%%%%%%%%%%%%%%%%%%%%%%%%%%%
Logic to get maximum and minimum principal strain values
%%%%%%%%%%%%%%%%%%%%%%%%%%%%%%%%%%%%%%%%%%%%%%%%%%%%%%%%%%%%%%%%%%%%%%%%%%%%%%%
if (E112 < E113 & E111 > E113)
   E113=E112
   E111=E111
elseif (E112 > E113 & E111 < E113)
   E111=E112
   E113=E113
elseif (E112 < E111 & E113 > E111)
   E111=E113
   E113=E112
 else
   E113=E113
   E111=E111
End
%%%%%%%%%%%%%%%%%%%%%%%%%%%%%%%%%%%%%%%%%%%%%%%%%%%%
% S111,S112,S113 calculate  Principal stresses
%%%%%%%%%%%%%%%%%%%%%%%%%%%%%%%%%%%%%%%%%%%%%%%%%%%%
S111=H/2+0.5*(H^2+4*Ta^2)^0.5
S112=0
S113=H/2-0.5*(H^2+4*Ta^2)^0.5
end


ER = (E11/2+E13/2)-(E111/2+E113/2) % calculates Δε_n
SR = (S11/2+S13/2)-(S111/2+S113/2) % calculates Δσ_n
ETR = (E11/2-E13/2)-(E113/2-E111/2) % calculates Δ(γ_max/2)
STR = (S11/2-S13/2)-(S113/2-S111/2) % calculates Δτ_max
Mst = (x+y)/2 %Mst represents the mean stress value
%%%%%%%%%%%%%%%%%%%%%%%%%%%%%%%%%%%%%%%%%%%%%%%%%%%%
%Fn represents damage for each half cycle
%%%%%%%%%%%%%%%%%%%%%%%%%%%%%%%%%%%%%%%%%%%%%%%%%%%%
Fn = (1/(SF*EF))*(ER)*(SR)+(1+(Mst/SF))*(1/(ST*ET))*(ETR)*(STR)
%%%%%%%%%%%%%%%%%%%%%%%%%%%%%%%%%%%%%%%%%%%%%%%%%%%%
%Fa represents cumulative damage
%%%%%%%%%%%%%%%%%%%%%%%%%%%%%%%%%%%%%%%%%%%%%%%%%%%%
Fa=Fn+Fa;

i1=2;
h2=0;
q2=0;
i2=0;
r2=0;
while i1 <= P-2
```

```
i1=i1+1;
yy=A(i1);
yy=abs(yy)

if ( yy >= 0.5*EL | yy <= 0.5*EL)

 yy1=abs(yy*0.10);

    if (yy ~= AA & H == BB & cont == 1)

       yq = H:yy/yy1:yy;
       yh = EB+(((-H+yq)/e)+2*((-H+yq)/(2*k)).^n)
       %%%%%%%%%%%%%%%%%%%%%%%%%%%%%%%%%%%%%%%%%%%
       %Record the max range from the last data
       %%%%%%%%%%%%%%%%%%%%%%%%%%%%%%%%%%%%%%%%%%%
       AA1 = abs(0.1*AA)
       y1q = H:AA/AA1:AA
       y1h = EB+(((-H+y1q)/e)+2*((-H+y1q)/(2*k)).^n)
       %%%%%%%%%%%%%%%%%%%%%%%%%%%%%%%%%%%%%%%%%%%%%%%%
       %Resume the original data to form small loop
       %%%%%%%%%%%%%%%%%%%%%%%%%%%%%%%%%%%%%%%%%%%%%%%%
       yh1 = length(yq)
       yH = yq(yh1);
       yE2 = length(yh)
       yEB = yh(yE2);
       EE=yEB/e
       EP = yEB-EE
       Veff=(Ve*EE+Vp*EP)/(EE+EP)

       %%%%%%%%%%%%%%%%%%%%%%%%%%%%%%%%%%%%%%%%%%%%%%%%
       % E211,E212,E213 calculate Principal strains
       %%%%%%%%%%%%%%%%%%%%%%%%%%%%%%%%%%%%%%%%%%%%%%%%
                   E211=(1-
       Veff)*yEB/2+0.5*(yEB^2*(1+Veff)^2+(Ya/2)^2)^0.5
                   E212=-Veff*yEB
                   E213=(1-Veff)*yEB/2-
       0.5*(yEB^2*(1+Veff)^2+(Ya/2)^2)^0.5

       %%%%%%%%%%%%%%%%%%%%%%%%%%%%%%%%%%%%%%%%%%%%%%%%%%%%%%%%%%%%%%%%%%%%%%%
       %Logic to get maximum and minimum principal strain values
       %%%%%%%%%%%%%%%%%%%%%%%%%%%%%%%%%%%%%%%%%%%%%%%%%%%%%%%%%%%%%%%%%%%%%%%
       if (E212 < E213 & E211 > E213)
            E213=E212
            E211=E211
         elseif (E212 > E213 & E211 < E213)
            E211=E212
            E213=E213
         elseif (E212 < E211 & E213 > E211)
            E211=E213
            E213=E212
          else
            E213=E213
            E211=E211
         end
       ER = E11/2-E13/2
```

```
%%%%%%%%%%%%%%%%%%%%%%%%%%%%%%%%%%%%%%%%%%%%%%%%%%%%
% S211,S212,S213 calculate Principal stresses
%%%%%%%%%%%%%%%%%%%%%%%%%%%%%%%%%%%%%%%%%%%%%%%%%%%%
S211=H/2+0.5*(H^2+4*Ta^2)^0.5
S212=0
S213=H/2-0.5*(H^2+4*Ta^2)^0.5
cont = cont+1;
elseif  (H ~= BB & yy == AA & cont >= 2)

   yq = H:yy/yy1:yy;
   yh = EB+(((-H+yq)/e)+2*((-H+yq)/(2*k)).^n)
   yh1 = length(yq)
   yH = yq(yh1);
   yE2 = length(yh)
   yEB = yh(yE2);
%%%%%%%%%%%%%%%%%%%%%%%%%%%%%%%%%%%%%%%%%%%%%%%%%%%%
% E211, E212, E213 calculate  Principal strains
%%%%%%%%%%%%%%%%%%%%%%%%%%%%%%%%%%%%%%%%%%%%%%%%%%%%
   E211=(1-Veff)*yEB/2+0.5*(yEB^2*(1+Veff)^2+(Ya/2)^2)^0.5
   E212=-Veff*yEB
   E213=(1-Veff)*yEB/2-0.5*(yEB^2*(1+Veff)^2+(Ya/2)^2)^0.5

%%%%%%%%%%%%%%%%%%%%%%%%%%%%%%%%%%%%%%%%%%%%%%%%%%%%%%%%%%%%%%%%%%%%%%%
%Logic to get maximum and minimum principal strain values
%%%%%%%%%%%%%%%%%%%%%%%%%%%%%%%%%%%%%%%%%%%%%%%%%%%%%%%%%%%%%%%%%%%%%%%
   if (E212 < E213 & E211 > E213)
     E213=E212
     E211=E211
   elseif (E212 > E213 & E211 < E213)
     E211=E212
     E213=E213
   elseif (E212 < E211 & E213 > E211)
     E211=E213
     E213=E212
   else
     E213=E213
     E211=E211
   end

   ER = E11/2-E13/2
   S211=H/2+0.5*(H^2+4*Ta^2)^0.5
   S212=0
   S213=H/2-0.5*(H^2+4*Ta^2)^0.5
   yq = y1q
   yh = y1h
   yh1 = length(yq)
   yH = yq(yh1);
   yy = yH
   yE2 = length(yh)
   yEB = yh(yE2);
```

```
%%%%%%%%%%%%%%%%%%%%%%%%%%%%%%%%%%%%%%%%%%%%%%%
% E211, E212, E213 calculate Principal strains
%%%%%%%%%%%%%%%%%%%%%%%%%%%%%%%%%%%%%%%%%%%%%%%

   E211=(1-Veff)*yEB/2+0.5*(yEB^2*(1+Veff)^2+(Ya/2)^2)^0.5
   E212=-Veff*yEB
   E213=(1-Veff)*yEB/2-0.5*(yEB^2*(1+Veff)^2+(Ya/2)^2)^0.5

%%%%%%%%%%%%%%%%%%%%%%%%%%%%%%%%%%%%%%%%%%%%%%%%%%%%%%%%%%%%
%Logic to get maximum and minimum principal strain values

%%%%%%%%%%%%%%%%%%%%%%%%%%%%%%%%%%%%%%%%%%%%%%%%%%%%%%%%%%%
   if (E212 < E213 & E211 > E213)
     E213=E212
     E211=E211
   elseif (E212 > E213 & E211 < E213)
     E211=E212
     E213=E213
   elseif (E212 < E211 & E213 > E211)
     E211=E213
     E213=E212
   else
     E213=E213
     E211=E211
   end

   ER = E11/2-E13/2

%%%%%%%%%%%%%%%%%%%%%%%%%%%%%%%%%%%%%%%%%%%%%%%%%
% S211, S212, S213 calculate Principal stresses
%%%%%%%%%%%%%%%%%%%%%%%%%%%%%%%%%%%%%%%%%%%%%%%%%
   S211=H/2+0.5*(H^2+4*Ta^2)^0.5
   S212=0
   S213=H/2-0.5*(H^2+4*Ta^2)^0.5

   else

   yq = H:yy/yy1:yy;
   yh = EB+(((-H+yq)/e)+2*((-H+yq)/(2*k)).^n)
   yh1 = length(yq)
   yH = yq(yh1);
   yE2 = length(yh)
   yEB = yh(yE2);

%%%%%%%%%%%%%%%%%%%%%%%%%%%%%%%%%%%%%%%%%%%%%%%%
% E211, E212, E213 calculate  Principal strains
%%%%%%%%%%%%%%%%%%%%%%%%%%%%%%%%%%%%%%%%%%%%%%%%
   E211=(1-Veff)*yEB/2+0.5*(yEB^2*(1+Veff)^2+(Ya/2)^2)^0.5
   E212=-Veff*yEB
   E213=(1-Veff)*yEB/2-0.5*(yEB^2*(1+Veff)^2+(Ya/2)^2)^0.5

%%%%%%%%%%%%%%%%%%%%%%%%%%%%%%%%%%%%%%%%%%%%%%%%%%%%%%%%%%%
%Logic to get maximum and minimum principal strain values
%%%%%%%%%%%%%%%%%%%%%%%%%%%%%%%%%%%%%%%%%%%%%%%%%%%%%%%%%%%
   if (E212 < E213 & E211 > E213)
     E213=E212
     E211=E211
```

```
    elseif (E212 > E213 & E211 < E213)
      E211=E212
      E213=E213
    elseif (E212 < E211 & E213 > E211)
      E211=E213
      E213=E212
    else
      E213=E213
      E211=E211
    end

    ER = E11/2-E13/2

  %%%%%%%%%%%%%%%%%%%%%%%%%%%%%%%%%%%%%%%%%%%%%%
  % S211, S212, S213 calculate  Principal stresses
  %%%%%%%%%%%%%%%%%%%%%%%%%%%%%%%%%%%%%%%%%%%%%%
    S211=H/2+0.5*(H^2+4*Ta^2)^0.5
    S212=0
    S213=H/2-0.5*(H^2+4*Ta^2)^0.5
   end


  i1=1+i1;
  yz=A(i1);
  yz1=abs(yz*0.1);
if ( yz <= 0.5*EL | yz >= 0.5*EL)

 if (yy == AA & yz ~= BB & cont1 == 1)

  if ( (yy > yz & yz >= 0) | ( yy < yz & yy <=0)  )
     pq = -(yz/yz1)
  else
     pq = yz/yz1
  end

  yr = yy:yz/yz1:yz;
  yi = yEB-((yy-(yr))/e)-2*((yy-(yr))/(2*k)).^n

  %%%%%%%%%%%%%%%%%%%%%%%%%%%%%%%%%%%%%%%%%%%%%%%%%%%%%%%%%%%
  %Record    the    min.    range    from    the    last    data
  %%%%%%%%%%%%%%%%%%%%%%%%%%%%%%%%%%%%%%%%%%%%%%%%%%%%%%%%%%%
  BB1 = abs(BB*0.1);
  y1r = yy:BB/BB1:BB;
  y1i = yEB-((yy-(y1r))/e)-2*((yy-(y1r))/(2*k)).^n
  %%%%%%%%%%%%%%%%%%%%%%%%%%%%%%%%%%%%%%%%%%%%
  %Resume the orginal data to form small loop
  %%%%%%%%%%%%%%%%%%%%%%%%%%%%%%%%%%%%%%%%%%%%
  yE1 = length(yi)
  EB = yi(yE1);
  yj1=length(yr);
  H = yr(yj1);
  %%%%%%%%%%%%%%%%%%%%%%%%%%%%%%%%%%%%%%%%%%%%%%%
  % E311, E312, E313 calculate  Principal strains
  %%%%%%%%%%%%%%%%%%%%%%%%%%%%%%%%%%%%%%%%%%%%%%%
  E311=(1-Veff)*EB/2+0.5*(EB^2*(1+Veff)^2+(Ya/2)^2)^0.5
  E312=-Veff*EB
  E313=(1-Veff)*EB/2-0.5*(EB^2*(1+Veff)^2+(Ya/2)^2)^0.5
```

```
%%%%%%%%%%%%%%%%%%%%%%%%%%%%%%%%%%%%%%%%%%%%%%%%%%%%%%%%%%%
%Logic to get maximum and minimum principal strain values
%%%%%%%%%%%%%%%%%%%%%%%%%%%%%%%%%%%%%%%%%%%%%%%%%%%%%%%%%%
 if (E312 < E313 & E311 > E313)
   E313=E312
   E311=E311
elseif (E312 > E313 & E311 < E313)
   E311=E312
   E313=E313
elseif (E312 < E311 & E313 > E311)
   E311=E313
   E313=E312
 else
   E313=E313
   E311=E311
 end

 cont1 = cont1 +1
 elseif  (yy ~= AA & yz == BB & cont1 >= 2)
 if ( (yy > yz & yz >= 0) | ( yy < yz & yy <=0)  )
    pq = -(yz/yz1)
 else
    pq = yz/yz1
 end
 yz = -yy
 yr = yy:pz:yz;
 yi = yEB-((yy-(yr))/e)-2*((yy-(yr))/(2*k)).^n
 yE1 = length(yi)
 EB = yi(yE1);
 yj1=length(yr);
 H = yr(yj1);

 %%%%%%%%%%%%%%%%%%%%%%%%%%%%%%%%%%%%%%%%%%%%
 % E11, E12, E13 calculate  Principal strains
 %%%%%%%%%%%%%%%%%%%%%%%%%%%%%%%%%%%%%%%%%%%%
 E311=(1-Veff)*EB/2+0.5*(EB^2*(1+Veff)^2+(Ya/2)^2)^0.5
 E312=-Veff*EB
 E313=(1-Veff)*EB/2-0.5*(EB^2*(1+Veff)^2+(Ya/2)^2)^0.5
 %%%%%%%%%%%%%%%%%%%%%%%%%%%%%%%%%%%%%%%%%%%%%%%%%%%%%%%%%%
 %Logic to get maximum and minimum principal strain values
 %%%%%%%%%%%%%%%%%%%%%%%%%%%%%%%%%%%%%%%%%%%%%%%%%%%%%%%%%%

 if (E312 < E313 & E311 > E313)
   E313=E312
   E311=E311
 elseif (E312 > E313 & E311 < E313)
   E311=E312
   E313=E313
 elseif (E312 < E311 & E313 > E311)
   E311=E313
   E313=E312
 else
   E313=E313
   E311=E311
 end

 yr =y1r
```

```
yi=y1i
yE1 = length(yi)
EB = yi(yE1);
yj1=length(yr);
H = yr(yj1);
%%%%%%%%%%%%%%%%%%%%%%%%%%%%%%%%%%%%%%%%%%%%%
% E311,E312,E313 calculate Principal strains
%%%%%%%%%%%%%%%%%%%%%%%%%%%%%%%%%%%%%%%%%%%%%
E311=(1-Veff)*EB/2+0.5*(EB^2*(1+Veff)^2+(Ya/2)^2)^0.5
E312=-Veff*EB
E313=(1-Veff)*EB/2-0.5*(EB^2*(1+Veff)^2+(Ya/2)^2)^0.5
%%%%%%%%%%%%%%%%%%%%%%%%%%%%%%%%%%%%%%%%%%%%%%%%%%%%%%%%%%
%Logic to get maximum and minimum principal strain values
%%%%%%%%%%%%%%%%%%%%%%%%%%%%%%%%%%%%%%%%%%%%%%%%%%%%%%%%%
if (E312 < E313 & E311 > E313)
  E313=E312
  E311=E311
elseif (E312 > E313 & E311 < E313)
  E311=E312
  E313=E313
elseif (E312 < E311 & E313 > E311)
  E311=E313
  E313=E312
else
  E313=E313
  E311=E311
end

else

if ( (yy > yz & yz >= 0) | ( yy < yz & yy <=0)  )
   pq = -(yz/yz1)
else
   pq = (yz/yz1)
end
yr = yy:pq:yz;
yi = yEB-((yy-(yr))/e)-2*((yy-(yr))/(2*k)).^n
yE1 = length(yi)
EB = yi(yE1);
%the value EB will be transferred back
yj1=length(yr);
H = yr(yj1);
%The value H will be transferred back to the cycle to take
care of Memory effect
%%%%%%%%%%%%%%%%%%%%%%%%%%%%%%%%%%%%%%%%%%%%%
% E311,E312,E313 calculate Principal strains
%%%%%%%%%%%%%%%%%%%%%%%%%%%%%%%%%%%%%%%%%%%%%
E311=(1-Veff)*EB/2+0.5*(EB^2*(1+Veff)^2+(Ya/2)^2)^0.5
E312=-Veff*EB
E313=(1-Veff)*EB/2-0.5*(EB^2*(1+Veff)^2+(Ya/2)^2)^0.5
%%%%%%%%%%%%%%%%%%%%%%%%%%%%%%%%%%%%%%%%%%%%%%%%%%%%%%%%%%
%Logic to get maximum and minimum principal strain values
%%%%%%%%%%%%%%%%%%%%%%%%%%%%%%%%%%%%%%%%%%%%%%%%%%%%%%%%%
if (E312 < E313 & E311 > E313)
  E313=E312
  E311=E311
elseif (E312 > E313 & E311 < E313)
```

```
            E311=E312
            E313=E313
          elseif (E312 < E311 & E313 > E311)
            E311=E313
            E313=E312
           else
            E313=E313
            E311=E311
           end
        end
        %%%%%%%%%%%%%%%%%%%%%%%%%%%%%%%%%%%%%%%%%%%%%%%%%%%%
        % S211, S212, S213 calculate  Principal stresses
        %%%%%%%%%%%%%%%%%%%%%%%%%%%%%%%%%%%%%%%%%%%%%%%%%%%%
        S311=H/2+0.5*(H^2+4*Ta^2)^0.5
        S312=0
        S313=H/2-0.5*(H^2+4*Ta^2)^0.5
        ER = (E211/2+E213/2)-(E311/2+E313/2) % calculates Δε_n
        SR = (S211/2+S213/2)-(S311/2+S313/2) % calculates Δσ_n
        ETR = (E211/2-E213/2)-(E313/2-E311/2) % calculates Δ(γ_max/2)
        STR = (S211/2-S213/2)-(S313/2-S311/2) % calculates Δτ_max
        Mst = (yy+yz)/2 %Mst represents the mean stress value
        %%%%%%%%%%%%%%%%%%%%%%%%%%%%%%%%%%%%%%%%%%%%%%%%%%%%
        %Fn represents damage for each half cycle
        %%%%%%%%%%%%%%%%%%%%%%%%%%%%%%%%%%%%%%%%%%%%%%%%%%%%
        Fn = 1/(SF*EF))*(ER)*(SR)+(1+(Mst/SF))*(1/(ST*ET))*(ETR)*(STR)
        %%%%%%%%%%%%%%%%%%%%%%%%%%%%%%%%%%%%
        %Fa represents cumulative damage
        %%%%%%%%%%%%%%%%%%%%%%%%%%%%%%%%%%%%
        Fa=Fn+Fa;
        plot(j,p,h,q,yh,yq,yi,yr),grid
        hold on
        title('Random Loading')
          xlabel('Strain value'),ylabel('Stress Value')

      else
    end
  else
 end
end

  if  ( cont <= 2)
for Nb = 0:10:100000000 % Checks values from 0 to 1000000000
Ft  =  ((SF/e)*((Nb)^b)+(EF)*((Nb)^c))+((ST/G)*((Nb)^b1)+  ET*((Nb)^c1))%
calculates Number of cycles
   if Ft <= Fa % Compare the Number of cycle with proposed parameter
      disp('The Number of Cycles are'), disp(Nb)
      break
   else

   end
end
elsedisp('The Data is below the Endurance Limit')
end
```